AN EMPIRICAL KINETIC APPROACH TO STUDY THE OCCURENCE OF ION EXCHANGE BETWEEN COUNTERIONS (X/Y) AT THE CATIONIC MICELLAR SURFACE

NORAZIZAH BINTI ABD RAZAK

FACULTY OF SCIENCE
UNIVERSITY OF MALAYA
KUALA LUMPUR

2018

AN EMPIRICAL KINETIC APPROACH TO STUDY THE OCCURENCE OF ION EXCHANGE BETWEEN COUNTERIONS (X/Y) AT THE CATIONIC MICELLAR SURFACE

NORAZIZAH BINTI ABD RAZAK

THESIS SUBMITTED IN FULFILMENT OF THE REQUIREMENTS FOR THE DEGREE OF DOCTOR OF PHILOSOPHY

DEPARTMENT OF CHEMISTRY
FACULTY OF SCIENCE
UNIVERSITY OF MALAYA
KUALA LUMPUR

2018

UNIVERSITY OF MALAYA

ORIGINAL LITERARY WORK DECLARATION

Name of Candidate: Norazizah Binti Abd Razak

Matric No: SHC130055

Name of Degree: Doctor of Philosophy

Title of Project Paper/Research Report/Dissertation/Thesis ("this Work"):

An Empirical Kinetic Approach to Study the Occurence of Ion Exchange between Counterions (X/Y) at the Cationic Micellar Surface

Field of Study: Physical Chemistry

I do solemnly and sincerely declare that:

(1) I am the sole author/writer of this Work;
(2) This Work is original;
(3) Any use of any work in which copyright exists was done by way of fair dealing and for permitted purposes and any excerpt or extract from, or reference to or reproduction of any copyright work has been disclosed expressly and sufficiently and the title of the Work and its authorship have been acknowledged in this Work;
(4) I do not have any actual knowledge nor do I ought reasonably to know that the making of this work constitutes an infringement of any copyright work;
(5) I hereby assign all and every rights in the copyright to this Work to the University of Malaya ("UM"), who henceforth shall be owner of the copyright in this Work and that any reproduction or use in any form or by any means whatsoever is prohibited without the written consent of UM having been first had and obtained;
(6) I am fully aware that if in the course of making this Work I have infringed any copyright whether intentionally or otherwise, I may be subject to legal action or any other action as may be determined by UM.

Candidate's Signature Date:

Subscribed and solemnly declared before,

Witness's Signature Date:

Name:

Designation:

AN EMPIRICAL KINETIC APPROACH TO STUDY THE OCCURENCE OF ION EXCHANGE BETWEEN COUNTERIONS (X/Y) AT THE CATIONIC MICELLAR SURFACE

ABSTRACT

In this study, the values of R_X^{Br} (relative CTABr micellar binding constants of counterions X^- and Br^-) for different counterion X^{v-} ($\nu = 1, 2$) were determined by a semi-empirical kinetic (SEK) and spectrophotometric (SESp) methods. In SEK method, the effects of $[M_vX]$ on pseudo-first-order rate constants (k_{obs}) for piperidinolysis of phenyl salicylate (PSa^-), in the presence of constant concentration of cetyltrimethylammonium bromide $[CTABr]_T$ or didodecyldimethylammonium bromide $[DDABr]_T$ and [NaOH], were studied. For SESp technique, the effects of $[M_vX]$ on the initial absorbance (A_{ob}) values of samples containing constant concentration of N-2-methoxyphenylphtalamic acid (N-2-MeOPhPTH), $[CTABr]_T$ and [NaOH] were obtained at 310 nm and 35 °C. The values of K_S^0, for S^- representing PSa^-, were determined as $(18.7 \times 10^3)\ M^{-1}$ and $(33.7 \times 10^3)\ M^{-1}$ in the presence of respective wormlike micelles (WM) and vesicles (Vs). The value of K_S^0, for S^- representing N-2-MeOPhPT$^-$, at 35 °C is 3624 M^{-1}. The mean values of R_X^{Br} for X^{v-} representing (i) 3- and 4-methylsalicylate (3-, 4-MeSa^{v-}) at 35, 40, 45 and 55 °C are $\geq 1.5 - 1.9$-fold larger than those of 4-methoxysalicylate (4-MeOSa^{v-}); (ii) aliphatic carboxylate groups at 35 °C are 0.31, 0.56, 0.77, 1.88, 15.3 and 74.3, for respective CH_3COO^-, $C_2H_5COO^-$, $C_3H_7COO^-$, $C_4H_9COO^-$, $C_6H_{13}COO^-$ and $C_7H_{15}COO^-$. The break in the plots of k_{obs} versus $[M_vX]$ reveals that the micellar binding of counterion X has initiated the morphological transformation of micelles' structure. Rheological flow measurements of aqueous 15 mM CTABr and different $[M_vX]$ solutions revealed the presence of WM or Vs due to observable shear thinning behavior and the presence of maxima in the plot of zero shear viscosity, η_0 versus $[M_vX]$. The values of η_0, critical shear rate, $\dot{\gamma}_{cr}$ as well as flow activation energy parameters, show a quantitative correlation between counterion (X^{v-}) binding affinity to cationic micelles and X^{v-}-induced micellar growth. The presence of turbidity maximum in the plot of corrected absorbance, A_{ob} versus $[M_vX]$ indirectly shows the presence of Vs in the aqueous system.

Keywords: relative CTABr micellar binding constant, semi-empirical kinetic, spectrophotometric, shear thinning, X^{v-}-induced micellar growth.

PENDEKATAN KINETIK EMPIRIKAL UNTUK MENGKAJI KEJADIAN PERTUKARAN ION ANTARA ION LAWAN (X/Y) DI PERMUKAAN MISEL KATIONIK

ABSTRAK

Dalam kajian ini, nilai R_X^{Br} (nisbah pemalar yang mengikat misel CTABr kepada ion X^- dan Br^-) untuk ion lawan yang berbeza $X^{\nu-}$ (ν = 1, 2) telah ditentukan melalui kaedah kinetik separa empirikal (SEK) dan spektrofotometri (SESp). Dalam kaedah SEK, kesan $[M_\nu X]$ terhadap pemalar kadar pseudo tertib pertama (k_{obs}) telah dikaji, di mana proses yang terlibat adalah piperidinolisis ion fenil salisilat (PSa^-), dengan kehadiran setiltrimetilammonium bromida $[CTABr]_T$ atau didodesildimetilammonium bromida $[DDABr]_T$ berkepekatan malar, dan [NaOH]. Untuk teknik SESp, kesan $[M_\nu X]$ terhadap nilai penyerapan awal (A_{ob}) sampel yang mengandungi asid N-2-metoksifenilftalamik (N-2-MeOPhPTH) berkepekatan malar, $[CTABr]_T$ dan [NaOH] direkod pada 310 nm dan suhu 35 °C. Nilai K_S^0, bagi S^- yang mewakili PSa^-, ialah (18.7 × 10^3) M^{-1} dan (33.7 × 10^3) M^{-1}, masing-masing ditentukan dengan kehadiran misel cacing (WM) dan vesikel (Vs). Nilai bagi K_S^0, bagi S^- yang mewakili N-2-MeOPhPT$^-$, pada suhu 35 °C ialah 3624 M^{-1}. Nilai purata R_X^{Br} bagi $X^{\nu-}$ yang mewakili (i) 3- dan 4-metilsalisilat (3-, 4-MeSa$^{\nu-}$) pada suhu 35, 40, 45 dan 55 °C adalah $\geq$ 1.5 - 1.9 kali lebih tinggi daripada nilai purata R_X^{Br} bagi ion 4-metoksisalisilat (4-MeOSa$^{\nu-}$); (ii) kumpulan karboksilat alifatik pada suhu 35 °C adalah 0.31, 0.56, 0.77, 1.88, 15.3 dan 74.3, masing-masing ditentukan untuk ion lawan CH_3COO^-, $C_2H_5COO^-$, $C_3H_7COO^-$, $C_4H_9COO^-$, $C_6H_{13}COO^-$ dan $C_7H_{15}COO^-$. Perubahan kecerunan pada plot k_{obs} terhadap $[M_\nu X]$ menunjukkan bahawa pengikatan misel kepada ion lawan X telah merangsang transformasi morfologi terhadap struktur misel. Pengukuran aliran rheologi bagi larutan akues yang mengandungi 15 mM CTABr dan $[M_\nu X]$ yang berbeza, menunjukkan kehadiran WM atau Vs, di mana sifat penipisan ricih dan kehadiran titik maksima dalam plot kelikatan ricih sifar, η_0 terhadap $[M_vX]$ boleh dilihat. Nilai parameter bagi η_0, kadar ricih kritikal, $\dot{\gamma}_{cr}$ dan juga tenaga pengaktifan aliran, menunjukkan korelasi kuantitatif antara ion lawan (X^{v-}) yang melekat pada misel kationik, dengan pertumbuhan misel yang disebabkan oleh X^{v-}. Kehadiran kekeruhan yang maksimum dalam plot serapan piawai, A_{ob} terhadap $[M_vX]$, secara tidak langsung menunjukkan kehadiran vesikel dalam sistem akues.

Kata kunci: nisbah pemalar pengikat misel CTABr, kinetik separa empirikal, spektrofotometri, penipisan ricih, pertumbuhan misel yang disebabkan oleh X^{v-}.

ACKNOWLEDGEMENTS

Syukur to Allah that I am able to finish my PhD work under His power and guidance. Although I have to face some of hurdles and hardness during my PhD work, it reminds me that there is no sweetness of being excellent without bitterness to compete for it. Working on this present project has been the most valuable experience in searching for knowledge during my course of study in Chemistry Department, UM. As far as I concerned, there are many important persons that contribute as a role in making the successfulness of this project. Needless to say, I would like to thank all of them and present my deepest gratitude for making this thesis possible.

First of all, I am heartily thankful my supervisor, Prof. Dr. Mohammad Niyaz Khan. His encouragement, guidance and support from the initial to the final level of my work have enabled me to develop a better understanding in the study of micelle. Despite his busy schedule and unstable health conditions, lately, he has shown me too much patients and was always willing to spare time to solve my problems. Thanks also to Prof. Dr. Azhar Ariffin for his advice during the final stage of my thesis. Not forget to all D223 lab members, who are their help, advice and guidance especially in the progression of technical and machinery. Thanks for being there during my research.

I would also like to thank my family, especially my beloved husband and my parents for inspiring me, as well as their support from the beginning of this work until the end. Thanks to my husband for his ability in accompanying me while I was doing my work during those days and nights before. Frankly, I would say from deep in my heart that, I am nothing without them. Thank you for being there.

Lastly, I would like to thank the Ministry of Higher Education (MOHE), University of Malaya (UM), for financial assistance through research grants UM.C/HIR/MOHE/SC/07. I would like to offer my regards and blessings to all of those who supported me in any respect during the completion of the present study.

Norazizah Binti Abd. Razak
SHC130055

TABLE OF CONTENTS

LIST OF FIGURES

LIST OF TABLES

LIST OF SYMBOLS AND ABBREVIATIONS

δ_{ap}	Apparent molar absorptivity
θ	Empirical parameter in Eq. 4.1
$\dot{\gamma}$	Shear rate
η	Shear viscosity
$[\ ]_T$	Total concentration
η_0^{max}	Zero shear viscosity maximum at $[M_vX]_{sc}$
A_{cald}	Calculated absorbance
A_{ob}	Observed absorbance
A_0	Observed absorbance at $t = 0$
A_∞	Observed absorbance at $t = \infty$
BWM	Branched wormlike micelles
C_D	Concentration of detergent (CTABr or DDABr)
cmc	Critical surfactant concentration at which spherical micelles begin to form
Cryo-TEM	Cryogenic Transmission Electron Microscopy
C_S	Concentration of M_vX
CTABr	Cetyltrimethylammonium bromide
CTACl	Cetyltrimethylammonium chloride
CTASal	Cetyltrimethylammonium salicylate
cvc	Critical surfactant concentration at which vesicle begin to form
DDABr	Didodecyldimethylammonium bromide
D_n	Micellized surfactant
E_a	Flow activation energy
Eq.	Equation
$F_{X/S}$	Empirical constant whose magnitude should be > 0 and ≤ 1

K_{Br}	CTABr micellar binding constant of Br^-
k_{cald}	Calculated rate constant
K_{Cl}	CTABr micellar binding constant of Cl^-
k_M	Rate constant of reaction occuring in micellar pseudophase
k_{obs}	Observed pseudo-first-order rate constant
$k_{obs}^{M_vX}$	k_{obs} at a typical value of $[M_vX]$ and $[CTABr]_T = 0$
K_{OH}	CTABr micellar binding constants of HO^-
K_S	CTABr micellar binding constants of PSa^- or N-2-MeOPhPT$^-$
K_S^0	K_S at $[M_vX] = 0$
k_W	Rate constant of reaction occuring in aqueous phase
K_X	CTABr micellar binding constant of X^-
$K^{X/S}$	Empirical constant in Eq. 4.1
$K_{X/S}$	Empirical constant whose magnitude represents the ability of counterion X^{v-} to expel S^- from cationic micellar pseudophase to aqueous phase
K_X^{Br}	Ratio of K_X and K_{Br} i.e $K_X^{Br} = K_X/K_{Br}$ where the values of CTABr micellar binding constants, K_{Br} and K_X, have been derived from kinetic parameters obtained in the presence of similar structure of micelles, respectively
K_X^Y	Ion-exchange constant for ion-exchange process X^{v-}/Y^-
4-MeOSaH	4-methoxysalicylic acid
4-MeOSa^{v-}	Anionic 4-methoxysalicylic acid
3-MeSaH	3-methylsalicylic acid
3-MeSa^{v-}	Anionic 3-methylsalicylic acid
4-MeSaH	4-methylsalicylic acid
4-MeSa^{v-}	Anionic 4-methylsalicylic acid
M	Molarity
MLV	Multilamellar vesicles

M_vX	Inert salt of anion
$[\mathrm{M_\nu X}]_\mathrm{S}^\mathrm{ef}$	Effective concentration of M_vX to expel PSa^- from micellar pseudophase to aqueous phase
$[\mathrm{M_\nu X}]_\mathrm{Br}^\mathrm{op}$	Optimum concentration of M_vX neededto expel Br^- ion from micellar pseudophase to aqueous phase
$[\mathrm{M_\nu X}]_\mathrm{OH}^\mathrm{op}$	Optimum concentration of M_vX needed to expel HO^- ion from micellar pseudophase to aqueous phase
$[\mathrm{M_\nu X}]_0^\mathrm{op}$	Optimum concentration of M_vX needed to expel both HO^- and Br^- ions from micellar pseudophase to aqueous phase
$[M_vX]_{sc}$	Specific concentration of M_vX at which the viscosity maximum occurs at zero or constant $\dot{\gamma}$ and [CTABr]
N_A	Avogadro's number
NMR	Nuclear magnetic resonance
PBLS	Planar bialyer sheets
PIE	Pseudophase ion exchange
Pip	Piperidine
pK_a	Acid dissociation constant at logarithmic scale
PM	Pseudophase micellar
PSaH	Phenyl salicylate
PSa^-	Ionized phenyl salicylate
RE	Residual error
RM	Rodlike micelles
R_X^{Br}	Ratio of K_X and K_{Br} i.e $R_X^{Br} = K_X/K_{Br}$ where the values of CTABr micellar binding constants, K_{Br} and K_X, have been derived from kinetic parameters obtained in the presence of spherical and non-spherical micelles, respectively
s	Second
S	Substrate/solubilizate
SANS	Small-angle neutron scattering
SEK	Semiempirical kinetic

SESp	Spectrophotometric
SM	Spherical micelles
S_M	Substrate/solubilizate in micellar pseodophase
Surf	Surfactant
SVs	Small vesicles
S_W	Substrate/solubilizate in aqueous phase
ULV	Unilamellar vesicles
WM	Wormlike micelles

LIST OF APPENDICES

CHAPTER 1: INTRODUCTION

1.1 Micelle

1.1.1 Characteristics of Micelles

Surfactant, which is also known as ‘surface active agent’, is ubiquitous both in physical, chemical and industrial processes (Khan, 2006). It is a chemical species which is amphiphilic in nature that has both hydrophilic (water-loving) head and hydrophobic (water-hating) tail (Khan, 2006). There are four main categories of surfactant which are anionic (negatively charged), cationic (positively charged), zwitterionic (negatively and positively charged) as well as non-ionic surfactants. The properties of surfactants fall into two broad categories which are adsorption and self-assembly (Yusof, 2011). The adsorption properties of surfactants make it suitable to lower the surface tension or interfacial tension between two phases like the surface tension between two liquids or between a liquid and a solid. For example, surfactants adsorb at the liquid-air interface, thus reduce the surface tension of water. Self-assembly property of surfactants is defined as the tendency of surfactant molecules to organize themselves into extended structures in solution, thus results in micelle formation. Surfactants start to aggregate to a micelle when it reach critical micelle temperature (Krafft temperature) as well as when the surfactant concentrations is above its well-defined critical micelle concentration (cmc) (Yusof, 2011).

A micelle is defined as an aggregation of colloidal molecules which exist in equilibrium with the surfactant molecules from which they are formed. Micelles are dynamic in the sense that they exist in rapid equilibrium with surfactant monomers. The structure of micelle (such as spherical, cylindrical, vesicles as well as lipid bilayers) is described by its surfactant packing parameter, N_S. The packing parameter of surfactant is given by $N_S = V_C/(aL_C)$, where V_C is the volume of hydrophobic chain of surfactant, a is the cross sectional area of the hydrophilic core per molecule of aggregate and L_C is the length of the hydrophobic chain. It is noteworthy that the packing parameter for a specific surfactant is not a constant because the magnitude of N_S is highly dependent on the physical properties of surfactant aggregates. Hassan and his coworkers (Hassan *et al.*, 2001) had described the main characteristics of micellar packing parameter as follows:

(a) The stabilization of micelles is governed by the hydrophobic attractive forces of the tail group as well as head group repulsion (electrostatic and steric forces).

(b) Each surfactant molecule moves in a fluid and its physical appearance such as size, shape and aggregation numbers are decided by the packing parameter (molecular self-assembly) for the individual surfactant.

(c) These micelles have a length scales of about 10-1000 Å and a life time of milliseconds where its aggregates disappear in milliseconds upon dilution below the cmc.

There are several factors which are affecting the formation of the micellar aggregates in terms of their sizes and shapes. These factors include surfactant concentration, temperature, pH and ionic strength which contribute to the balance of interaction (hydrophilic, hydrophobic, van der Waals'/steric as well as electrostatic interaction (with ionic micelle)) between surfactant and solvent molecules (Khan, 2010). In aqueous system, the hydrophilic heads of micelle-forming surfactants point outward, exposing themselves to the aqueous surrounding, whilst the hydrophobic tails remain in the core of the aggregate. Water is a polar molecule, thus the hydrophilic head groups which are also polar in nature facing towards the water due to the attractive interaction between these two types of molecules. In contrast, the hydrophobic effect occurs due to the characteristic nature of hydrophobic tails (nonpolar), which drew away from water and pointing inward, forming the core of the aggregate.

It is noteworthy that any additional surfactants added to the micellar system, above its cmc, will go to micelles. This is due to the saturated concentration of surfactant above this critical concentration value. The reported cmc values for CTABr and DDABr micelles in water at 25 °C are 0.9 – 1.0 mM (Yusof, 2011) and 0.046 mM (Soltero *et al.*, 2000), respectively. The presence of critical vesicle concentration (cvc) in aqueous DDABr micellar system, also at 25 °C was reported by Soltero et al. as 0.73 mM (Soltero *et al.*, 2000). However, the cmc and cvc values for different surfactant systems may vary from each other depending on their environment such as temperature, pressure as well as the presence of surface active substances such as cosurfactant (Rojas *et al.*, 2008; Schubert *et al.*, 2003) or salts (Khan *et al.*, 2010; Ruan *et al.*, 2001; Yusof & Khan, 2010, 2011).

1.1.2 Application of Micelles

It is relevant to note that the micelles have drawn great attention in many applications. Such applications include drug carriers (health and pharmaceutical area) as well as industrial textiles, cosmetics, paper production and paint. Industrial detergents which also use the surfactant system are used widely in a number of applications for removing dirt from various surfaces. The amphiphilic nature of it, as well as the micelle size and charge are the key properties that influence product performance.

The micelles are used widely in industrial applications due to their fascinating viscoelastic behavior. The viscoelasticity is defined as the property of materials/systems that exhibit both viscous and elastic properties when undergoing deformation. The unique flexibility of micellar system when undergoing deformation makes it interesting to be explored. Early studies on viscoelastic micellar system had reported the rheological behavior along with its large potential in various applications (Yang, 2002). This characteristic behavior of micellar system has been used widely in petrochemical (Qi & Zakin, 2002), health and pharmaceutical area (Ideta *et al.*, 2004; Nishiyama *et al.*, 2005) as well as drag reduction in centralized heating and cooling system (Lin *et al.*, 2001).

1.1.3 Micelle Catalysis

The addition of micelle-forming surfactant above its cmc to a reaction mixture is believed to affect the solution environment, which is the cause for acceleration or inhibition of the rate of a reaction (Khan & Ahmad, 2001a, 2001b; Khan *et al.*, 2010; Ruan *et al.*, 2001; Yusof & Khan, 2010, 2011). Catalysis by micelles involves at least three main steps (Engberts, 1992):

i) Binding of the substrate(s) to the micelles,

ii) The actual chemical transformation in the micelle (usually at the micellar surface) and

iii) Release of product(s).

In micellar phase, the changes on the rate of reaction is attributed to the presence of electrostatic interaction (for ionic micelles) and hydrophobic interaction between the micellar phase and reactants as well as transition state and products (Khan, 2006; Yusof, 2011). The electrostatic interaction results from the presence of attractive or repulsive force between two charged particles (ionic headgroup of micelles and ionic solubilizate) which could affect the formation of an activated-complex (transition state). The formation of an activated-complex was determined by a sufficient energy of colliding molecules to overcome an activation energy barrier to react. It is relevant to note that this transition state posses charge/partial charge which is opposite to that of the micellar surface relative to the reactant side. The hydrophobic interaction between the hydrophobic tail of micelles, along with the hydrophobic nature of reactants and activated-complex species will cause them to orient their position during the course of a reaction. Both interactions (electrostatic and hydrophobic interactions) affecting the product formation rate and thus, the rate of reaction as well.

The rate of a chemical reaction in a micellar system could be affected by the presence of ions due to the occurrence of ion-exchange process. The ion-exchange process is defined as the process in which ions of one substance are replaced by similarly charged ions of another substance. The occurrence of ion-exchange between counterions and ionic reactants of charge similar to the charge of counterions of micellar-mediated ionic reactions or semi-ionic bimolecular reactions has been known to enhance the rate of chemical reactions in certain cases as well as inhibiting the rate of reaction in other cases (Khan, 1989, 1997; Khan *et al.*, 1997, 1999, 2010; Khan & Ismail, 2009; Ruan *et al.*, 2001; Yusof & Khan, 2010, 2011). It is possible to describe the occurrence of ion-exchange between the aqueous and micellar phases by an equilibrium process described below by **Eq. 1.1**,

$$[Y_M] + [X_W] \overset{K_S^0}{\rightleftharpoons} [Y_W] + [X_M] \qquad \textbf{Eq. 1.1}$$

where Y_M and X_M represent Y and X counterions, respectively in micellar pseudophase where as Y_W and X_W correspond to respective Y and X counterions, in aqueos phase. The corresponding selectivity coefficient or ion exchange constant, K_X^Y may be expressed as

$$K_X^Y = \frac{[Y_W][X_M]}{[Y_M][X_W]} \qquad \textbf{Eq. 1.2}$$

Several attempts have been made, where a number of models had been proposed in order to discuss and give a brief explanation on the properties and condition of micellar solution that exhibit ion-exchange processes (Minero & Pelizzetti, 1993; Yunes *et al.*, 2005). Khan (2006) had discussed extensively two of them which are Pseudophase Ion-Exchange (PIE) (Brinchi *et al.*, 2007) and Pseudopase Micellar (PM) (Chaimovich *et al.*, 1975) model. However, only PM model will be applied in the present study due to some weaknesses of PIE model. The reasons and probable explanations could be found elsewhere (Khan, 2006).

1.1.3.1 Pseudophase Micellar Model

The aggregation numbers of surfactant molecules that constitute a micelle vary from <100 to >100, depending on the physicochemical characteristics of surfactant, as well as its concentration, the presence of additives and temperatures. The word pseudophase is perhaps the best to describe a micellar phase, rather than real phase itself. Early report (Khan, 2010) summarized the assumptions introduced in PM model of micelles which are as follows: (a) There is no complex formation of substrate and surfactant monomer. (b) Substrate does not perturb micellization. (c) Substrate associates with the micelles in a 1:1 stoichiometry. (d) Micellization takes place exactly at the cmc rather than over a small concentration range. (e) The relationship $[D_n] = ([Surf]_T - cmc)/n$ is valid. (f) There is strictly definite reaction region for both micellar and bulk aqueous solvents. (g) The changes in the size and shape of micelles due to the increase in surfactant concentration will not affect the reaction rates and equilibria of micelles. (h) Both k_S and k_{-S} are larger than the respective k_W and k_M, where k_S and k_{-S} stand for respective rate constant for micellar incorporation and micellar exit of solubilizate/substrate S, hence $k_S/k_{-S} = K_S$, where K_S is the micellar binding constant of substrate; k_W and k_M represent the rate of reaction occur in respective aqueous and micellar system (i) The equilibrium process for micellar incorporation, are independent of each other for different solubilizates. (j) The cross-interface reaction for a bimolecular reaction, such as between a reactant in the micellar pseudophase R_M and other reactant in aqueous phase S_W, or vice versa does not take place. The micellar-mediated bimolecular reactions exhibit parallel reaction steps occuring simultaneously in both aqueous phase and micelar pseudophase. (k) K_M, K_S and k_M are independent to each other where K_M and K_S stand for equilibrium constant for the formation of micelles and solubilizate, respectively while k_M is the rate constant for micellar mediated reaction. In other words, $k_M^f >> k_W$ and $k_M^d >> k_M$ where k_M^f and k_M^d stand for respective rate constant for micelle formation and disintegration, and therefore $k_M^f / k_M^d = K_M$. In **Eq. 1.3**,

$$((n - N)/N_A)\text{monomers} \rightleftharpoons (N/rN_A)\text{micelles} \qquad \textbf{Eq. 1.3}$$

where n represents total number of surfactant molecules, N is the number of total surfactant molecules used up in the formation of number of micelles (N/r), r is the mean aggregation number of a micelle and N_A is Avogadro's number.

1.1.4 Aims of the Study

Numerous studies highlighted the origin of micellar structural transition (from spherical to long linear and entangled wormlike micelles (WM)) occurs whenever counterion (X) binds strongly to ionic micelles. However, the micellar binding affinity of different counterion X had been discussed only qualitatively, while the quantitative determination of this is rare. Thus, this study was designed with the following aims:

(i) To determine the values of micellar binding constant of different counterions X to CTABr micelles, where X^{v-} (ν = ionization number) represents 4-MeOSa^{v-}, 3- and 4-MeSa^{v-}, CH_3COO^-, $C_2H_5COO^-$, $C_3H_7COO^-$, $C_4H_9COO^-$, $C_6H_{13}COO^-$ and $C_7H_{15}COO^-$.

(ii) To investigate the characteristic behavior of dialkyl chain cationic surfactant (i.e. DDABr) system in aqueous environment.

(iii) To investigate the different possibilities of counterions X^{v-}- and temperature-induced micellar growth.

(iv) To provide a new knowledge and idea on micellar growth for industrial applications, and

(v) To provide better understanding on the rheological properties and characteristic behavior of surfactant solution containing different structure of aggregates

CHAPTER 2: LITERATURE REVIEW

Counterionic effect on surfactant aggregate structures has been attracting attention since nearly six decades ago. The specific counterion/ion effects on aqueous interfaces, occurring in almost all branches of science, are of great interest both in physical and chemical processes. Micelles and vesicles are surfactant aggregate structures/nanoparticles which have been known for more than 100 years (Menger, 1979; Razak *et al.*, 2014) and vast studies had been done to examine their physicochemical characteristics as well as organization aspect on reaction rates (Khan, 2006). In 1959, Duynstee and Grunwald, in their excellent report has highlighted the effects of micelles on the rate and equilibrium constants of chemical reactions (Duynstee & Grunwald, 1959a, 1959b). Until the mid-1960s, the kinetic data which stressed on the rates of micellar-mediated reaction was explained only qualitatively due to the absence of an acceptable kinetic micellar model based on relevant and convincing mechanisms of micellar-mediated reactions. It is noteworthy that the mechanism of a chemical reaction is crucial, hence difficult to understand. Several methods and techniques, for instance electrospray ionization mass spectrometry (Santos *et al.*, 2005) and crossover experiments had been used to diagnose the reaction mechanism. But the kinetic method is perhaps the best mechanistic tool that established the most refined mechanism at the molecular level of any reaction (Khan, 2006).

Gravsholt (1976) and Rao et. al (1987) had reported the astonishing and unpredictable discovery of viscoelastic behavior of aqueous solution containing ~2.0×10^{-4} M cetyltrimethylammonium salicylate (CTASal). Since then, a number of researches to have a better understanding on viscoelasticity and related behavior exhibited by micelle solutions can be seen from the emergence and growth of significant number of fairly recent papers (Herle *et al.*, 2008; Lin *et al.*, 2009b; Oelschlaeger *et al.*, 2010; Takeda *et al.*, 2011). Numerous numbers of reports highlighted the origin of micellar structural transition (from spherical to long linear and entangled wormlike micelles (WM)) occurs whenever counterion (X) binds to ionic micelles (Abezgauz *et al.*, 2010; Davies *et al.*, 2006; Oelschlaeger *et al.*, 2010; Penfold *et al.*, 2004; Takeda *et al.*, 2011; Vermathen *et al.*, 2002). In other words, a strong counterion (X) binding with ionic micelles has a great power in enhancing the origin of X-induced micellar structural growth. The strength of binding between counterion (X) and micelle, at a constant concentration of micelle-forming surfactant, reflects the specific concentration of counterion (X) for the beginning of the micellar growth. The moderately hydrophobic counterion (X) includes benzoate and substituted benzoate ions. In those studies (Gravsholt, 1976; Oelschlaeger *et al.*, 2010; Penfold *et al.*, 2004; Rao *et al.*, 1987; Singh *et al.*, 2009; Vermathen *et al.*, 2002), the binding of moderately hydrophobic counterion (X), such as benzoate or substituted benzoate ions to ionic micelles had been discussed only qualitatively. The quantitative measure of counterion (X) affinity to ionic micelles could be determined from the values of ion exchange constants, K_X^Y, where X and Y are the competing ions in the ionic micellar system studied. A search of literature reveals a limited number on the values of K_X^Y, which had been obtained in the presence of cationic micelles or vesicles, for Y = Br or Cl and X = moderately hydrophobic anions (Bachofer & Simonis, 1996; Gamboa *et al.*, 1989; Magid *et al.*, 1997; Scarpa *et al.*, 2000). However, the determination of K_X^Y values is very technique-dependent (Khan, 1995, 1996; Khan *et al.*, 1988; Magid *et al.*, 1997), which needs an appropriate and relevant method to be used. Several techniques used to determine the ion exchange constant are ^{1}H NMR, ion-selective electrode as well as flotation technique (Magid *et al.*, 1997). For an example, the reported values of K_X^Y for X = 2,6-Cl_2Bz^- on the CTACl micellar surface, determined by the use of ion-selective electrode, ^{1}H NMR and flotation technique are 1.3 ± 0.1, 16.2 ± 5.5 and 16.8 ± 1.0, respectively.

Since the K_X^Y value is very technique-dependent, it is difficult to get a reliable correlation between the values of K_X^Y, determined by different techniques, and X-induced micellar growth. Thus, the use of a uniform-technique for the determination of K_X^Y value is needed. In the present study, a semi-empirical kinetic (SEK) and semi-empirical spectrophotometric (SESp) methods have been used to determine the values of K_X^Y (Khan, 2010; Khan *et al.*, 2013). It is noteworthy that the determination of K_X^Y value involves the determination of the micellar binding affinity of counterions X and Y, where the X and Y ions represent the respective counterion of inert organic salt (MX) and reference counterion of ionic micelles. In the present SEK method, the values of K_X^{Br} (for Y = Br) were determined using an empirical kinetic approach that consists of the classical pseudophase micellar (Chaimovich *et al.*, 1975) model coupled with an empirical equation (**Eq. 2.1**) (Khan, 1997; Khan & Arifin, 2000; Yusof & Khan, 2010),

$$K_S = \frac{K_S^0}{1 + K_{X/S}[MX]} \qquad \textbf{Eq. 2.1}$$

where K_S and K_S^0 are the micellar binding constants of a reactive counterion S, in the presence and absence of salt, respectively. $K_{X/S}$ represents the empirical constant which measures the ability of counterion X to expel another counterion S from the cationic micellar surface to the bulk aqueous phase through the occurrence of ion exchange X^-/S^- at the cationic micellar surface. It is relevant to note that the SESp method also uses **Eq. 2.1** where the value of micellar binding constant, K_S of ionized N-2-methoxyphenylphthalamic acid (N-2-MeOPhPTH) was derived spectrophotometrically, instead of kinetically (Khan *et al.*, 2013). On the other hand, a recent study had reported the K_X^{Br} values for different counterion X, which were determined using SEK and SESp methods, appear to be almost similar for both (Khan *et al.*, 2013; Yusof & Khan, 2011, 2012).

A search on the literature reveals a very restricted number on the reported values of K_X^{Br} or R_X^{Br}, obtained in the presence of cationic micelles with X representing hydrophilic or moderately hydrophobic counterions (Bachofer & Simonis, 1996; Gamboa *et al.*, 1989; Khalid *et al.*, 2017a, 2017b; Khan *et al.*, 2013; Magid *et al.*, 1997). It is noteworthy that the K_X^{Br} or R_X^{Br} values, for moderately hydrophilic and hydrophobic counterion X, could be determined by the present SEK (Khalid *et al.*, 2016; 2017a; Razak *et al.*, 2014; Yusof & Khan, 2012; Yusof *et al.*, 2013) and SESp methods (Khan *et al.*, 2013). The use of kinetic parameter, K_X^{Br} or R_X^{Br} depends on the values of $K_{X/S}$ and $K_{Br/S}$, whether they were obtained in the presence of similar or different micellar aggregate structures. Early study had reported the values of K_X^{Br} or R_X^{Br} for X = 5-MeOSa^{2-} and 5-MeSa^{2-} on the CTABr micellar surface, determined by the use of SEK method are 89 ± 6 and 796 ± 48, respectively (Khan *et al.*, 2013; Yusof & Khan, 2012). It is important to note that the value of R_X^{Br} is higher in the presence of higher apparent hydropbobicity of the benzoate substituent attached to the benzoate ions (Fagge *et al.*, 2017). Khan and his coworkers had reported that the R_X^{Br} values, determined by the use of SESp method were found to be 100 ± 3 and 729 ± 31 for respective X = 5-MeOSa^{2-} and 5-MeSa^{2-}, which the values are not appreciably different from that obtained with SEK method (Khan *et al.*, 2013). On the other hand, the K_X^{Br} or R_X^{Br} values obtained for X = 2-; 3-; and 4-BrC$_6$H$_4$COO$^-$, under SEK and SESp methods appear to be almost similar for both (Khan *et al.*, 2013).

Lin et al. (1994) had reported the effects of 3-, 4-, and 5-methylsalicylic acid (3-, 4-, and 5-MeSaH) as well as 3-, and 4-hydroxybenzoic acid (3-, and 4-HOBzH) concentration on cetyltrimetylammonium bromide (CTABr) micellar growth by the use of cryo-TEM while the presence of wormlike micelles (WM) had been detected using rheological measurements on mixed 5-MeSaH-CTABr aqueous solutions. It is proven from this and a few related studies (Manohar *et al.*, 1986; Rao *et al.*, 1987; Shikata *et al.*,

1989) that: (a) for 3-, 4-, and 5-MeSaH, the micellar transition from spherical micelles-to-wormlike micelles occurs at about the same C_A/C_D ratio where C_A and C_D represent the concentration of counterionic acid (MeSaH) and surfactant/detergent (CTABr), respectively and (b) sodium salicylate (SaNa) and salicylic acid (Ono *et al.*, 2005) are about equally effective in driving the micellar structural transition compared to 3-, and 4-hydroxybenzoic acid (3-, and 4-HOBzH). A deep discussion has been made on such observations in terms of widely accepted view of relative cationic micellar binding affinity of counterions which is derived based upon qualitative observations (Brianáborak, 2010; Gaidamauskas *et al.*, 2010; Oelschlaeger *et al.*, 2010; Singh *et al.*, 2009; Sreejith *et al.*, 2010; Takeda *et al.*, 2011; Vermathen *et al.*, 2002). Some of these observations correlate quantitatively with the reported values of R_X^{Br} for X = $2\text{-}^{-}OC_6H_4CO_2^{-}$ (R_X^{Br} = 44) (Khan *et al.*, 2010), and X = 3- and $4\text{-}^{-}OC_6H_4CO_2^{-}$ (K_X^{Br} = 4.9 and 2.7 for respective X = 3- and $4\text{-}^{-}OC_6H_4CO_2^{-}$) (Khan *et al.*, 2010).

The effects of 3-, 4-, and 5-MeSaH on CTABr micellar growth should be similar, according to the concept of molecular critical packing parameter (CPP) in surfactant self-assembly (Israelachvili *et al.*, 1976; Mitchell & Ninham, 1981; Nagarajan, 2002). This concept is used to describe the shape of a molecule, which takes into account the volume and chain length of the hydrophobic chain as well as cross sectional area per molecule at the aggregate surface. This prediction is consistent with the cryo-TEM results reported by Lin and his coworkers (Lin *et al.*, 1994). However, it appears that the rheological data obtained for aqueous CTABr-MX (with MX = 5-Me-, and 5-MeOSaNa_2) systems (Yusof & Khan, 2012) as well as CPCl-MX (with CPCl and MX represent respective cetylpyridinium chloride and 2-, 3-, and 4-MeBzH) systems (Rehage & Hoffmann, 1991) are incompatible with the prediction of CPP. On the other hand, Zheng et al. used cryo-TEM to deduce the presence of vesicles in the mixtures of 5 mM CTACl and 5 mM 3-MeSaNa (Zheng *et al.*, 2000). Yusof and Khan (2012), in their report could not detect the presence of WM in the micellar growth from spherical micelles (SM)-to-vesicles in the mixtures of 5-MeSaNa_2 and CTABr at 35 °C. However, Davies et al. had detected the presence of WM in the micellar growth from SM-to-vesicles in the aqueous mixture of 5-MeSaH and CTABr at 25 °C and within [5-MeSaH]/[CTABr] range between 0.4 to 2.0 at a constant 12.5 mM CTABr (Davies *et al.*, 2006). Thus, it can be concluded that the appearance of WM in such studies could be attributed to the change in the temperature (from 25 to 35 °C), as well as the nature of the counterions (from 5-$MeSa^{2-}$ to 5-$MeSa^{-}$).

Recent studies had reported the effects of salicylate, $^{-}OC_6H_4COO^{-}$ (Fagge *et al.*, 2016) and 4-chlorobenzoate, 4-$ClC_6H_4COO^{-}$ (Fagge *et al.*, 2018a) ions concentration on CTABr and mixed CTABr-$C_{16}E_{20}$ (cationic–nonionic) micelle, where $C_{16}E_{20}$ represents poly(ethylene glycol hexadecyl ether). In both studies, the micellar binding constants of counterions X and Br, R_X^{Br} as well as X-induced micellar structural growth were investigated. The value of R_X^{Br} for aqueous CTABr/MX solution (for X = $^{-}OC_6H_4COO^{-}$ and 4-$ClC_6H_4COO^{-}$) were found to be ~42 (Fagge *et al.*, 2016) and 50.3 (Fagge *et al.*, 2018a), respectively, where the rheological observations clearly demonstrate the presence of WM in the micellar system. The R_X^{Br} value decrease to 16 (Fagge *et al.*, 2016) and 21.7 (Fagge *et al.*, 2018a) in the presence of different amounts of $C_{16}E_{20}$ mixed with a constant concentration of CTABr for X = respective $^{-}OC_6H_4COO^{-}$ and 4-$ClC_6H_4COO^{-}$, which reveals the presence of only SM in the aqueous CTABr–$C_{16}E_{20}$/MX solution mixture.

Apart from this, Kreke et al. (Kreke *et al.*, 1996; Yusof *et al.*, 2013) had conducted experiments using ^{1}H and ^{13}C NMR to show that 2,6-$Cl_2C_6H_3CO_2^{-}$ (2,6-Cl_2Bz^{-}) and 3,5-Cl_2Bz^{-} counterions were intercalated within the cationic micellar headgroups and that 3,5-Cl_2Bz^{-} counterions inserted further into the interface of rodlike micelles while 2,6-Cl_2Bz^{-} counterions remained at the surface of the spherical micelles (Kreke *et al.*, 1996; Yusof *et al.*, 2013). Cryo-TEM images, small angle neutron scattering (SANS) and rheological measurements are the well known techniques which have been used to study the micelle formation and growth of aqueous CTAX solutions (X = 2-ClBz$^-$, 4-ClBz$^-$, 2,6-ClBz$^-$, 3,4-ClBz$^-$ and 3,5-ClBz$^-$) (Carver *et al.*, 1996). Meanwhile, the surfactants CTA2-ClBz$^-$ and CTA2,6-Cl$_2$Bz form Newtonian fluids containing spherical micelles at $\leq$ 0.07 M CTAX, whereas CTAX (with X = 4-ClBz$^-$, 3,4- and 3,5-Cl$_2$Bz$^-$) form highly viscoelastic aqueous solutions at ~0.002 – 0.035 M CTAX and SANS data turns out to be same for all three CTAX (X = 4-ClBz$^-$, 3,4- and 3,5-Cl$_2$Bz$^-$) at the same concentration of CTAX (Carver *et al.*, 1996; Yusof *et al.*, 2013). A fairly recent study had reported the quantitative correlation between counterion (X) binding to cationic micelles and X-induced micellar growth for different moderately hydrophobic X, where X represents 2,4-; 2,5-; 2,6-, and 3,4- Cl$_2$Bz$^-$ (Yusof *et al.*, 2013). On the other hand, a recent paper had also reported the quantitative correlation of those ions, as well as 3,5-Cl$_2$Bz$^-$ binding affinity to cationic micelles and the probable effect of temperature on the aggregate CTAX structural transitions (Razak *et al.*, 2016). In both studies, they asserted the presence of only WM in aqueous CTAX solution of X = 2,4-, 2,5-, and 3,4-Cl$_2$Bz$^-$, as well as the presence of the mixture of WM and vesicles in aqueous CTAX solution (for X = 3,5-Cl$_2$Bz$^-$) (Razak & Khan, 2013; Yusof *et al.*, 2013). A recent study by Fagge and his coworkers had reported the presence of wormlike/twisted micelles and vesicle at various concentration of 3,5-Cl$_2$Bz$^-$ and a contant CTABr concentration by rheological measurements at 25 and 35°C, where the average R_X^{Br} value for CTABr/MX (X = 3,5-Cl$_2$Bz$^-$) was found to be 198 (Fagge *et al.*, 2018b).

Even though a vast research study had been made upon CTABr aggregate structural transitions, a great attention, also has been put towards the effects of dialkyl chain cationic surfactants concentrations on such surfactant aggregate structural transitions (Grillo *et al.*, 2008; Junquera *et al.*, 2004; Kaur *et al.*, 2012; Marques *et al.*, 1999; Ono *et al.*, 2005). However, studies on the kinetics and mechanism of didodecyldimetylamonium bromide

(DDABr) micellar-catalyzed reactions is rare (Brinchi *et al.*, 2007; Kunitake *et al.*, 1980). Detailed kinetic studies reported by Brinchi et al. and Kunitake et al., assert the presence of respective premicellar aggregates and ammonium bilayer membranes, under essentially similar experimental kinetic conditions. On the other hand, Grillo et al. had reported that the DDABr/H_2O system shows the aqueous DDABr aggregate structural transitions as: globular prolate micelles (WM)-very small vesicles (SVs)-large multilamellar vesicles (MLV) (Grillo *et al.*, 2008). It has been concluded elsewhere that the value of $K_{Br/S}$, obtained in the presence of aqueous cationic CTABr spherical micelles is 25 M^{-1} at 35 °C for S = PSa^- (Khan *et al.*, 2000). However, such value for aqueous cationic DDABr micelles, under the same condition is unknown. Thus, it would be necessary to determine the value of $K_{Br/S}$ (for S = PSa^-) in the presence of aqueous cationic DDABr aggregates at 35 °C.

CHAPTER 3: MATERIALS AND EXPERIMENTAL METHODS

3.1 Micelle

The probe molecules used in SEK and SESp techniques were respective (i) phenyl salicylate (PSaH) from Fluka with ≥ 98 % purity, and (ii) N-(2-methoxyphenyl)phthalamic acid (N-2-MeOPhPTH) which was synthesized as described in the early report (Leng *et al.*, 2004). Other materials used in this study were obtained from Aldrich, Merck and Fluka which are also of highest available purity (≥ 98 % purity). The materials used are as follows: (a) sodium hydroxide (NaOH), (b) piperidine (Pip), (c) cetyltrimethylammonium bromide (CTABr) and (d) didodecyldimethylammonium bromide (DDABr), (e) sodium bromide (NaBr) and (f) inert organic acids/organic salts which are listed in **Table 3.1**. The chemical structures of compounds used are shown in **Figure 3.1**.

Table 3.1: List of Inert Organic Acids/Organic Salts Used in the Study.

Chemical	Manufacturer	Purity
4-methoxysalicylic acid (4-MeOSaH)	Aldrich	99 %
3-methylsalicylic acid (3-MeSaH)	Aldrich	97 %
4-methylsalicylic acid (4-MeSaH)	Aldrich	99 %
2,3-dichlorobenzoic acid (2,3-$Cl_2BzCOOH$)	Aldrich	97 %
2,4-dichlorobenzoic acid (2,4-$Cl_2BzCOOH$)	Aldrich	98 %
2,5-dichlorobenzoic acid (2,5-$Cl_2BzCOOH$)	Aldrich	97 %
2,6-dichlorobenzoic acid (2,6-$Cl_2BzCOOH$)	Merck	≥ 98 %
3,4-dichlorobenzoic acid (3,4-$Cl_2BzCOOH$)	Aldrich	99 %
3,5-dichlorobenzoic acid (3,5-$Cl_2BzCOOH$)	Aldrich	97 %
Sodium acetate (CH_3COONa)	Fisher Scientific	99 %
Sodium propanoate (C_2H_5COONa)	Merck	≥ 99 %
Sodium butanoate (C_3H_7COONa)	Merck	≥ 98 %
Pentanoic acid (C_4H_9COOH)	Sigma-Aldrich	> 99 %
Heptanoic acid ($C_6H_{13}COOH$)	Sigma-Aldrich	97 %
Octanoic acid ($C_7H_{15}COOH$)	Aldrich	≥ 98 %

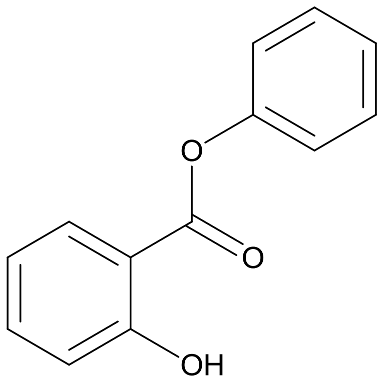

phenyl salicylate

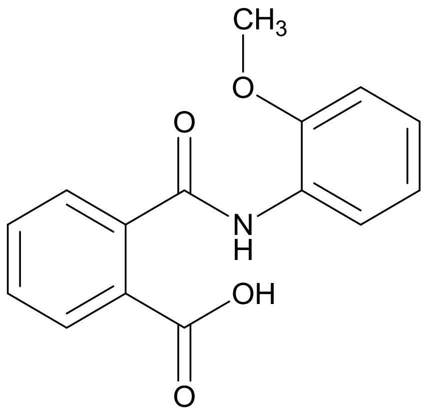

N-(2-methoxyphenyl)phthalamic acid

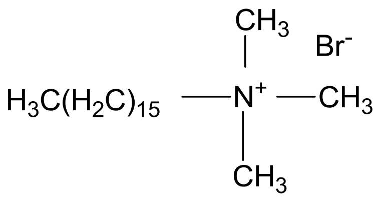

$H_3C(H_2C)_{15}-N^+(CH_3)_3\ Br^-$

cetyltrimethylammonium bromide

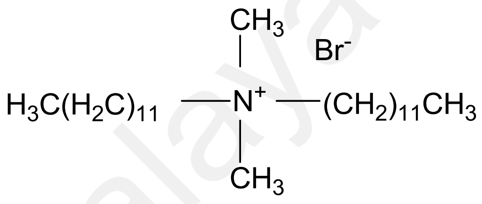

$H_3C(H_2C)_{11}-N^+(CH_3)_2-(CH_2)_{11}CH_3\ Br^-$

didodecyldimethylammonium bromide

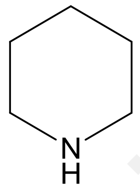

piperidine

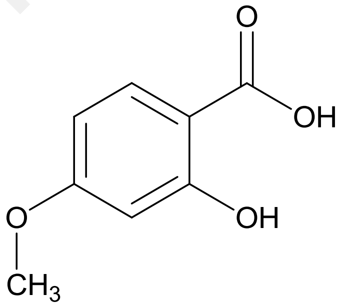

4-methoxysalicylic acid

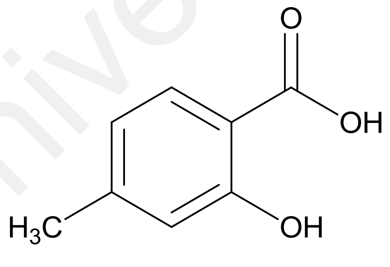

4-methylsalicylic acid

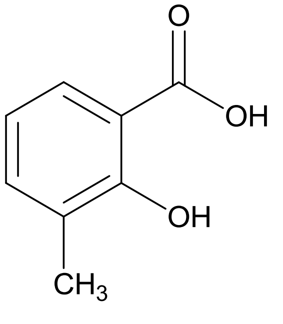

3-methylsalicylic acid

Figure 3.1: Chemical structures of compounds used in this study.

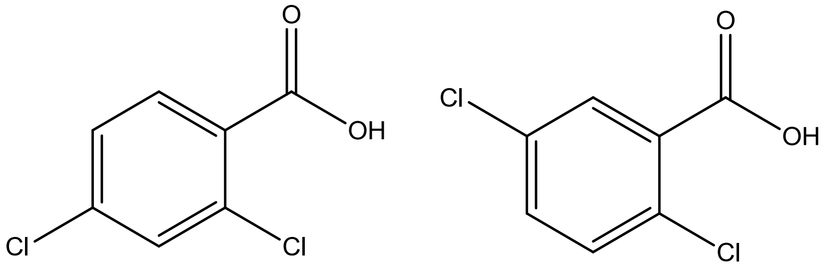

2,4-dichlorobenzoic acid 2,5-dichlorobenzoic acid

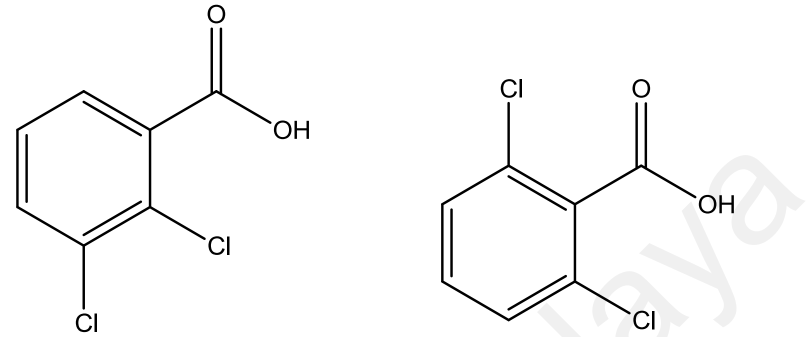

2,3-dichlorobenzoic acid 2,6-dichlorobenzoic acid

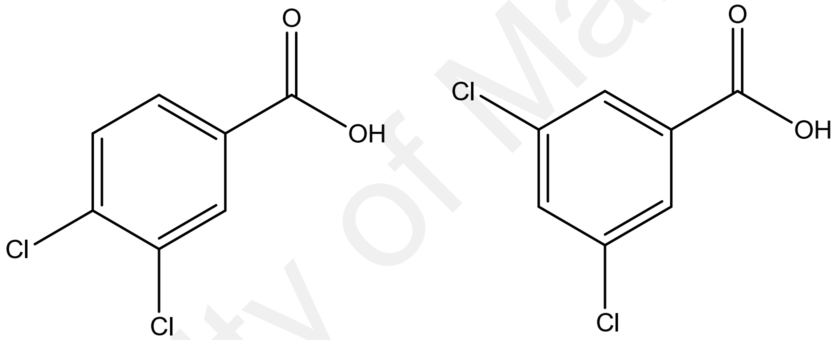

3,4-dichlorobenzoic acid 3,5-dichlorobenzoic acid

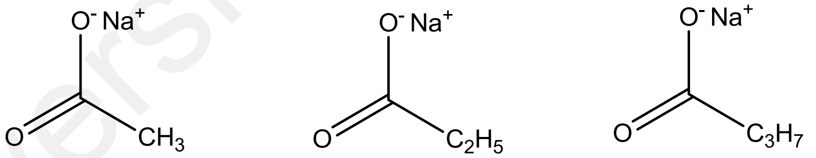

sodium acetate sodium propanoate sodium butanoate

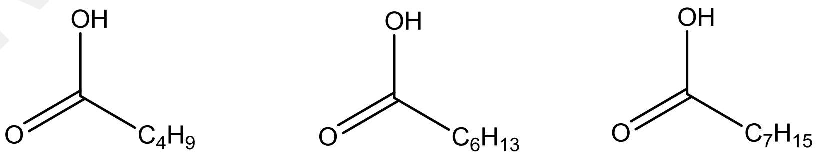

pentanoic acid heptanoic acid octanoic acid

Figure 3.1, continued

The stock solutions of organic salts ($M_\nu X$) with $\nu = 1$ or 2 (subscript ν represents ionization number of counterion X) were prepared by adding respective 0.52 – 0.55 M, 1.05 M and 1.25 M NaOH to the corresponding 0.5 M solutions of each organic acid. However, stock solutions' preparation of some organic salts used in the study showed the presence of impurities. Thus, recrystallizations of their organic acids were carried out using distilled water as recrystallizing solvents. The stock solutions of PSaH as well as N-2-MeOPhPTH were prepared in acetonitrile.

3.2 Experimental Methods

This study contains two parts of experimental work, which focuses on the use of UV-spectrophotometer (for spectrophotometric study) and Anton Paar MCR301 rheometer (for rheological study). The main part was the spectrophotometric work which consists of:

(i) the effects of $[M_vX]$ on the pseudo-first-order rate constants (k_{obs}) for the nucleophilic reaction between anionic phenyl salicylate (PSa^-) and Pip, where the disappearance of PSa^- at different time, t was monitored spectrophotometrically as well as

(ii) the effects of $[M_vX]$ on the initial absorbance (A_{ob}) of anionic N-(2-methoxyphenyl)phthalamic acid (N-2-MeOPhPT$^-$).

The rheological part was carried out at a constant temperature within its range 35 – 55 °C, which gave indication on the structure of micelles, although indirectly. The results obtained from rheological and spectrophotometric measurements were used to correlate to each other, thus give a better understanding on the counterion and temperature induced micellar growth.

3.2.1 Kinetic Measurements

The kinetic measurements for the nucleophilic substitution reaction between Pip and PSa^- were carried out at a constant temperatures using Shimadzu UV-Visible Spectrophotometer Double Beam Model UV-1601 along with its electronically temperature controlled cell compartment. The wavelength for each set of organic salts used was chosen and fixed at a certain typical value, where the largest difference of absorbance with variable time was obtained in the plots of A_{ob} versus wavelengths. For each kinetic run, the aqueous solution contains all the chemical ingredients (4.9 mL) except the probe molecule or substrate (i.e. PSaH), which was then equilibrated in water bath at a constant temperature, i.e. 35 °C for at least 15 minutes. An appropriate amount of substrate (0.1 mL) was injected to the equilibrated solution mixture. The mixture was then swirled gently and transferred carefully to quartz cuvette which was then placed in the UV's cell compartment as fast as possible. For highly viscous solution, the swirl time was longer so that the substrates could mix uniformly throughout the reaction mixture. The same procedures were repeated for a few set of kinetic runs at 40, 45, and 55 °C. The reaction period was carried out for more than ~8 half-lives.

3.2.1.1 Derivation of Kinetic Equation of First-Order Reaction

In the present study, the kinetic measurements were carried out under pseudo-first-order reaction condition where the concentration of Pip ($[Pip]_T$) was fixed at 500 times larger than the concentration of PSaH ($[PSaH]_T$). The reaction step of this reaction is described as below,

$$R \xrightarrow{k_{obs}} P \qquad \textbf{Eq. 3.1}$$

where R and P represent reactant and product, respectively and k_{obs} is the pseudo-first-order rate constant for the reaction (i.e. $k_{obs} = k_n[Pip]$ with k_n representing nucleophilic second-order rate constant). The rate law for this reaction is expressed as,

$$\text{Rate} = \frac{-\,d[R]}{dt} = \frac{-\,d[Pip]}{dt} = \frac{+\,d[P]}{dt} = k_{obs}[R]$$

Eq. 3.2

or

$$\text{Rate} = \frac{-\,d[R]}{dt} = k_{obs}[R] \qquad \textbf{Eq. 3.3}$$

The integration of **Eq. 3.3** will give the following **Eq. 3.4**,

$$[\mathrm{R}] = [\mathrm{R_0}]\exp(-\mathrm{k_{obs}t}) \qquad \textbf{Eq. 3.4}$$

where $[R_0]$ is the initial concentration of R and [R] is the concentration of R at any reaction time, t. According to Beer-Lambert law,

$$\mathrm{A_{ob}} = \delta\ell[\mathrm{C}] \qquad \textbf{Eq. 3.5}$$

where A_{ob} is the absorbance value, δ is the molar absorptivity/molar extension coefficient, ℓ is path length of cuvette which in this case is equal to 1 cm and [C] is molar concentration. In this study, the observed absorbance was reflected due to reaction mixture of both reactant and product, thus,

$$\mathrm{A_{ob}} = \mathrm{A^R_{ob}} + \mathrm{A^P_{ob}} \qquad \textbf{Eq. 3.6}$$

By applying **Eq. 3.5** into **Eq. 3.6**,

$$\mathrm{A_{ob}} = \delta_\mathrm{R}[\mathrm{R}] + \delta_\mathrm{P}[\mathrm{P}] \qquad \textbf{Eq. 3.7}$$

where δ_R and δ_P represent molar extension coefficient of respective reactant and product. From **Eq. 3.2**,

$$[\mathrm{R_0}] = [\mathrm{R}] + [\mathrm{P}] \qquad \textbf{Eq. 3.8}$$

Thus,

$$[\mathrm{P}] = [\mathrm{R_0}] - [\mathrm{R}] \qquad \textbf{Eq. 3.9}$$

By substituting **Eq. 3.9** into **Eq. 3.7**, thus will give the following equation,

$$\mathrm{A_{ob}} = \delta_\mathrm{R}[\mathrm{R}] + \delta_\mathrm{P}([\mathrm{R_0}] - [\mathrm{R}]) \qquad \textbf{Eq. 3.10}$$

By rearranging **Eq. 3.10**, A_{ob} is equal to,

$$\mathrm{A_{ob}} = (\delta_\mathrm{R} - \delta_\mathrm{P})[\mathrm{R}] + \delta_\mathrm{P}[\mathrm{R_0}] \qquad \textbf{Eq. 3.11}$$

where under the experimental conditions of the present study, $(\delta_\mathrm{R} - \delta_\mathrm{P}) = \delta_\mathrm{ap}$ where as $\delta_\mathrm{P}[\mathrm{R_0}] = \mathrm{A_\infty}$ with δ_{ap} is apparent molar extension coefficient and A_∞ is the absorbance value at t = ∞. Thus,

$$\mathrm{A_{ob}} = \delta_\mathrm{ap}[\mathrm{R}] + \mathrm{A_\infty} \qquad \textbf{Eq. 3.12}$$

Finally, the substitution of **Eq. 3.4** into **Eq. 3.12** will results in,

$$A_{ob} = [R_0]\delta_{ap}\exp(-k_{obs}t) + A_\infty \qquad \textbf{Eq. 3.13}$$

Under the conditions of the experimental study, it is evident that the values of A_{ob} at different t were found to fit well to **Eq. 3.13** under the limit of uncertainty. Therefore, **Eq. 3.13** has been used to find the values of unknown parameters i.e. k_{obs}, δ_{ap} and A_∞ for each kinetic run. If the reaction reveals the product appearance as a function of t, then following **Eq. 3.14** has been used.

$$A_{ob} = [R_0]\delta_{ap}[1 - \exp(-k_{obs}t) + A_0 \qquad \textbf{Eq. 3.14}$$

3.2.2 Spectrophotometric Measurements for SESp Method

In this technique, the experimental procedures were almost the same as in kinetic measurements. The probe molecule used was N-2-MeOPhPTH, where the effects of the concentration of inert salt, $[M_vX]$ on A_{ob} of aqueous samples were monitored spectrophotometrically at a fixed wavelength, 310 nm and 35 °C. It is noteworthy that some substituted benzoate ions show significant absorption at wavelengths < 310 nm (Khan *et al.*, 2013). For each spectrophotometric run, the aqueous solution contains all the chemical ingredients (4.9 mL) except the substrate (i.e. N-2-MeOPhPTH), which was then equilibrated in water bath at a constant temperature, i.e. 35 °C for at least 15 minutes. An appropriate amount of substrate (0.1 mL) was injected to the equilibrated solution mixture. The mixture was then swirled gently and transferred carefully to quartz cuvette which was then placed in the UV's cell compartment and the value of A_{ob} was recorded at 310 nm. It is noteworthy that the alkaline hydrolysis (1 %) of N-2-MeOPhPTH, under the present conditions, requires > 465 days (Khan *et al.*, 2013). The same procedures were carried out in order to measure the turbidity of the surfactant solution, except that the wavelength used for this measurement was 600 nm (visible region).

3.2.3 Rheological Measurements

A series of rheological measurements has been carried out to find their probable characteristic behavior and viscosity under steady and dynamic shear flow at 15 mM CTABr and constant temperatures. The rheometer used was Anton Paar MCR301 with double gap cylinder, DG26.7/T200/SS measuring system. In rheological measurement, the samples' preparation was similar to that in kinetic measurement, where the substrate was injected into the aqueous solution containing all the chemical ingredients of desired amount of concentrations (except the probe molecule), when a constant desired temperature was achieved. However, the volumes of each ingredient were doubled resulting in the total volume of 10 mL of the solution mixture. The sample solution was left in the measuring cylinder until the desired temperature has been achieved (controlled by Peltier temperature control unit). For rotational measurement, two tests have been carried out which are flow test and step rate test. In start-up flow measurement, a total time of ~300 s with constant shear rate in the range 0.01 – 5 s^{-1} was applied for a sample with the highest viscosity value. This sample at this specific concentration of M_vX was chosen due to its high sensitivity towards the conditions of solution mixture. Thus, this sample has been set up as a reference to find out the best relaxation time for each sample. In steady shear flow measurement, a wide range of shear rate range from 0.01 – 1000 s^{-1} has been applied in order to get the viscosity values by set up the logarithmic preset for the flow test profile. Longer time has been given at lower shear rate than at the higher one, beginning at t = 100 s and ending at t = 10 s. The test was repeated for different temperatures i.e. at 40, 45, and 55 °C. Amplitude and frequency sweep experiments have also been carried out within the linear viscoelastic regime (LVER). A new sample was used for every repeat measurement.

CHAPTER 4: RESULTS AND DISCUSSION

This chapter is divided into two parts, which focus on:

i) the determination of kinetic parameters (such as K_S, K_S^0, R_X^{Br}) using the SEK or SESp technique, and

ii) the determination of rheological behavior of aqueous system containing CTABr or DDABr micelles.

In SEK and SESp method, the effects of $[M_vX]$ on the absorbance values was monitored spectrophotometrically. In SEK method, the rate of a chemical reaction is monitored by observing the absorbance values of a sample solution at a certain typical wavelength, by time. Although there are several any other techniques that can be used to study the kinetic, perhaps the most easy and effective one is by spectrophotometric study, using UV-spectrophotometer. In SEK method, the primary data (absorbance value) obtained from the spectrophotometric study, are required for the determination of a secondary data (k_{obs}), while in SESp technique, only the primary data are required. Therefore, the absorbance values of a sample, at different values of wavelength were obtained.

In SEK method, the effects of inert organic salt concentration, $[M_vX]$ (with v = 1 or 2) on k_{obs} for the piperidinolysis of PSa^- in the absence/presence of CTABr micelle have been studied. However, such studies on the system containing DDABr micelles have not been carried out. The reported value of K_S^0 (for S representing PSa^-) to CTABr micelles, in the presence of spherical micelles, is 7000 M^{-1} (Khan, 2010). But, K_S^0 value (for S representing PSa^-) to DDABr micelles is unknown. Thus, this value was explored in the present study.

In SESp method, the effects of $[M_vX]$ (with v = 1) on the initial absorbance, A_{ob} value of aqueous CTABr micellar solution mixture, which contains a constant desired concentration of probe (N-2-MeOPhPT$^-$), NaOH, CTABr and M_vX have been studied. In this method, the probe used was different compared to that in SEK method. As a result, the value of K_S^0 (for S representing N-2-MeOPhPT$^-$) to CTABr micelles would be different as well. This value of K_S^0 has been evaluated in the present study.

It is evident from the present study, as well as few related studies (Khan, 1989, 1997, 2006; Khan & Ahmad, 2001a; Khan *et al.*, 1997, 2002, 2010; Khan & Ismail, 2009; Yusof & Khan, 2010) that: (a) the nucleophilic substitution reaction between piperidine (Pip) and anionic phenyl salicylate (PSa$^-$) results in the formation of N-piperidinylsalicylate and phenol. (b) the concentrations of protonated Pip, [PipH$^+$] is very low compared to the concentration of nonprotonated Pip, [Pip] (i.e. [PipH$^+$] << [Pip]). Thus, $[Pip]_T = [Pip] + [PipH^+] \approx [Pip]$ and is evident from the observed value of rate constant (k_{obs}) exhibited by **Table 4.1, S1** and **S2** (see Appendix A - **Table S1** and **S2**). (c) the concentrations of nonionized phenyl salicylate (PSaH) was almost zero. This is also evident from the initial values of absorbance (A_0), where its value is found to be independent of $[CTABr]_T$ as well as [HO$^-$] in the present study (Yusof, 2011). It is also proven from a few related studies that the PSa$^-$ absorbs strongly rather than PSaH which does not show any detectable absorption at wavelength 365 and 370 nm in the present study. (d) the rate of hydrolysis of PSa$^-$ is negligible compared to the rate of piperidinolysis of PSa$^-$ under the experimental conditions of the present study.

It is well known that the presence of micelles (CTABr or DDABr) under the reaction conditions of the present study has no effect on the formation of products as well as the mechanism of the reaction. However, it certainly affects the values of k_{obs} of the present study (Khan & Fagge, 2018). The k_{obs} values, in the presence of CTABr or DDABr micelles in the aqueous reaction mixtures has been found to decrease by ~10-fold as compared to the values of k_{obs} for the reaction in the absence of CTABr or DDABr micelles. Thus, the micelles act as a medium inhibitor under such reaction conditions of the present study. In view of these observations, the reaction between Pip and PSa^- under the present experimental conditions are represented by **Figure 4.1**,

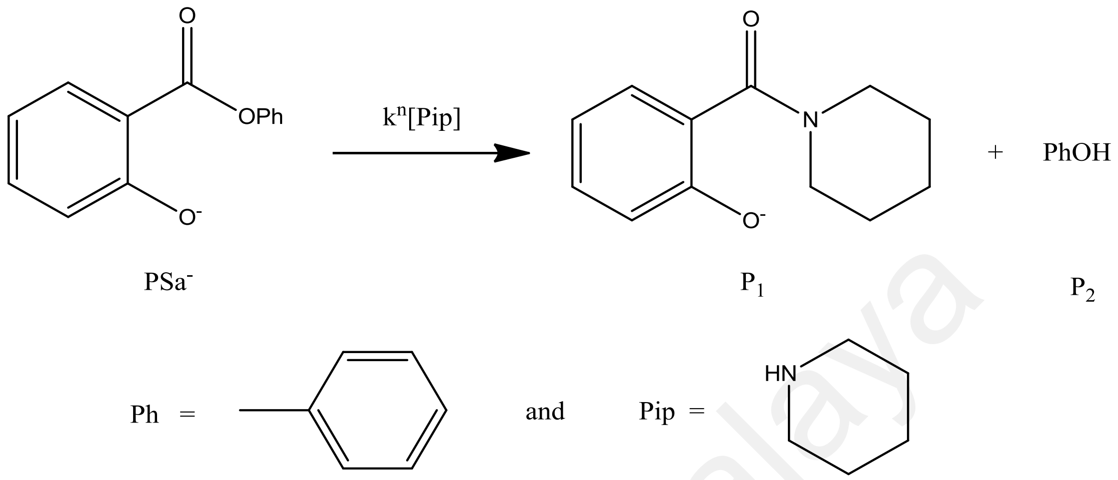

Figure 4.1: The reaction between PSa^- and Pip in the presence of CTABr or DDABr micelles.

where k^n represents nucleophilic second-order rate constant and $k_{obs} = k^n[Pip]_T$, with $k^n = k[PSa^-]$, where k represents pseudo-first-order rate constant, and $[Pip]_T$ representing total concentration of Pip.

Table 4.1: Values of the Kinetic Parameters, k_{obs}, δ_{ap}, and A_∞, Calculated from **Eq. 3.13** for the Piperidinoloysis of PSa^- with $M_\nu X$ = 4-MeO-, 3-Me- and 4-MeSaNa$_\nu$ ($\nu = 2$), in the Absence of CTABr Micelles at 35 °C.[a]

$M_\nu X$[b]	4-MeOSaNa$_\nu$			3-MeSaNa$_\nu$			4-MeSaNa$_\nu$		
$[M_\nu X]$ (mM)	10^3 k_{obs}[c] (s^{-1})	δ_{ap}[c] ($M^{-1}cm^{-1}$)	10^2 A_∞[c]	10^3 k_{obs}[c] (s^{-1})	δ_{ap}[c] ($M^{-1}cm^{-1}$)	10^2 A_∞[c]	10^3 k_{obs}[c] (s^{-1})	δ_{ap}[c] ($M^{-1}cm^{-1}$)	10^2 A_∞[c]
0	30.5 ± 0.2[d]	2570 ± 9[d]	0.0 ± 0.1[d]	30.9 ± 0.2[d]	1734 ± 5[d]	0.16 ± 0.05[d]	31.2 ± 0.2[d]	1690 ± 5[d]	-0.1 ± 0.1[d]
2	30.6 ± 0.1	2553 ± 5	0.3 ± 0.1						
5	31.0 ± 0.2	2559 ± 6	0.4 ± 0.1	31.4 ± 0.1	1723 ± 4	1.25 ± 0.04	31.9 ± 0.2	1733 ± 5	0.2 ± 0.1
7	30.9 ± 0.2	2588 ± 7	0.4 ± 0.1						
10	30.7 ± 0.2	2588 ± 8	0.4 ± 0.1	31.3 ± 0.1	1746 ± 4	1.85 ± 0.04	32.7 ± 0.2	1739 ± 4	0.6 ± 0.1
15	30.3 ± 0.2	2621 ± 7	1.6 ± 0.1						
20	30.8 ± 0.2	2588 ± 8	1.0 ± 0.1	30.4 ± 0.1	1723 ± 4	3.46 ± 0.04	32.1 ± 0.2	1756 ± 6	1.1 ± 0.1
30	29.8 ± 0.2	2603 ± 8	1.2 ± 0.1	30.8 ± 0.1	1718 ± 4	5.17 ± 0.03	31.5 ± 0.2	1737 ± 5	1.8 ± 0.1
40	30.8 ± 0.1	2608 ± 6	1.6 ± 0.1	31.1 ± 0.1	1711 ± 4	7.07 ± 0.05	32.1 ± 0.3	1729 ± 7	2.6 ± 0.1
50	30.1 ± 0.1	2596 ± 6	1.6 ± 0.1	31.1 ± 0.1	1716 ± 4	8.96 ± 0.04	31.6 ± 0.2	1721 ± 5	3.2 ± 0.1
60	30.5 ± 0.2	2594 ± 6	1.9 ± 0.1	30.4 ± 0.2	1724 ± 6	11.0 ± 0.06	31.2 ± 0.2	1724 ± 5	4.0 ± 0.1
70	29.9 ± 0.2	2606 ± 6	2.1 ± 0.1	29.8 ± 0.1	1716 ± 3	13.1 ± 0.03	30.8 ± 0.2	1726 ± 6	4.7 ± 0.1
80	29.8 ± 0.2	2593 ± 8	2.7 ± 0.1	29.4 ± 0.1	1733 ± 4	15.5 ± 0.04	30.5 ± 0.2	1697 ± 5	6.0 ± 0.1
90	29.0 ± 0.2	2607 ± 7	2.7 ± 0.1	29.7 ± 0.1	1716 ± 5	17.7 ± 0.05	29.8 ± 0.2	1695 ± 4	6.0 ± 0.1
100	29.4 ± 0.1	2599 ± 6	3.3 ± 0.1	29.2 ± 0.2	1714 ± 5	19.9 ± 0.05	29.7 ± 0.1	1710 ± 4	6.8 ± 0.1
150				28.0 ± 0.2	1728 ± 5	32.0 ± 0.05			
200				27.7 ± 0.2	1720 ± 5	45.0 ± 0.05	27.4 ± 0.2	1697 ± 5	15.1 ± 0.1
300				25.2 ± 0.3	1701 ± 10	73.1 ± 0.12	26.3 ± 0.2	1718 ± 6	25.8 ± 0.1

[a] $[PSa^-]_0$ = 0.2 mM, 30 mM NaOH, 100 mM Pip and λ = 370 nm for $M_\nu X$ = 3-Me- and 4-MeSaNa$_\nu$; λ = 365 nm for $M_\nu X$ = 4-MeOSaNa$_\nu$ at 35 °C, and aqueous reaction mixture for each kinetic run contains 2 % v/v CH_3CN. [b] MvX = 3-Me-; 4-Me- and 4-MeOSaNa$_\nu$ with $\nu = 2$. [c] Calculated using **Eq. 3.13** by the use of observed data (A_{ob} versus reaction time) obtained from kinetic runs. [d] Error limits are standard deviations.

4.1 The Use of SEK or SESp Technique for the Determination of R_X^{Br} Values in the Presence of CTABr or DDABr Micelles

4.1.1 Determination of R_X^{Br} Value by SEK Technique

4.1.1.1 Effects of [M_vX] (ν = 1, 2) with M_vX = 4-MeO- and 3-Me-, 4-MeSaNa$_v$ on k_{obs} for the Piperidinoloysis of PSa$^-$ in the Absence of CTABr Micelles at 35 °C

In SEK method, the determination of the effects of [M_vX] on k_{obs} in the absence of cationic micelles is needed. In order to find out the probable kinetic salt/ionic strength effect of inert salts, M_vX on k_{obs} (k_{obs} represents rate of piperidinoloysis of PSa$^-$), a series of kinetic runs was carried out at 35 °C for the reaction mixture containing constant concentrations of 0.2 mM PSaH, 30 mM NaOH, 100 mM Pip and [M_vX] range between 0.0 – 300 mM. The [NaOH] value was varied within its range 30 - < 40 mM. The values of kinetic parameters k_{obs}, δ_{ap} and A_∞ are shown in **Table 4.1** for M_vX = 4-MeO- and 3-Me-, 4-MeSaNa$_v$ (ν = 2) and **Table S1 and S2** (see Appendix A - **Table S1 and S2**) for respective M_vX (ν = 1 and 2). The least-squares calculated values of k_{obs}, δ_{ap} and A_∞ at different values of [M_vX], (M_vX = 4-MeO- and 3-Me-, 4-MeSaNa$_v$ (ν = 1, 2)) reveal the following observations: (a) The effect of salt was insignificant for M_vX = 4-MeO-, 3-Me-, and 4-MeSaNa$_v$ (ν = 2) but the calculated value of k_{obs} at 100 mM M_vX is lowered by 3.6 – 5.5 % than the corresponding calculated values of k_{obs} at zero concentration of M_vX (**Table 4.1**). However, the effect of salt M_vX = 3-Me-, and 4-MeSaNa$_v$ (ν = 2) beyond this concentration range (i.e. > 100 mM M_vX) show a mild negative salt effect (**Table 4.1**). Similar results were obtained for the system containing M_vX = 4-MeO- and 4-MeSaNa$_v$ (ν = 2). However, slightly mild negative salt effect was detected for the system containing M_vX = 4-MeO- and 3-Me-, 4-MeSaNa$_v$ (ν = 1). (b) The values of δ_{ap} remain unchanged with the increase of [M_vX] from 0.0 – 0.30 M for M_vX = 4-MeOSaNa$_v$ (δ_{ap}^{avg} = 2736 ± 20 and 2592 ± 19, 2755 ± 25 for respective ν = 1 and 2 at λ = 365 nm) as well as from 0.0 – 0.30 M for M_vX = 4-MeSaNa$_v$ (δ_{ap}^{avg} = 1813 ± 34 and 1719 ± 19, 1723 ± 26 for respective $\nu = 1$ and 2 at $\lambda = 370$ nm) and $M_\nu X$ = 3-MeSaNa$_\nu$ (δ_{ap}^{avg} = 1782 ± 24 and 1722 ± 11 for respective $\nu = 1$ and 2 at $\lambda = 370$ nm), where δ_{ap}^{avg} corresponds to the mean value of δ_{ap}. (c) The A_∞ values of $M_\nu X$ = 4-MeOSaNa$_\nu$ ($\nu = 1$ and 2) increase from 0.0 – 0.054 and 0.0 – 0.033, 0.028 – 0.133, respectively at 365 nm with the increase in [4-MeOSaNa$_\nu$] from 0.0 - ≤ 0.30 M. (d) The increase in [$M_\nu X$] ($M_\nu X$ = 3- and 4-MeSaNa$_\nu$) from 0.0 – 0.30 M increases A_∞ at 370 nm, from 0.0 – 0.40 and 0.0 – 0.73 for $M_\nu X$ = 3-MeSaNa$_\nu$ at respective $\nu = 1$ and 2, as well as from 0.0 – 0.15 and 0.0 – 0.26, 0.01 – 0.26 for $M_\nu X$ = 4-MeSaNa$_\nu$ at $\nu = 1$ and 2, respectively. These concluded observations (b) – (d) show that (i) there is no turbidity development during the course of such reaction conditions, (ii) intial absorbance values (i.e. $A_0 = A_{ob}$ at t = 0, **Eq. 3.13**) due to [4-MeOSaNa$_\nu$] within its range 0.0 - ≤ 0.30 M are almost insignificant, and (iii) the values of A_0 increase significantly with the increase in [3- and 4-MeSaNa$_\nu$] from 0.0 – 0.30 M.

4.1.1.2 Effects of [$M_\nu X$] (ν = 1, 2) with $M_\nu X$ = 4-MeO- and 3-Me-, 4-MeSaNa$_\nu$ on k_{obs} for the Piperidinoloysis of PSa$^-$ in the Presence of a Constant [CTABr]$_T$ at a Constant Temperature

A few series of kinetic runs was carried out at a constant temperature of 35, 40, 45 and 55 °C for the system containing constant concentrations of 0.2 mM PSaH, 100 mM Pip, 5 ≤ [CTABr]$_T$ (mM) ≤ 15 and varying values of [$M_\nu X$] range between 0.0 – 60, 70 and 100 mM for respective 3-Me-, 4-Me- and 4-MeOSaNa$_\nu$ (ν = 1, 2). The [NaOH] values were varied between the range 30 - < 40. The observed values of k_{obs} versus [$M_\nu X$] (ν = 2) for X = 4-MeO-, 3-Me- and 4-MeSa$^{\nu-}$ at 35, 40, 45 and 55 °C are shown in **Figures 4.2 – 4.7**. Similar plots were obtained for the series of kinetic runs of $M_\nu X$ = 4-MeO-, 3-Me- and 4-MeSaNa$_\nu$ (ν = 1, 2) at 35 °C, which are shown in **Figure S1, S2** and **S3** (see Appendix B - **Figure S1, S2** and **S3**), respectively.

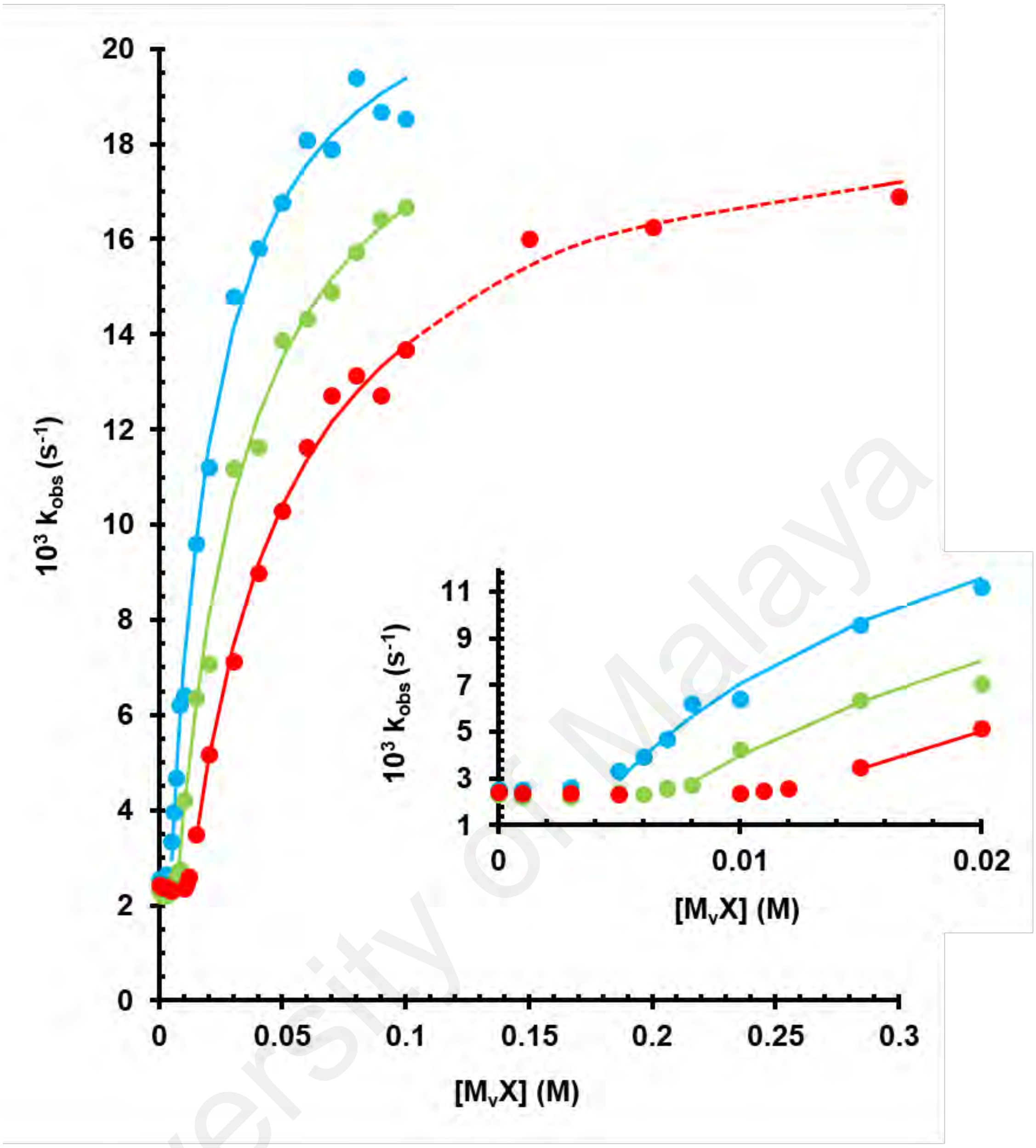

Figure 4.2: Plots showing the dependence of k_{obs} upon [M_vX] (M_vX = 4-MeOSaNa$_v$ with ν = 2) for piperidinolysis of PSa$^-$ at 0.2 mM PSa$^-$, 0.1 M Pip, and [CTABr]$_T$/mM = 6 (blue), 10 (green) and 15 (red), at 35 °C. The solid lines are drawn through the calculated data points using Eq. 4.1, with θ and $K^{X/S}$ listed in Table 4.2. Dotted line is drawn through the calculated data points using Eq. 4.1, assuming the presence of WM at $[M_\nu X]_0^{op} < [M_\nu X] \leq 300$ mM (ν = 2).

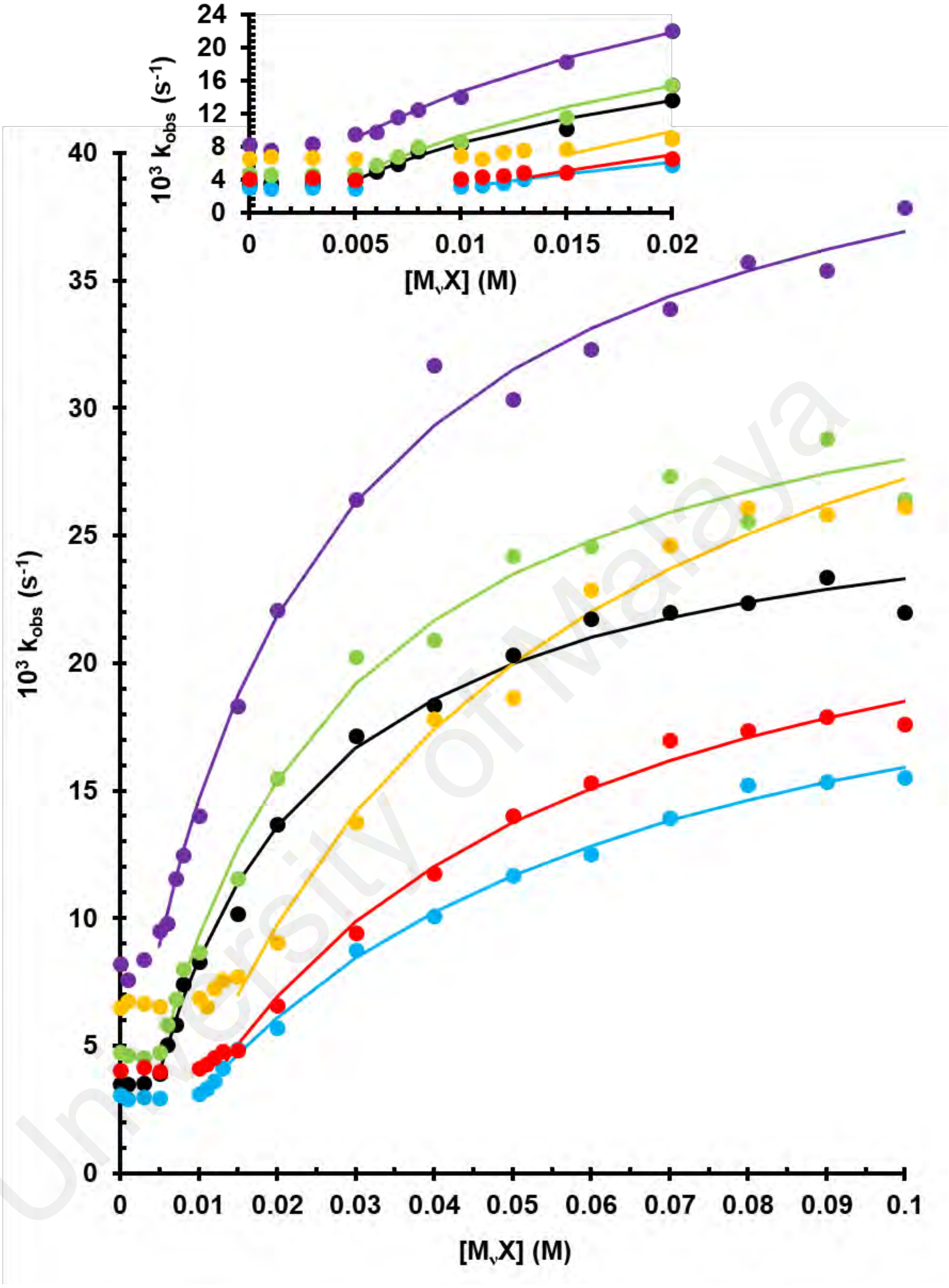

Figure 4.3: Plots showing the dependence of k_{obs} upon [$M_\nu X$] ($M_\nu X$ = 4-MeOSaNa$_\nu$ with ν = 2) for piperidinolysis of PSa$^-$ at 0.2 mM PSa$^-$, 0.1 M Pip, and [CTABr]$_T$/mM = 6 (black), 15 (blue) at 40 °C; 6 (green), 15 (red) at 45 °C; and 6 (purple), 15 (orange) at 55 °C. The solid lines are drawn through the calculated data points using Eq. 4.1, with θ and $K^{X/S}$ listed in Table 4.2.

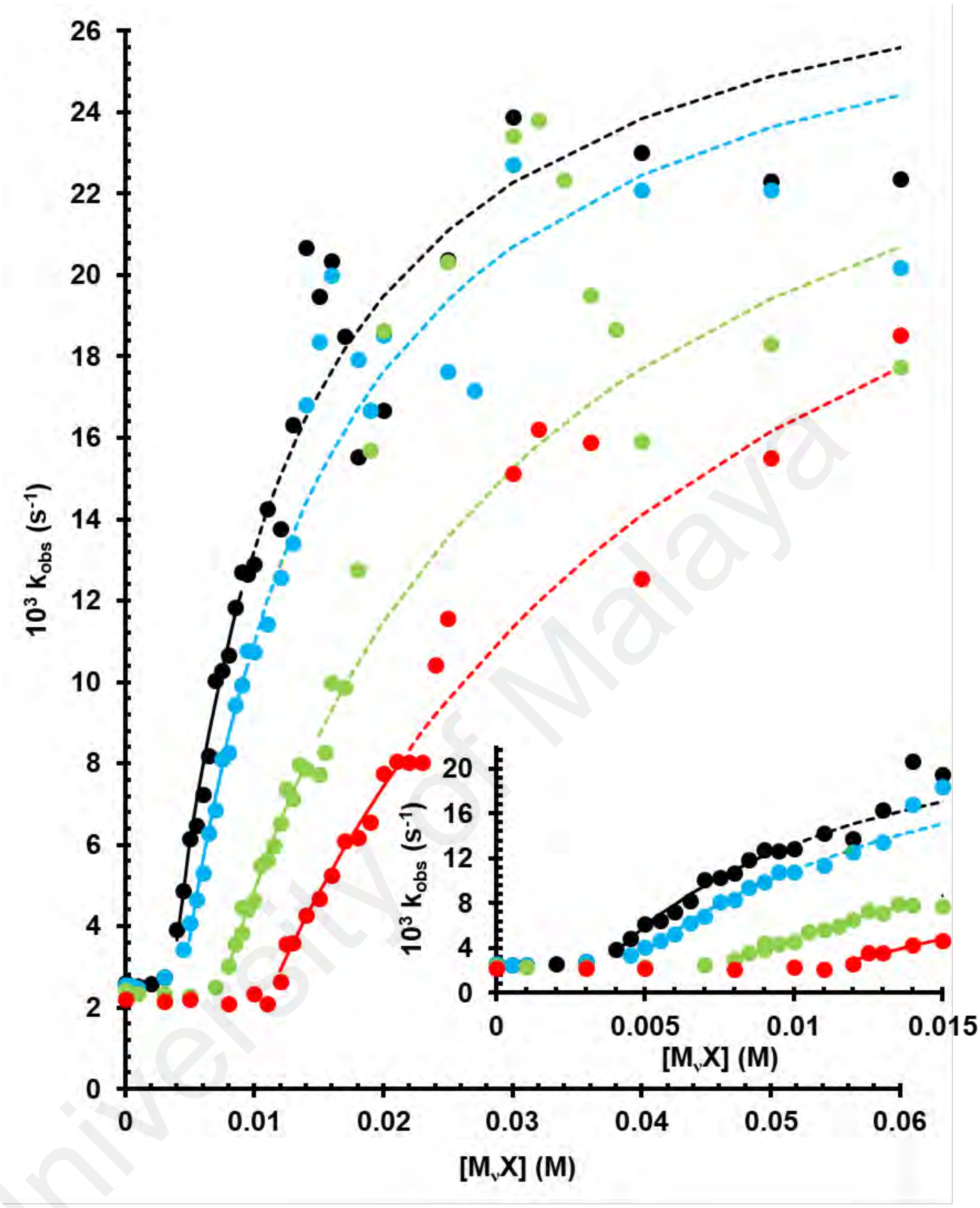

Figure 4.4: Plots showing the dependence of k_{obs} upon [M$_v$X] (M$_v$X = 3-MeSaNa$_v$ with ν = 2) for piperidinolysis of PSa$^-$ at 0.2 mM PSa$^-$, 0.1 M Pip, and [CTABr]$_T$ (mM) = 5 (black), 6 (blue), 10 (green) and 15 (red) at 35 °C. The solid lines are drawn through the calculated data points using Eq. 4.1, with θ and $K^{X/S}$ listed in Table 4.2. The dotted lines are drawn through the calculated data points using Eq. 4.1, assuming the presence of WM at $[M_vX]_0^{op} < [M_vX] \leq 500$ mM.

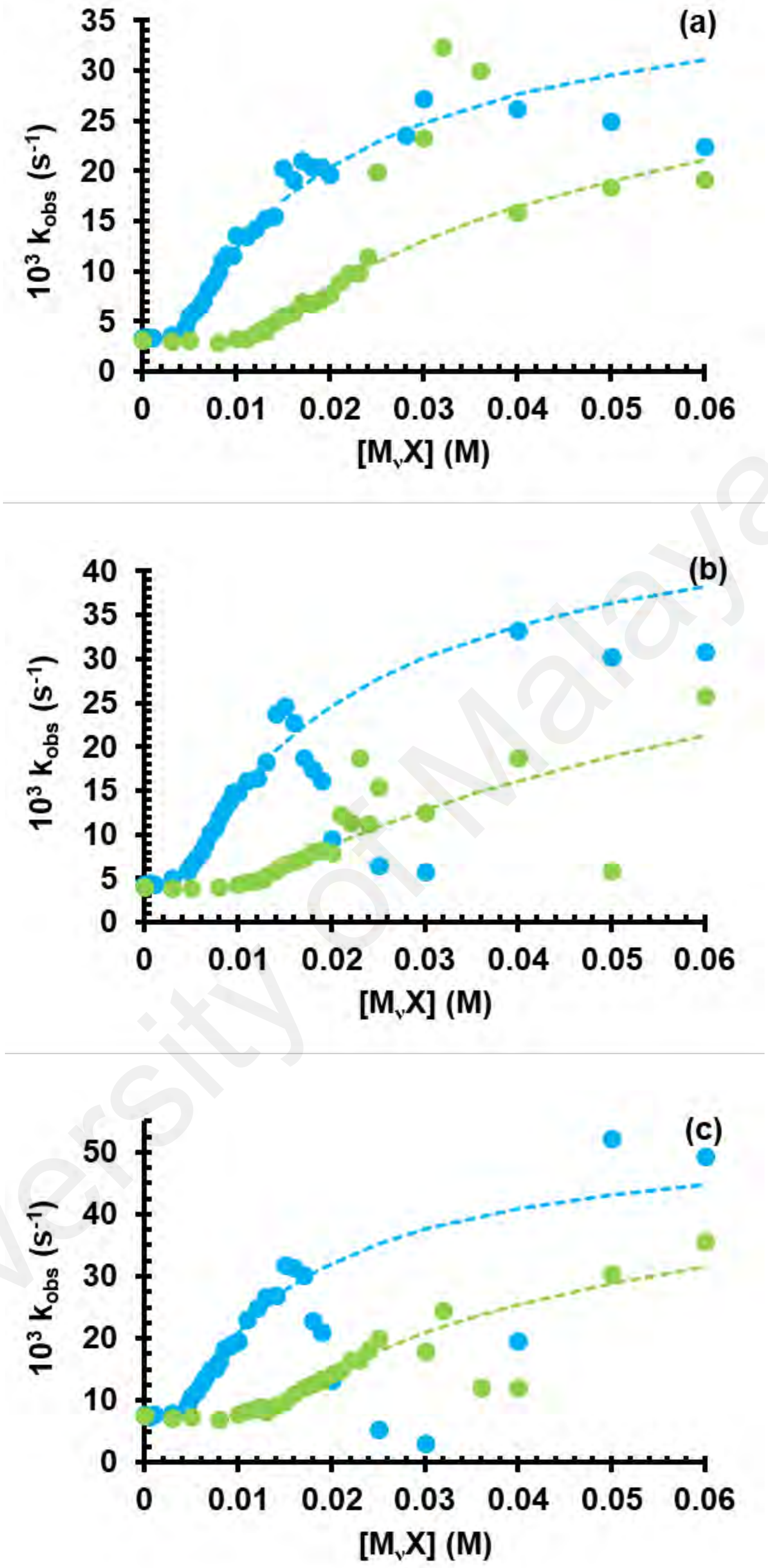

Figure 4.5: Plots showing the dependence of k_{obs} upon $[M_{\nu}X]$ ($M_{\nu}X$ = 3-MeSaNa$_{\nu}$ with $\nu = 2$) for piperidinolysis of PSa^- at 0.2 mM PSa^-, 0.1 M Pip, and $[CTABr]_T$ (mM)= 6 (blue) and 15 (green) at (a): 40 °C, (b): 45 °C and (c): 55 °C. The solid lines are drawn through the calculated data points using Eq. 4.1, with θ and $K^{X/S}$ listed in Table 4.2. The dotted lines are drawn through the calculated data points using Eq. 4.1, assuming the presence of WM at $[M_{\nu}X]_0^{op} < [M_{\nu}X] \leq 500$ mM.

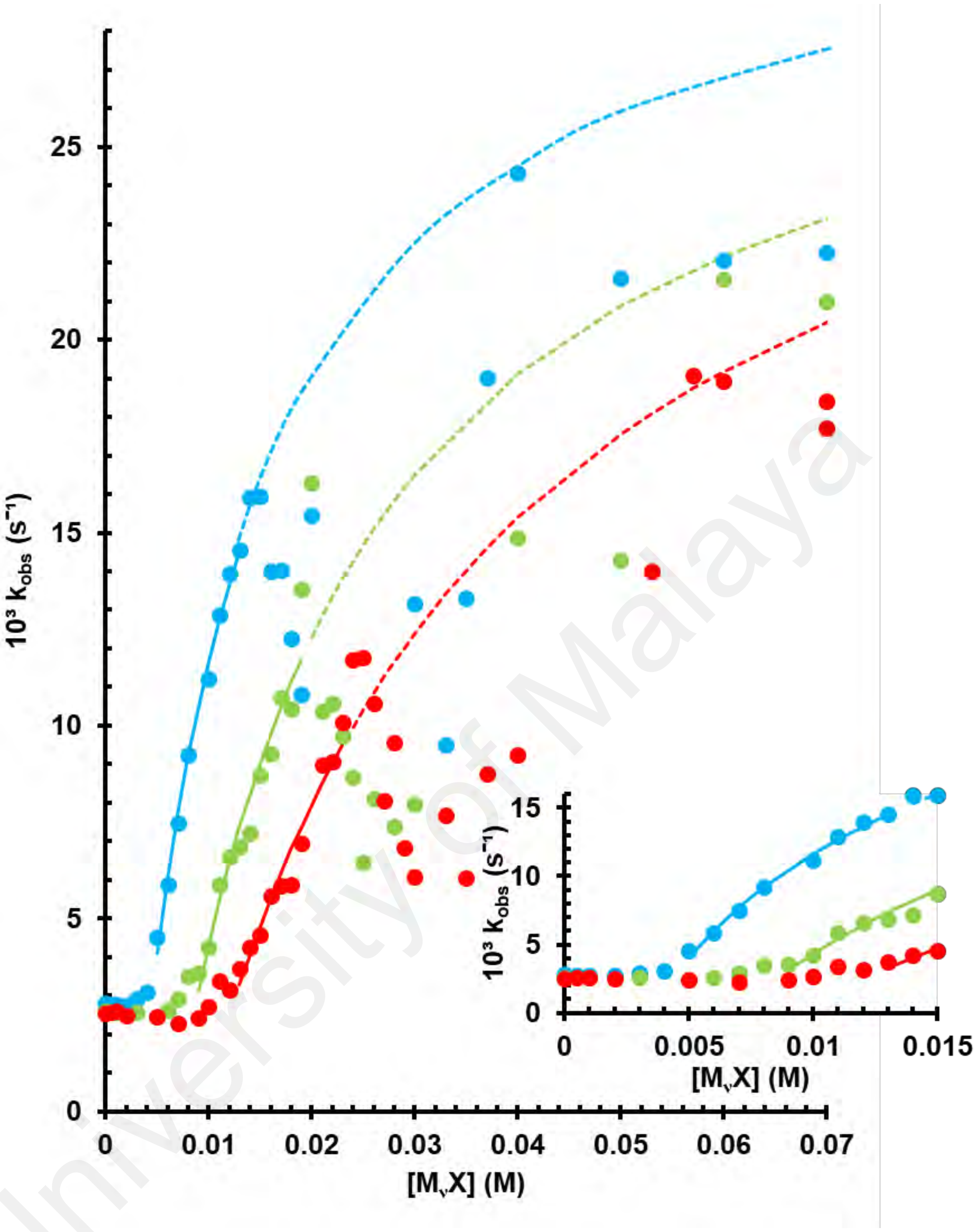

Figure 4.6: Plots showing the dependence of k_{obs} upon $[M_vX]$ (M_vX = 4-MeSaNa$_v$ with $v = 2$) for piperidinolysis of PSa^- at 0.2 mM PSa^-, 0.1 M Pip, and $[CTABr]_T$ (mM) = 6 (blue), 10 (green), and 15 (red) at 35 °C. The solid lines are drawn through the calculated data points using Eq. 4.1, with θ and $K^{X/S}$ listed in Table 4.2. The dotted lines are drawn through the calculated data points using Eq. 4.1, assuming the presence of WM at $[M_vX]_0^{op} < [M_vX] \leq 500$ mM.

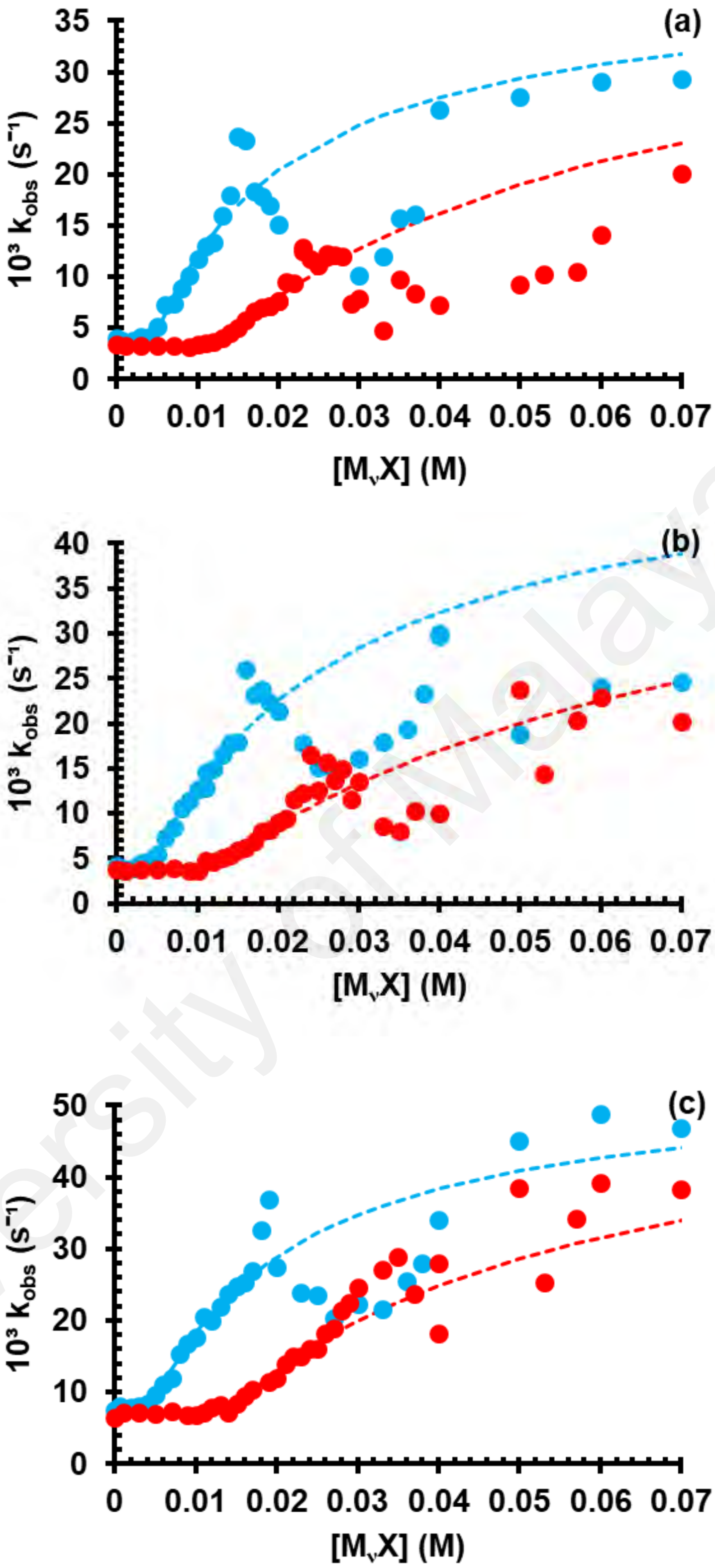

Figure 4.7: Plots showing the dependence of k_{obs} upon [$M_\nu X$] ($M_\nu X$ = 4-MeSaNa$_\nu$ with $\nu = 2$) for piperidinolysis of PSa$^-$ at 0.2 mM PSa$^-$, 0.1 M Pip, and [CTABr]$_T$ (mM) = 6 (blue) and 15 (red) at (a): 40 °C, (b): 45 °C and (c): 55 °C. The solid lines are drawn through the calculated data points using Eq. 4.1, with θ and $K^{X/S}$ listed in Table 4.2. The dotted lines are drawn through the calculated data points using Eq. 4.1, assuming the presence of WM at $[M_\nu X]_0^{op} < [M_\nu X] \le 500$ mM.

In **Figures 4.2** and **4.3**, the plots reveal that the k_{obs} values are almost independent of $[M_vX]$ (M_vX = 4-MeOSaNa$_v$, ν = 2) at the initial low values of $[M_vX]$, then followed a trend where the values of k_{obs} reveal monotonic increase with increasing $[M_vX]$. Similar plots could be seen in **Figure S1** where (M_vX = 4-MeOSaNa$_v$, ν = 1, 2). **Figures 4.4 – 4.7** for M_vX = 3-, 4-MeSaNa$_v$ and ν = 2 show a similar plots of k_{obs} versus $[M_vX]$ when $[M_vX]$ < ~25 mM. After this concentration, the values of k_{obs} reveals a mild increase at certain $[M_vX]$, followed by a decrease, then increase again at higher values of $[M_vX]$. Similar breaks were obtained in the plots of k_{obs} versus $[M_vX]$ (M_vX = 3-, 4-MeSaNa$_v$) when ν = 1, 2 at 15 mM CTABr and 35 °C. These plots are shown in **Figures S2** and **S3** for respective M_vX = 3- and 4-MeSaNa$_v$. However, such observations were not detected with M_vX = 5-MeSaNa$_2$ under similar experimental conditions (Yusof & Khan, 2012).

The reaction mixtures of M_vX (= 4-MeOSaNa$_v$, ν = 2) were moderately viscous, yet clear under the conditions of almost entire kinetic runs. Similar observations were obtained for the reaction mixtures of M_vX (= 4-MeOSaNa$_v$, ν = 1, 2). However, the reaction mixtures of M_vX (= 3- and 4-MeSaNa$_v$, ν = 2) were clear and moderately viscous at C_S/C_D = 1.3, then appear to be mild cloudy and viscous at 1.3 < C_S/C_D < 11.6 and 35 °C, where C_S and C_D represent $[M_vX]$ and $[CTABr]_T$, respectively. It is noteworthy that almost similar observations were exhibited for the reaction mixtures of M_vX (= 3- and 4-MeSaNa$_v$, ν = 1, 2). It is also important to note that the quality of the observed data (A_{ob} versus t) fit to **Eq. 3.13** was better, in terms of standard deviations (std) associated with the calculated parameters (k_{obs}, δ_{ap} and A_∞), at C_S/C_D < 1.5 and 35 °C, where the values of respective maximum and minimum std are 1.3 and 0.4 %. In contrast, the values of maximum and minimum std are 7.4 and 3.8, respectively when C_S/C_D > 1.5 and 35 °C.

In order to reveal the extent of reliability of the observed data fit to **Eq. 3.13**, the kinetic parameters of k_{obs}, δ_{ap} and A_∞ were calculated using the nonlinear least-square technique exhibited by **Eq. 3.13**. To test the validity of this, the observed data (A_{ob} versus t) of a kinetic run, which corresponds to the maximum turbidity in the plot of A_{ob} versus [4-

MeSaNa$_v$] with ν = 2 (**Figure 4.8**), was chosen and summarized in **Table S3** (see Appendix A - **Table S3)** as well as **Figure S4** (see Appendix C - **Figure S4**). The calculated values of k_{obs}, δ_{ap} and A_∞ are $(5.50 \pm 0.41) \times 10^{-3}$ s^{-1}, 2005 ± 85 $M^{-1}cm^{-1}$ and 0.156 ± 0.006, respectively. The extent of reliability of the observed data fit to **Eq. 3.13** was evident from the values of standard deviations (std) associated with calculated values of k_{obs}, δ_{ap} and A_∞ as well as from the percent residual errors (% RE) listed in **Table S3**. Until nearly 5 halflives (i.e. 97 %) completion of the reaction, the maximum and minimum absolute values of % RE are 3.7 and 0.4, respectively as exhibited from **Table S3**. Furthermore, the maximum and minimum values of std associated with least-squares calculated parameters are 4.2 and 3.8 %, respectively. In addition, it is relevant to mention that the values of k_{obs} obtained throughout the study are reliable by considering the fact that the observed data of **Table S3** were obtained under the experimental conditions of maximum turbidity as exhibited by **Figure S4**. Besides, the k_{obs} values that were used to calculate the unknown kinetic parameters (θ and $K^{X/S}$) in the present study were selected

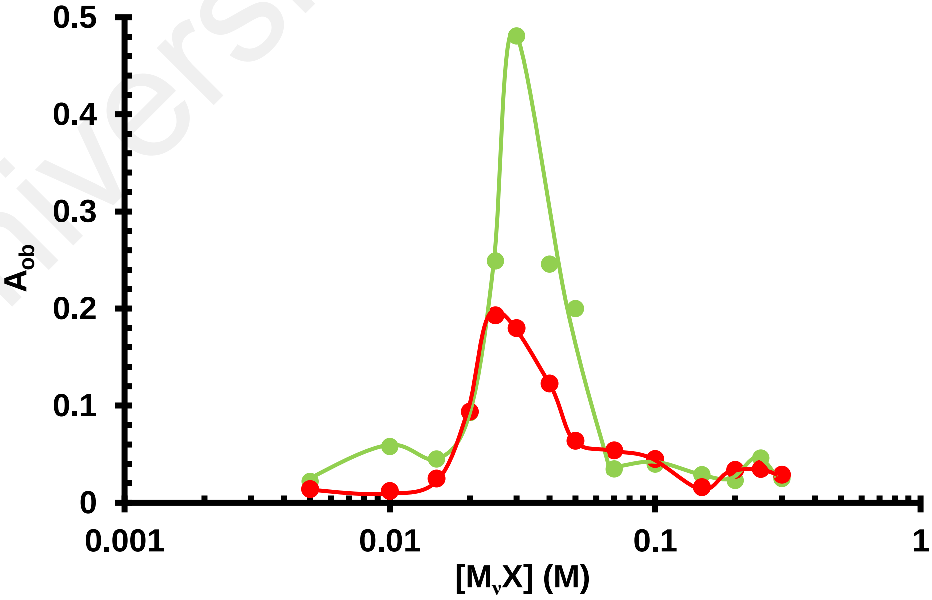

Figure 4.8: Effects of [M$_v$X] = 3-MeSaNa$_v$ (ν = 1) and 4-MeSaNa$_v$ (ν = 2) on corrected absorbance at 600 nm, A_{ob}, (i. e. absorbance due to presence of CTABr/M$_v$X aggregates) of aqueous solutions containing 15 mM CTABr, 0.1 M Pip, 0.03 M NaOH and 0.2 mM PSaH at 35 °C where plots with (red) and (green) represent the A_{ob} values of 3-MeSaNa$_v$ (ν = 1) and 4-MeSaNa$_v$ (ν = 2), respectively.

at less than the critical values of $[M_vX]$. This critical value of $[M_vX]$ corresponds to the value of $[M_vX]$ where the k_{obs} values start to deviate from monotonic solid plots of k_{obs} versus $[M_vX]$.

4.1.1.3 Determination of R_X^{Br} Values for M_vX = 4-MeO- and 3-Me-, 4-MeSaNa$_v$ (v = 1, 2)

Khan et al. had described in detail in the earlier reports (Khan, 2010; Yusof & Khan, 2010, 2012) that the nonlinear increase in k_{obs} with increasing values of $[M_vX]$ at a constant $[CTABr]_T$ and temperature (**Figures 4.2 – 4.7, S1 – S3**) is due to the transfer of micelle-bound PSa$^-$ ions to bulk water phase through the occurrence of ion exchange process between X^{v-}/PSa$^-$ at the cationic micellar surface. The values of k_{obs}, obtained at 0.2 mM PSa$^-$, 100 mM Pip, a constant $[CTABr]_T$ and temperature as well as different $[M_vX]$ (= 4-MeO- and 3-Me-, 4-MeSaNa$_v$ (ν = 1, 2)) were found to fit to empirical relationship, **Eq. 4.1** (Khan, 2010; Yusof & Khan, 2012).

$$k_{obs} = \frac{k_0 + \theta K^{X/S}([M_vX] - [M_vX]_0^{op})}{1 + K^{X/S}([M_vX] - [M_vX]_0^{op})} \qquad \textbf{Eq. 4.1}$$

All symbols in **Eq. 4.1** are described as follows: k_0 represents the value of k_{obs} when $[M_vX] = 0$ and $[CTABr]_T \neq 0$, θ and $K^{X/S}$ are the empirical constants, and $[M_vX]_0^{op}$ represents the M_vX value of optimum concentration, where the concentration value of both micellized HO$^-$ and Br$^-$, i.e. ($[HO_M^-] + [Br_M^-]$) becomes independent with increasing $[M_vX]$ (Khan, 2010; Yusof & Khan, 2012). In **Eq. 4.1**, if $k_0 << K^{X/S}([M_vX] - [M_vX]_0^{op}$ and $1 << K^{X/S}([M_vX] - [M_vX]_0^{op})$, then the k_{obs} value is under the limiting conditions.

It is noteworthy that the determination of the ion-exchange constant, R_X^{Br}, involves a reaction kinetic probe, where this probe consists of the effects of inert organic salts on the pseudo-first-order rate constants for a bimolecular reaction of an anionic and a nonionic reactants at a constant concentration of cationic micelles and temperature. It has been described in details in the early report that **Eq. 4.1** has been derived based upon a reaction scheme explaining the mechanism of CTABr-micelle catalyzed reaction of Pip with PSa^- in terms of PM model and **Eq. 2.1** (described in literature review part) (Khan, 2010). The effects of CTABr micelles on the rate of piperidinolysis of PSa^-, in the presence and absence of an inert salt is discussed in the latter discussion, under subtopic 4.1.1.5 (Piperidinolysis of PSa^- in DDABr/M_vX System). Although the surfactant used are different for both system, the mechanism of CTABr-micelle catalyzed reaction of Pip with PSa^-, in terms of PM model are similar for both.

Iterative technique was used for the determination of $[M_vX]_0^{op}$ values (Khan, 2010; Yusof & Khan, 2012). The calculated values of $[M_vX]_0^{op}$, as well as θ and $K^{X/S}$ at different $[CTABr]_T$ and a constant temperature (35 – 55 °C) are listed in **Table 4.2** for M_vX = 4-MeO-, 3-Me- and 4-MeSaNa$_v$ (ν = 1, 2). The empirical value of $K^{X/S}$ measures the ability of counterion X^{v-} to expel another counterion PSa^- from micellar pseudophase to the bulk aqueous phase through the ion exchange process between X^{v-}/PSa^- at the cationic micellar surface.

By considering k_0 as a known parameter, the values of θ, $K^{X/S}$ and least-squares, Σdi^2 (where di = $k_{obs\ i} - k_{cald\ i}$ with $k_{obs\ i}$ and $k_{cald\ i}$ represent observed and calculated rate constant at the ith value of $[M_vX]$, respectively) were calculated using the nonlinear least-squares technique exhibited by **Eq. 4.1**. The calculated values of these kinetic parameters, (θ, $K^{X/S}$ and Σdi^2), at different $[CTABr]_T$ and a constant temperature are summarized in **Table 4.2** for M_vX = 4-MeO-, 3-Me- and 4-MeSaNa$_v$ (ν = 1, 2). It is noteworthy that the quality of the observed data fit to **Eq. 4.1** was reflected by the values of the standard deviations of calculated parameters (θ and $K^{X/S}$). It is also important to note that the effects of various inert inorganic and organic salts on k_{obs} for alkaline hydrolysis of phthalimide, phenyl salicylate, phenyl benzoate and N-benzylphtalimide had been explained satisfactorily by using **Eq. 4.1** (Khan, 2006, 2010; Yusof & Khan, 2012).

Table 4.2: Values of the Empirical Constants θ and $K^{X/S}$ for $M_{\nu}X$ = 4-MeO-, 3- and 4-MeSaNa$_{\nu}$ (ν = 2) in CTABr Micelles at 35, 40, 45 and 55 °C.[a]

$[CTABr]_T$[b] (mM)	10^4 k_0[c] (s^{-1})	$[M_{\nu}X]_0^{op}$ (mM)	10^3 θ (s^{-1})	$K^{X/S}$ (M^{-1})	$F_{X/S}$[d]	$K_{X/S}$[e] (M^{-1})	$K^{n}_{X/S}$[f] (M^{-1})	K_X^{Br} or R_X^{Br}[g]	$[M_{\nu}X]$[h] (mM)	10^6 Σdi^2
4-MeOSaNa$_{\nu}$										
Temp = 35 °C										
6.0	25.5 ± 0.1[i]	4.5	22.3 ± 0.4[i]	55.1 ± 4.1[i]	0.74[j]	2369[k]	1753	70[l]	5 - 100	2.57
10.0	23.3 ± 0.2	7.2	21.2 ± 0.8	33.9 ± 3.5	0.70	2405	1684	67	8 - 100	2.46
15.0	24.4 ± 0.2	12.3	19.2 ± 0.9	24.1 ± 3.1	0.63	2555	1609	64	12 - 100	1.01
15.0[v]	22.2 ± 0.3	11.7	23.6 ± 0.6	17.6 ± 0.9	0.77	1866	1437	57	15 - 100	0.21
15.0[w]	22.9 ± 0.3	13.2	20.8 ± 0.4	23.6 ± 1.3	0.68	2502	1701	68	15 - 120	0.34
Temp = 40 °C										
6.0	34.9 ± 0.3	4.6	27.8 ± 0.7	46.5 ± 4.2	0.67[m]	1530[n]	1025	28[o]	5 - 100	4.96
15.0	30.9 ± 0.3	10.3	24.3 ± 1.1	17.2 ± 1.7	0.58	1391	807	22	11 - 100	0.96
Temp = 45 °C										
6.0	47.6 ± 0.4	5.3	34.4 ± 1.4	38.3 ± 5.3	0.65[p]	692[q]	450	10[r]	6 - 100	12.62
15.0	40.2 ± 0.4	12.6	26.9 ± 1.7	19.7 ± 3.1	0.51	861	439	9	13 - 100	2.53
Temp = 55 °C										
6.0	82.3 ± 0.6	4.5	44.7 ± 1.2	38.7 ± 3.6	0.79[s]	440[t]	347	7[u]	5 - 100	10.36
15.0	65.2 ± 0.7	14.2	40.3 ± 3.5	18.5 ± 3.8	0.72	499	359	7	15 - 100	7.10
3-MeSaNa$_{\nu}$										
Temp = 35 °C										
5.0	24.9 ± 0.2[i]	3.6	29.6 ± 0.4[i]	101.5 ± 3.8[i]	0.96[j]	3672[k]	3525	141[l]	4 - 9	1.83
5.0[v]	22.3 ± 0.2	4.1	29.6 ± 0.3	97.0 ± 2.1	0.96	3493	3353	134	5 - 11	0.78

Table 4.2 continued

$[\mathrm{CTABr}]_T^{b}$ (mM)	$10^4\ k_0^{c}$ (s^{-1})	$[M_\nu X]_0^{op}$ (mM)	$10^3\ \theta$ (s^{-1})	$K^{X/S}$ (M^{-1})	$F_{X/S}^{d}$	$K_{X/S}^{e}$ (M^{-1})	$K^{n}_{X/S}$ ^{f} (M^{-1})	K_X^{Br} or R_X^{Br} ^{g}	$[M_\nu X]^{h}$ (mM)	$10^6\ \Sigma di^2$
6.0	25.7 ± 0.1	4.5	29.1 ± 0.3	84.4 ± 2.2	0.94	3629	3411	136	5 – 9.5	0.66
6.0^{v}	21.9 ± 0.2	5.0	29.1 ± 0.3	84.5 ± 2.3	0.94	3634	3415	137	6 – 10	0.65
10.0	24.3 ± 0.2	7.5	29.3 ± 0.2	40.5 ± 0.9	0.96	2876	2760	110	8 - 14	0.50
10.0^{v}	20.7 ± 0.3	7.8	29.4 ± 0.3	38.2 ± 1.2	0.95	2712	2577	103	8 - 14	0.82
15.0	22.2 ± 0.2	11.0	30.1 ± 0.3	25.6 ± 0.8	0.97	2714	2632	105	12 – 21	0.62
15.0^{v}	19.8 ± 0.2	12.2	30.2 ± 0.2	24.5 ± 0.5	0.98	2597	2545	102	12 - 20	0.18
				Temp = 40 °C						
6.0	34.5 ± 0.2	4.0	40.3 ± 0.5	53.1 ± 1.6	0.96^{m}	1749^{n}	1679	46^{o}	4.5 - 14	3.59
15.0	31.6 ± 0.4	11.5	39.4 ± 0.6	20.2 ± 0.8	0.94	1633	1535	42	12 – 24	2.91
				Temp = 45 °C						
6.0	44.0 ± 0.7	4.0	50.9 ± 0.5	47.9 ± 1.0	0.97^{p}	866^{q}	840	18^{r}	4.5 - 13	2.37
15.0	39.9 ± 0.6	11.3	51.0 ± 0.3	11.7 ± 0.3	0.97	511	496	11	11 - 19	0.31
				Temp = 55 °C						
6.0	77.9 ± 1.1	4.3	54.5 ± 0.8	68.6 ± 2.5	0.97^{s}	781^{t}	787	15^{u}	4.5 - 14	8.87
15.0	74.8 ± 0.7	12.5	52.5 ± 0.3	24.2 ± 0.4	0.93	652	607	12	13 - 23	0.58
				4-MeSaNa$_\nu$						
				Temp = 35 °C						
6.0	28.1 ± 0.3^{i}	4.4	32.6 ± 0.3^{i}	75.4 ± 1.8^{i}	1.03^{j}	3242^{k}	3339	134^{l}	5 - 13	0.55
10.0	26.0 ± 0.2	8.6	30.2 ± 0.9	47.4 ± 3.3	0.95	3365	3197	128	9 - 19	5.98

Table 4.2 continued

$[CTABr]_T$[b] (mM)	10^4 k_0[c] (s^{-1})	$[M_\nu X]_0^{op}$ (mM)	10^3 θ (s^{-1})	$K^{X/S}$ (M^{-1})	$F_{X/S}$[d]	$K_{X/S}$[e] (M^{-1})	$K^n_{X/S}$[f] (M^{-1})	K_X^{Br} or R_X^{Br}[g]	$[M_\nu X]$[h] (mM)	10^6 Σdi^2
15.0	25.4 ± 0.3	12.1	30.8 ± 0.5	29.9 ± 1.5	0.97	3169	3074	123	12 - 23	1.93
15.0[v]	22.0 ± 0.3	12.2	30.9 ± 0.8	30.0 ± 2.6	1.04	3180	3307	132	12.5 - 21	4.44
15.0[w]	22.0 ± 0.3	10.0	29.4 ± 0.7	30.4 ± 4.2	0.97	3222	3125	125	12 – 21	0.74
				Temp = 40 °C						
6.0	39.8 ± 0.4	4.7	39.3 ± 1.0	56.6 ± 3.7	0.94[m]	1864[n]	1752	48[o]	5 - 14	7.58
15.0	34.0 ± 0.4	12.4	41.9 ± 0.5	18.1 ± 0.7	1.00	1463	1463	40	13 - 22	1.53
				Temp = 45 °C						
6.0	41.8 ± 0.5	4.3	52.4 ± 0.3	39.1 ± 0.7	1.00[p]	707[q]	707	15[r]	5 - 15	0.94
15.0	38.2 ± 0.3	11.3	51.3 ± 0.4	13.4 ± 0.4	0.98	586	574	12	12 - 21	0.60
				Temp = 55 °C						
6.0	74.3 ± 0.9	4.4	54.8 ± 0.7	52.7 ± 1.6	0.97[s]	600[t]	582	11[u]	5 - 17	5.06
15.0	65.0 ± 0.9	13.4	55.0 ± 0.6	22.9 ± 0.7	0.98	617	605	12	14 - 26	2.78

[a] $[PSa^-]_0$ = 0.2 mM at λ = 365 nm ($M_\nu X$ = 4-MeOSaNa$_\nu$) and λ = 370 nm ($M_\nu X$ = 3-, and 4-MeSaNa$_\nu$), and aqueous reaction mixture for each kinetic run contains 2 % v/v CH_3CN. [b] Total concentration of CTABr. [c] $k_0 = k_{obs}$ at $[M_\nu X]$ = 0. [d] $F_{X/S} = \theta / k_w$. [e] $K_{X/S} = K^{X/S}(1 + K_S^0\ [CTABr]_T)$. [f] $K^n_{X/S} = F_{X/S}K_{X/S}$. [g] K_X^{Br} or R_X^{Br} = $K^n_{X/S} / K^n_{Br/S}$. [h] Total concentration range of $M_\nu X$ used in the data analysis. [i] Error limits are standard deviations. [j] k_W= mean value of k_{obs} obtained within $[M_\nu X]$ range where k_{obs} values remained independent of $[M_\nu X]$ at $[CTABr]_T$ = 0. [k] K_S^0 = 7000 M^{-1} (Khan, 2010). [l] $K^n_{Br/S}$ = 25 M^{-1} (Khan, 2010). [m] k_W = 41.8 X 10^{-3} s^{-1} (Yusof & Khan, 2012). [n] K_S^0 = 5322 M^{-1} (Yusof & Khan, 2012). [o] $K^n_{Br/S}$ = 36.6 M^{-1} (Yusof & Khan, 2012). [p] k_W = 52.6 X 10^{-3} s^{-1} (Yusof & Khan, 2012). [q] K_S^0 = 2847 M^{-1} (Yusof & Khan, 2012). [r] $K^n_{Br/S}$ = 46.8 M^{-1} (Yusof & Khan, 2012). [s] k_W = 56.3 X 10^{-3} s^{-1} (Yusof & Khan, 2012). [t] K_S^0 = 1730 M^{-1} (Yusof & Khan, 2012). [u] $K^n_{Br/S}$ = 51.3 M^{-1} (Yusof & Khan, 2012). [v] $M_\nu X$ (ν = 1). [w] $M_\nu X$ (ν = 2).

From the observed plots of **Figures 4.2** and **4.3** as well as **Figure S1**, the k_{obs} values for M_vX = 4-MeOSaNa$_v$ ($v = 1, 2$) reveal a monotonic increase with the increase in $[M_vX] - [M_vX]_0^{op}$ within the entire range of $[M_vX] - [M_vX]_0^{op}$ investigated in this study. Indeed, the results were obtained as predicted. However, the plots of **Figures 4.4 – 4.7** as well as **Figures S2** and **S3** indicate monotonic increase in k_{obs} with increasing $[M_vX]$ only until $[M_vX]_0^{op} < [M_vX] < 25$ mM for both M_vX = 3- and 4-MeSaNa$_v$ ($v = 1, 2$). The k_{obs} values start to deviate after this concentration, and the reasons for this may be explained qualitatively as follows. Recent reports (Khan, 2010; Yusof & Khan, 2012) by Khan et al. had shown that the empirical constant $K^{X/S}$ is a function of CTABr micellar binding constants K_X and K_S of respective counterions X and S. It is noteworthy that the K_S value decrease with the increase of $[M_vX]$ (as exhibitd by **Eq. 2.1**). The increase in $[M_vX]$ may results in the changes of CTABr/M_vX aggregates, which will eventually change the magnitude of K_X as well. A recent study had reported that the magnitude of K_X was higher in the presence of vesicles, slightly lower in the presence of WM, and the lowest in the presence of SM (Yusof & Khan, 2012). From these reports, it is evident that the values of $K^{X/S}$ will remain constant only within a specific range of $[M_vX]$ where the structure of mixed CTABr/M_vX aggregates remained essentially unchanged. The $K^{X/S}$ value is expected to be higher in the presence of vesicles than that in WM, and the lowest in the presence of SM. Thus, the $K^{X/S}$ value should vary in the order: $K^{X/S}$ (SM) < $K^{X/S}$ (WM) << $K^{X/S}$ (vesicles) for a system at a constant temperature and $[\text{CTABr}]_T$ (Yusof & Khan, 2012). In relation to that, the cause of breaks in the plots of k_{obs} versus $[M_vX]$ as exhibited by **Figures 4.4 – 4.7** as well as **Figures S2** and **S3** is probably due to the transition of the structure of micellar aggregates from SM-to-WM-to-planar/curved bilayer aggregates at a constant $[\text{CTABr}]_T$ and temperature. The rheological measurements of M_vX = 4-MeOSaNa$_v$ ($v = 1, 2$), which will be explained further in latter discussion, reveals the presence of WM and its structure remains unchanged with the change in $[M_vX]$ covered in this study. Similar observations that were obtained for M_vX = 3- and 4-MeSaNa$_v$ (v = 1, 2) only until ~25 mM of M_vX, also indicates the unchanged behavior of structural WM. However, the structure of mixed CTABr/3- or 4-MeSaNa$_v$ system becomes Vs/planar bilayers–to–MLV after that concentration. It is noteworthy that the kinetic data of k_{obs} versus [M_vX] at a constant [CTABr]$_T$ and temperature are insensitive to the micellar microstructural changes of short WM-to-long linear WM-to-entangled WM-to-branched WM. In contrast, such kinetic data appear to be sensitive to surfactant aggregate structural changes of SM-to-WM-to-planar or curved bilayer aggregates.

The possible occurrence of ion exchange processes between counterions at the cationic micellar pseudophase are Br^-/HO^-, Br^-/X^-, Br^-/PSa^-, X^-/HO^-, X^-/PSa^- and HO^-/PSa^-. But, the kinetically effective ion exchange process under the present reaction system is X^-/PSa^-. The reasons for this are described as follows: (i) the ion exchange between Br^-/HO^-, X^-/HO^- and HO^-/PSa^- remained kinetically insignificant due to the rate of the reaction between Pip and PSa^- was independent of [HO^-] within the [HO^-] range of the present study. (ii) X^- and Br^- are nonreactive ions. Therefore, they should not affect the rate of piperidinolysis of PSa^-. (iii) the ion exchange Br^-/PSa^- may be ignored compared to X^-/PSa^- due to the values of [X^-] which are generally many fold larger than [Br^-], also the large difference in the hydrophobicity between X^- and Br^- as well as constant values of [Br^-]$_T$ and [PSa^-]$_T$ with variable [X^-]$_T$.

Thus, the kinetically effective occurrence of ion exchange between X^- and PSa^- (in CTABr system) at the cationic micellar surface will definitely decrease the value of cationic micellar binding constant of PSa^- (K_S) with the increase of [M_vX] through the empirical relationship given by **Eq. 2.1**. The empirical definition of those kinetic parameters obtained in **Eq. 2.1** was explained earlier, where K_S^0 = K_S at zero concentration of M_vX (Khan, 2006, 2010; Khan *et al.*, 2000) while the magnitude of the empirical constant $K_{X/S}$ measures the ability of counterion X^- to expel another counterion

S^- from the cationic micellar pseudophase to the bulk aqueous phase through the occurrence of ion exchange process between X^-/S^- at the cationic micellar surface. It has been shown elsewhere that a kinetic equation derived from a reaction scheme explaining the mechanism of CTABr micelle-catalyzed reaction of Pip with PSa^-, in terms of PM model under the experimental conditions and **Eq. 2.1**, (with the change of $[M_vX] = [M_vX] - [M_vX]_0^{op}$) can lead to **Eq. 4.1** with θ and $K^{X/S}$ expressed by respective **Eqs. 4.2** and **4.3** (Khan, 2010; Yusof & Khan, 2010, 2012),

$$\theta = F_{X/S}k_W^{M_vX} \qquad \textbf{Eq. 4.2}$$

where $F_{X/S}$ is an empirical constant which by definition, represents the fractions of transferred micellized counterion S^- (i.e. S_M), from micellar pseudophase to the aqueous phase through ion exchange X^-/S^-. The value of $k_W^{M_vX}$ is the average value of k_{obs} obtained at a certain concentration range of M_vX and $[CTABr]_T = 0$, where the k_{obs} values under this concentration range remain unchanged, and

$$K^{X/S} = K_{X/S}/(1 + K_S^0[CTABr]_T) \qquad \textbf{Eq. 4.3}$$

The appearance of empirical parameter $F_{X/S}$ had been discussed in details by Khan in his excellent review article (Khan, 2010). This parameter do exist in **Eq. 4.2** and its value should be less than 1.0, just to take account that the hydrophilic counterions, in the physical reality cannot expel completely (i.e. 100 %) hydrophobic counterions from micellar pseudophase to the bulk aqueous phase (Khan, 2010; Khan *et al.*, 2013).

It is relevant to note that the values of θ and $F_{X/S}$, as exhibited by **Eq. 4.2** should be independent of $[CTABr]_T$, which is proven in the present study and those values are summarized in **Table 4.2**. The mean values of $F_{X/S}$ for M_vX = 4-MeOSaNa$_v$ and 3-, 4-MeSaNa$_v$ are shown in **Table 4.3**. However, the mean values of $F_{X/S}$ for M_vX = 4-MeOSaNa$_v$ (ν = 2) are mildly lower than those reported for M_vX = 5-MeOSaNa$_v$ (ν = 2) (Yusof & Khan, 2012).

Table 4.3: Mean Values of $F_{X/S}$ and R_X^{Br}, Determined by SEK Method for Different M_vX Used in the Presence of CTABr Micelles.

X	Temp (°C)	$[M_vX]_0^{op}$	Z1[a] (mM)	Z2[b] (mM)	10^2 $F_{X/S}$	R_X^{Br}	η_0^{max} [c] (mPa·s)	η_0^{max2} [d] (mPa·s)	W [e]
4-MeOSa^{2-}	35	Nonzero	15		69 ± 6[f]	67 ± 1[f]	327	g	1.3
	40	Nonzero	14		63 ± 5	25 ± 3	63.8	g	1.5
	45	Nonzero	19		58 ± 10	9.5 ± 0.5	31.6	g	1.3
	55	Nonzero	20		76 ± 5	7.0 ± 0	5.8	g	1.0
3-MeSa^{2-}	35	Nonzero	12	100	96 ± 2	118 ± 20	435	13.2	6.8
	40	Nonzero	13	80	95 ± 1	44 ± 3	282	8.4	8.5
	45	Nonzero	13	100	97 ± 0	15 ± 5	76.2	6.0	6.3
	55	Nonzero	14	100	95 ± 3	14 ± 2	14.7	3.3	3.8
4-MeSa^{2-}	35	Nonzero	12	150	98 ± 4	128 ± 5	938	50.5	6.3
	40	Nonzero	13	150	97 ± 4	45 ± 4	287	26.5	8.3
	45	Nonzero	14	150	99 ± 1	14 ± 2	94.1	12.0	6.8
	55	Nonzero	14	150	98 ± 1	12 ± 1	27.0	5.6	4.4
2,3-Cl_2Bz^- [h]	35	Nonzero	40		70 ± 4	25 ± 2	1.6	g	
2,4-Cl_2Bz^- [h]	35	Nonzero	30		75 ± 3	45 ± 2	7.8	g	
2,5-Cl_2Bz^- [h]	35	Nonzero	40		87 ± 3	25 ± 3	3.6	g	
2,6-Cl_2Bz^- [h]	35	Nonzero			63 ± 2	4.7± 0.6	g	g	
3,4-Cl_2Bz^- [h]	35	Nonzero	13	40	94 ± 4	119 ± 10	174	37.3	
3,5-Cl_2Bz^- [h]	35	Nonzero	13	40	95 ± 3	206 ± 4	60.7	5.2	

[a] Z1 = $[M_vX]_{sc1}$, specific concentration of M_vX at which the first zero shear viscosity maximum occurs at 15 mM CTABr. [b] Z2 = $[M_vX]_{sc2}$, specific concentration of M_vX at which the second zero shear viscosity maximum occurs at 15 mM CTABr. [c] Zero shear viscosity at $[M_vX]_{sc1}$. [d] Zero shear viscosity at $[M_vX]_{sc2}$. [e] W = Y1/Y2 where Y1 = R_X^{Br} for X = 5-MeO- or 5-MeSa^{2-} and Y2 = R_X^{Br} for X = 4-MeO- or 3-, 4-MeSa^{2-}. [f] Error limits are standard deviations. [g] Absence of well defined maximum for X = 2,6-Cl_2Bz^- and second maximum for X = 4-MeOSa^{2-}. [h] The mean values of $F_{X/S}$, R_X^{Br}, η_0^{max} and η_0^{max2} were obtained from Razak & Khan (2013), Razak et al. (2014) and Yusof et al. (2013).

The values of $K_{X/S}$ were calculated using **Eq. 4.3** for different M_vX = 4-MeOSaNa$_v$ and 3-, 4-MeSaNa$_v$ (v = 1, 2), [CTABr]$_T$ and temperatures. The values of K_S^0 were reported as 7000, 5322, 2847, and 1730 M^{-1} cm^{-1} at 35, 40, 45 and 55 °C, respectively (Yusof & Khan, 2012). These calculated values of $K_{X/S}$ are summarized in **Table 4.2** for M_vX = 4-MeO-, 3- and 4-MeSaNa$_v$ (v = 1, 2) at different [CTABr]$_T$ and temperatures. From the table, the values of normalized $K_{X/S}$, i.e. $K_{X/S}^n$ (= $F_{X/S}K_{X/S}$) were found to be almost independent of [CTABr]$_T$. The value of $K_{X/S}$ has been normalized due to empirical consequences that the hydrophilic counterions cannot expel completely (i.e. 100 %) hydrophobic counterions from micellar pseudophase to the bulk aqueous phase (Khan, 2010; Khan *et al.*, 2013). The values of R_X^{Br} were calculated by using the relationship $K_{X/S}^n / K_{Br/S}^n$, where the values of $K_{Br/S}^n$ at a specific temperatures are listed in **Table 4.2** (Khan, 2010; Yusof & Khan, 2012). These calculated values of R_X^{Br} are essentially independent of [CTABr]$_T$ at a constant temperature (**Table 4.2**). Thus, the mean values of R_X^{Br} at different temperatures are shown in **Table 4.3**.

It is noteworthy that the magnitude of $K_{X/S}$ is used to measure the ability of counterion X^- to expel another counterion S^-, from micellar pseudophase to the bulk aqueous phase. Thus, it means that the magnitude of $K_{X/S}$ is directly proportional to the micellar binding constant of counterion X^- (K_X) and inversely proportional to the micellar binding constant of counterion S^- (K_S) (Khan, 2010). This relationship is given mathematically as $K_{X/S} = \Omega_S K_X/K_S$ where Ω_S represents proportionality constant (Khan, 2010; Yusof & Khan, 2010). Similarly, for another ion exchange Br^-/S^-, $K_{Br/S} = \Omega_S K_{Br}/K_S$. The magnitude of Ω_S depends on the molecular characteristics of counterion S^- only which means that this parameter is not affected by the molecular characteristics of other counterions such as Br^-. The relationship between $K_{X/S} = \Omega_S K_X/K_S$ and $K_{Br/S} = \Omega_S K_{Br}/K_S$ results in $K_{X/S}/K_{Br/S} = K_X/K_{Br} = K_X^{Br}$ or R_X^{Br}. The use of kinetic parameter, K_X^{Br} or R_X^{Br} depends on the values of $K_{X/S}$ and $K_{Br/S}$, whether they were obtained in the presence of similar or different micellar aggregate structures. It is noteworthy that the penetration of cationic micelles by counterion X cannot be determined clearly by the magnitude of K_X^{Br} or R_X^{Br} (Khan *et al.*, 2013). However, the plausible correlation between the magnitude of K_X^{Br} or R_X^{Br} as well as X-penetration to cationic micelles would be affected by the position of substituents in benzoate ion (Khan *et al.*, 2013).

The R_X^{Br} values obtained for M_vX = 4-MeO- and 5-MeOSaNa_v (ν = 2) at 35 °C are 67 and 89, respectively, which is 25 % smaller for 4-MeO- than that for 5-MeOSaNa_v (ν = 2) (Yusof & Khan, 2012). At 40 and 45 °C, similar observations were obtained for both 4-MeO- and 5-MeOSaNa_v (ν = 2), while at 55 °C, the values of R_X^{Br} become the same (Yusof & Khan, 2012). The values of R_X^{Br} obtained within 35 – 55 °C, for M_vX = 4-Me- and 5-MeSaNa_v (ν = 2), are larger than those for M_vX = 4-MeO- and 5-MeOSaNa_v (ν = 2) by respective ~1.7- and ~8-fold (Yusof & Khan, 2012). Similarly, the R_X^{Br} values reported by earlier study for X = 3- and 4-$MeC_6H_4CO_2^-$ are ~3-fold larger than that for 4-$MeOC_6H_4CO_2^-$ (Khan, 2006, 2010). These observations indicate quantitatively that the magnitude of R_X^{Br} is higher in the presence of higher apparent hydrophobicity of benzoate substituent attached to the benzoate ions, i.e. 4-Me than that of 4-MeO.

4.1.1.4 Turbidity Measurements of Aqueous CTABr/M_vX System Containing 15 mM CTABr and Different [M_vX] with M_vX = 3-MeSaNa_v (ν = 1) and 4-MeSaNa_v (ν = 2)

The reaction mixtures of M_vX (= 4-MeOSaNa_v, ν = 1, 2) were moderately viscous, yet clear under the conditions of almost entire kinetic runs. However, the reaction mixtures of M_vX (= 3- and 4-MeSaNa_v, ν = 1 and 2, respectively) were clear and moderately viscous at C_S/C_D = 1.3, then appear to be mild cloudy and viscous at 1.3 < C_S/C_D < 11.6 and 35 °C. It is also noteworthy that almost similar observations were shown by the reaction mixtures of M_vX (= 3- and 4-MeSaNa$_v$, ν = 1, 2). In order to find out the reliability of this qualitative observation on the present kinetic data, a few series of spectrophotometric runs was carried out at a constant wavelength of 600 nm, 35 °C, 15 mM CTABr, 0.1 M Pip, 0.03 M NaOH, 0.2 mM PSaH as well as different ranges of [M_vX] (ν = 1 and 2 for respective 3-MeSaNa$_v$ and 4-MeSaNa$_v$). Wavelength 600 nm has been chosen due to the visible spectra (scanned within wavelength range 350 – 900 nm) of samples containing all chemical ingredients used for kinetic and rheological measurements. Turbidity was expressed in absorbance units, A_{ob}. The plots of A_{ob} versus [M_vX] are shown in **Figure 4.8** for M_vX = 3-MeSaNa$_v$ and 4-MeSaNa$_v$, ν = 1 and 2, respectively. It is necessary to note that the values of A_{ob} represent the corrected absorbance due to the presence of CTABr/M_vX aggregates only. Turbidity maximum exhibited from the plots of **Figure 4.8** lies within [M_vX] range of > ~20 - < ~30 mM. In relation to that, the k_{obs} values (**Figures 4.4 – 4.7** and **Figures S2 – S3**) begin to deviate from the plots of initial monotonic increase of k_{obs} with increasing [M_vX] at ~0.02 M (M_vX = 3-MeSaNa$_v$ and 4-MeSaNa$_v$, ν = 1 and 2, respectively).

4.1.1.5 Piperidinolysis of PSa$^-$ in DDABr/M_vX System

Effects of cationic micelles (CTABr or DDABr) on the rate of piperidinolysis of PSa$^-$, in the absence as well as presence of an inert salt have been explained qualitatively in terms of PM model (Khan *et al.*, 2000, 1997). The formation of micelles in such reaction conditions may create different medium for reactions to occur. The reactions may take place in both aqueous phase and micellar pseudophase. The observed rate constant for the reaction that occurs in micellar pseudophase is reduced due to the lower reaction rate in micellar pseudophase (Khan *et al.*, 1999, 2002, 2010; Khan & Ismail, 2001, 2009; Yusof & Khan, 2010). A reaction scheme for the piperidinolysis of PSa$^-$ under the present experimental conditions, which was derived in terms of PM model, is expressed in **Figure 4.9**,

$$\mathrm{PSa^{-}_{W}} + \mathrm{D_n} \xrightleftharpoons{K_S} \mathrm{PSa^{-}_{M}}$$

$$\mathrm{N_W} + \mathrm{D_n} \xrightleftharpoons{K_N} \mathrm{N_M}$$

$$\mathrm{PSa^{-}_{W}} + \mathrm{N_W} \xrightarrow{k^{n}{}_{W}} \text{N-Piperidinylsalicylate + Phenol}$$

$$\mathrm{PSa^{-}_{M}} + \mathrm{N_M} \xrightarrow{k^{n}{}_{M}} \text{N-Piperidinylsalicylate + Phenol}$$

Figure 4.9: The reaction between PSa$^-$ and Pip in aqueous phase and micellar pseudophase.

where D_n represents CTABr or DDABr micelles (i.e. $[D_n]$ = [CTABr or DDABr]$_T$ – cmc with cmc representing critical micelle concentration), K_S and K_N represent respective micellar binding constant of PSa$^-$ and Pip, k_W^n and k_M^n stand for nucleophilic second-order rate constant for the piperidinolysis of PSa$^-$ in the respective aqueous and micellar phase, while subscripts W and M represent water phase and micellar pseudophase, respectively. It is noteworthy that such reaction does not involve cross-interface reaction (Khan, 2006), which means that the reactions between PSa$^-$ and Pip occur simultaneously in both phases resulting in the same products. The value of k_M^n is significantly lower than k_W^n value due to the distribution of both reactants in aqueous phase as well as micellar pseudophase (Khan, 1997; Khan *et al.*, 1997). The observed rate law for such reaction is given as

$$\text{Rate} = k_{\text{obs}}[\text{PSa}^-]_T \qquad \textbf{Eq. 4.4}$$

where $[\text{PSa}^-]_T$ represents total concentration of PSa$^-$ (i.e. $[\text{PSa}^-]_T = [\text{PSa}^-_W] + [\text{PSa}^-_M]$). The observed rate law, **Eq. 4.4**, and reaction scheme (**Figure 4.9)** lead to **Eq. 4.5**,

$$k_{\text{obs}} = \frac{(k_W^n + k_m^{mr} K_N K_S [D_n])[N]_T}{(1 + K_S[D_n])(1 + K_N[D_n])} \qquad \textbf{Eq. 4.5}$$

where k_M^{mr} = k_M^n/V_M with V_M is the micellar molar volume in M^{-1} and $[N]_T = [N_W] + [N_M]$ (Bunton & Savelli, 1987; Khan, 2010). The value of cmc of CTABr in the presence of 0.2 mM PSa$^-$ was reported to be < 1 × 10^{-4} M (Chaimovich *et al.*, 1975; Khan & Fagge, 2018; Modaressi *et al.*, 2007; Sotgiu *et al.*, 1996), while the reported cmc value of DDABr in water only was ~5 × 10^{-5} M (Grillo *et al.*, 2008; Ono *et al.*, 2005). However, the expected value of cmc is reduced by the presence of additives such as inert salt (Chaimovich *et al.*, 1975; Khan & Fagge, 2018; Liu *et al.*, 2001; Modaressi *et al.*, 2007; Para *et al.*, 2005; Sotgiu *et al.*, 1996). Therefore, $[D_n] \approx [CTABr]_T$ or $[DDABr]_T$ under the conditions of the present study. It should be noted also that the value of K_N is very low due to the highly hydrophilic behavior of nonionic Pip. Thus, $1 >> K_N[D_n]$ under the present experimental conditions (Khan *et al.*, 1997). Therefore, **Eq. 4.5** is reduced to **Eq. 4.6**.

$$k_{obs} = \frac{(k_W^n + k_m^{mr} K_N K_S [D_n])[N]_T}{1 + K_S [D_n]} \qquad \textbf{Eq. 4.6}$$

(a) Effects of $[DDABr]_T$ on k_{obs}, δ_{ap} and A_∞ for the Piperidinoloysis of PSa^- in the Absence and Presence of a Constant [NaBr] at 35 °C

In order to find out the value of micellar binding constant (K_S) of PSa^- in aqueous DDABr system, several kinetic runs were carried out at a constant [NaBr], within its range 0.0 – 100 mM and 35 °C for the system containing constant concentrations of 0.2 mM PSaH, 30 mM NaOH, 100 mM Pip and $[DDABr]_T$ range between 0.0 – 0.8 mM. The [NaOH] values were varied between its ranges 30 - < 40 mM. The observed values of k_{obs} at different $[DDABr]_T$ are shown in **Figure 4.10** at a few representative values of [NaBr] series, as well as **Figures S5(a)** and **5(b)** (see Appendix D - **Figures S5(a)** and **5(b)**). The calculated values of δ_{ap} and A_∞ at different range of $[DDABr]_T$ are shown in **Figures 4.11, S6** and **Figure S7** (see Appendix D - **Figures S6** and **S7**), respectively.

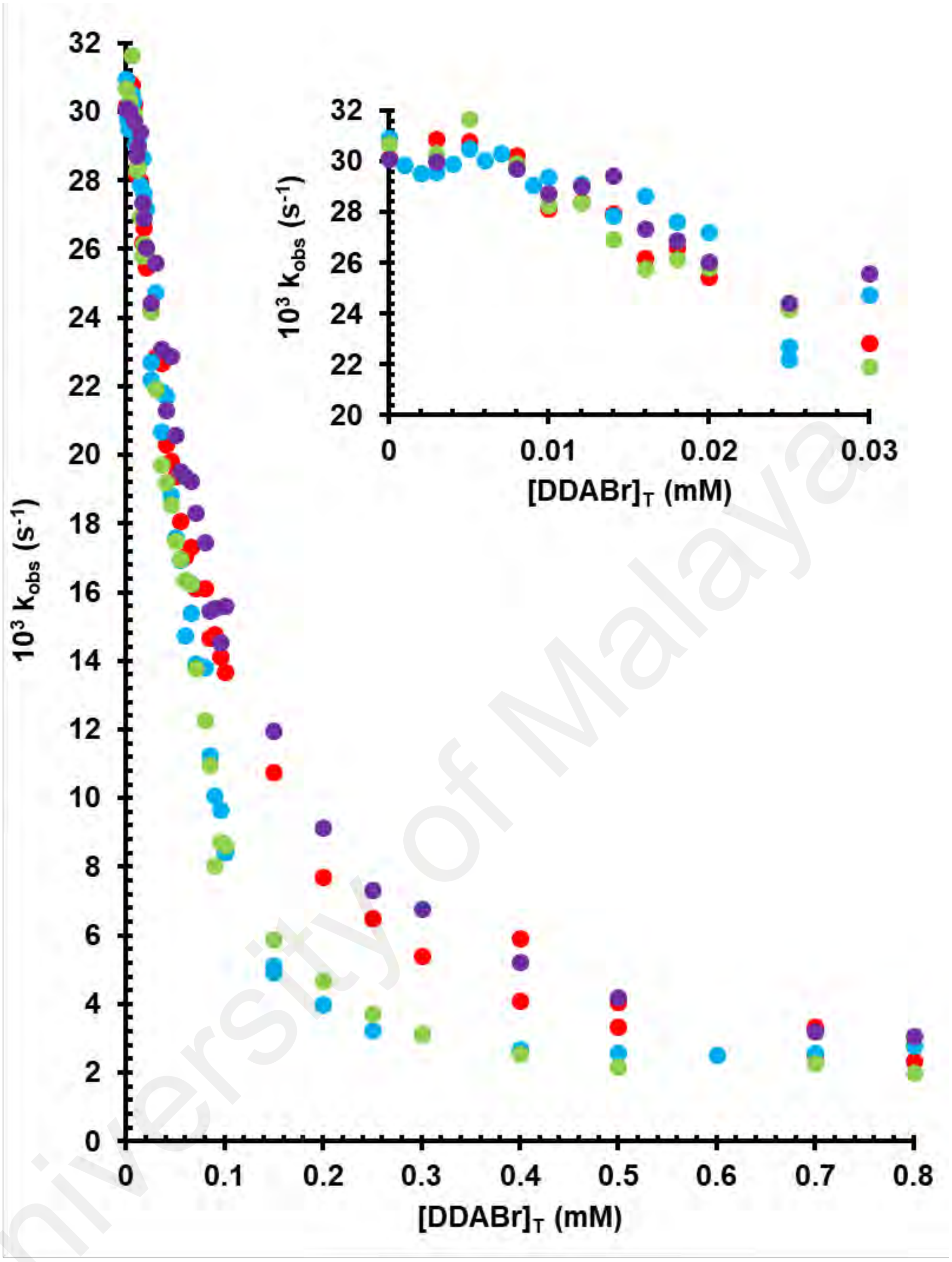

Figure 4.10: Plots showing the dependence of k_{obs} upon $[DDABr]_T$ for piperidinolysis of PSa^- at 0.2 mM PSa^-, 0.03 M NaOH, 0.1 M Pip and [NaBr] (mM) = 0 (blue), 1 (green), 5 (red) and 10 (purple) at 35 °C. Inset: The plots for the data points at the lowest values of $[DDABr]_T$ are shown at magnified scale.

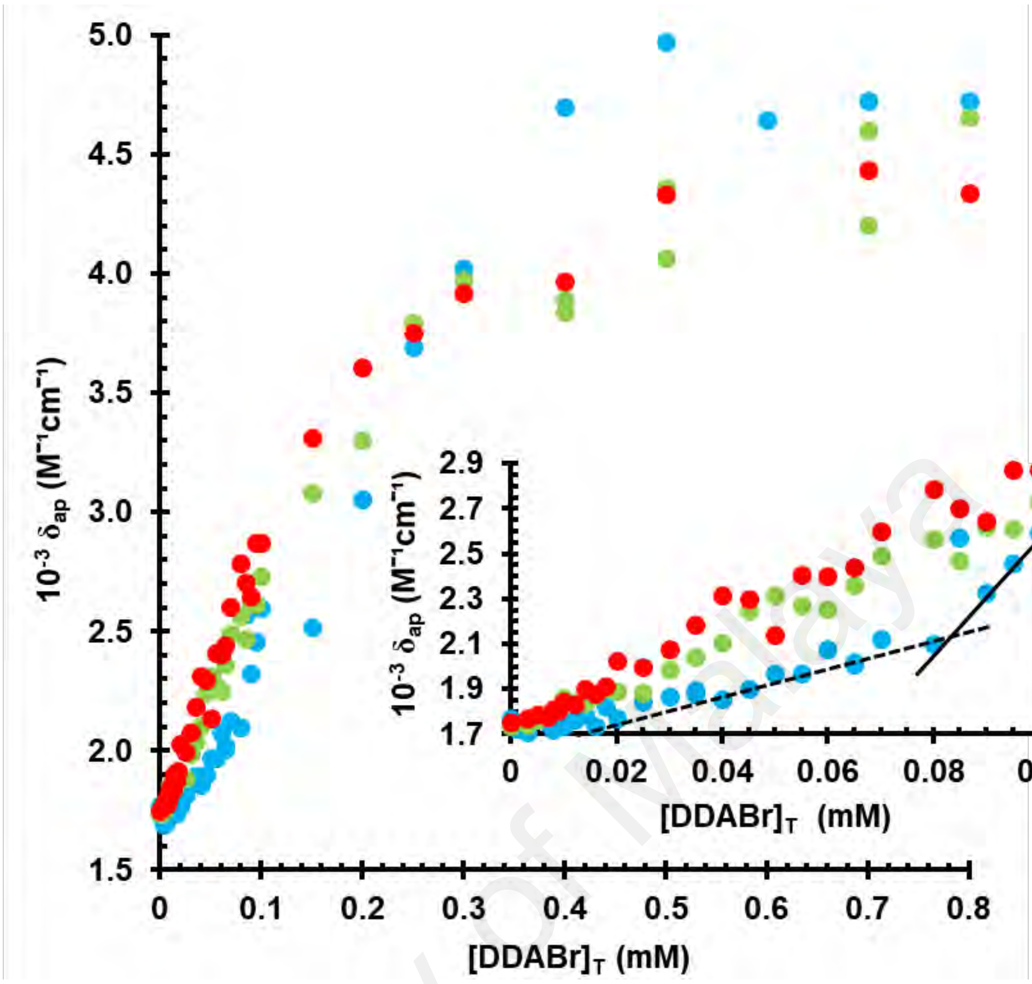

Figure 4.11: Plots showing the dependence of δ_{ap} upon $[DDABr]_T$ for piperidinolysis of PSa^- at 0.2 mM PSa^-, 0.1 M Pip, 0.03 M NaOH, 35 °C and [NaBr] (mM) = 0 (blue), 5 (green) and 20 (red). Inset: The plots at magnified scale for the data points at the lowest values of $[DDABr]_T$.

(b) CH_3CN-H_2O: Mixed Solvents Effect on Rate of Piperidinolysis of PSa^- at 35 °C

In **Figures 4.11** and **S6**, the plots exhibited by a different series of [NaBr] at 370 nm show a nonlinear increase of δ_{ap} with increasing values of $[DDABr]_T$. In contrast, the values of δ_{ap} at 370 nm did not show any significant changes due to different $[CTABr]_T$ and constant [NaBr] as well as different [NaBr] and $[CTABr]_T = 0$. It is believed that these observations occurred due to medium polarity changes of micellar-catalyzed reactions with increasing values of $[DDABr]_T$. However, this micellar effects give only partial contribution to the total micellar catalytic effects on reaction rate constants (Brinchi *et al.*, 2010; Khan *et al.*, 2000; Khan & Fagge, 2018; Scarpa *et al.*, 2000). In order to explore the reliability of this, a series of kinetic runs was carried out on piperidinolysis of PSaH within CH_3CN range 2 - ≤ 96 % v/v in mixed aqueous solvents at a constant [NaOH], 100 mM Pip, 370 nm and 35 °C. The values of kinetic parameters, k_{obs}, δ_{ap} and A_∞ are summarized in **Table S4** (see Appendix A - **Table S4**), for both series of kinetic runs at 5 and 10 mM NaOH. It is relevant to note that the observed data fit to the pseudo-first-order kinetic equation, **Eq. 3.13** was satisfactory even though the reaction mixtures were slightly cloudy to the naked eye at ≥ 90 % v/v CH_3CN. The reliability of these kinetic parameters is evaluated from the percent residual errors (RE = 100 × ($A_{ob\ i}$ – $A_{cald\ i}$)/$A_{ob\ i}$) listed in **Table S4** for these two representative kinetic runs.

(c) Determination of K_S^0 Values for Piperidinolysis of PSa$^-$ in Aqueous DDABr System

The effects of $[DDABr]_T$ on k_{obs} values has been attempted to be explain in terms of PM model of micelles (Bunton & Savelli, 1987). The values of k_{obs} as exhibited by a plot of k_{obs} versus $[DDABr]_T$ in **Figure 4.10** show a monotonic decrease with increasing $[DDABr]_T$. The quality of the observed data (A_{ob} versus t) fit to **Eq. 3.13** was better in terms of standard deviations associated with the calculated kinetic parameters (k_{obs}, δ_{ap} and A_∞). The values of k_{obs} were obtained by carrying out kinetic runs at $0.0 \leq [DDABr]_T \leq 0.8$ mM as well as at 35 °C and constant [NaBr]. It is noteworthy that the values of k_{obs} appear to be independent of $[DDABr]_T$ less than cmc. Thus, a more reliable value of k_{obs} (=k_W) was obtained which represents the mean value of several k_{obs} obtained within $[DDABr]_T$ range 0 - < cmc. The values of cmc, obtained from iterative (Khan, 2010) as well as graphical (Broxton *et al.*, 1988) techniques for different set of [NaBr] within its range 0 – 100 mM and 35 °C, are not significantly different from each other. The cmc is expected to decrease with increasing [NaBr] which is evident within [NaBr] range 0.0 – 6.0 mM. However, the values of cmc appear to be almost similar within [NaBr] range 10 – 100 mM. The calculated values of cmc and k_W are summarized in **Table 4.4** for different [NaBr] values.

Table 4.4: Values of the Intercept (α) and Slope (K_S) of Linearized Form of **Eq. 4.6** Using k_{obs} Values Obtained at Cmc < $[DDABr]_T \le 0.08$ mM and Different [NaBr].[a]

[NaBr] (mM)	10^2 cmc [b] (mM)	10^2 cmc [c] (mM)	10^3 k_W [d] (s^{-1})	α[e]	10^{-3} K_S (M^{-1})	10^{-3} K_S^{cald} [f] (M^{-1})	10^2 $[DDABr]_T$ range (mM)
0.0	1.2	1.2	29.8 ± 0.6[g]	0.78 ± 0.04[g]	17.9 ± 0.9[g]	-	1.2 – 8.0
0.0	1.0	1.0	30.3 ± 0.1	0.81 ± 0.05	19.4 ± 1.1	-	1.0 – 8.0
1.0	0.7	0.6	30.7 ± 0.8	0.91 ± 0.02	16.3 ± 0.6	16.8	1.0 – 6.5
2.0	1.0	0.9	30.4 ± 0.3	0.86 ± 0.02	15.6 ± 0.5	15.6	1.2 – 8.0
3.0	0.7	0.6	30.1 ± 0.3	0.91 ± 0.02	15.7 ± 0.5	14.7	1.0 – 8.0
5.0	0.6	0.5	30.5 ± 0.4	0.94 ± 0.02	13.1 ± 0.4	13.1	1.0 – 8.0
6.0	0.3	0.2	31.6 ± 0.2	0.97 ± 0.02	12.1 ± 0.7	12.4	1.0 – 8.0
10.0	0.8	0.7	29.5 ± 0.6	0.93 ± 0.02	9.64 ± 0.67	10.2	1.6 – 8.0
20.0	0.4	0.4	29.9 ± 0.4	0.97 ± 0.02	7.47 ± 0.40	7.1	1.0 – 8.0
50.0	0.0	0.0	30.3 ± 0.1	1.00 ± 0.01	6.61 ± 0.37	(3.75)[h]	0.7 – 8.0
100.0	0.6	0.5	29.9 ± 0.3	0.96 ± 0.02	8.85 ± 0.43	(2.09)	1.2 – 6.5

[a] [PSaH] = 0.2 mM, 30 mM NaOH, 100 mM Pip, 35 °C, λ = 370 nm and aqueous reaction mixture, for each kinetic run, contains 2 % v/v CH_3CN. [b] Values of cmc were obtained from graphical technique. [c] Values of cmc were calculated from the relationship: $\alpha = 1 - \text{cmc}K_S$ with α and K_S values listed in **Table 4.4**. [d] k_W represents mean value of several k_{obs} obtained within $[DDABr]_T$ range 0 - < cmc. [e] $\alpha = 1 - \text{cmc}K_S$. [f] Calculated from **Eq. 2.1** with M_vX = NaBr, 10^{-3} K_S^0 = 18.0 M^{-1} and $K_{Br/S}$ = 76 M^{-1} as described into the text. [g] Error limits are standard deviations. [h] Parenthesized values represent K_S^{cald} calculated from **Eq. 2.1** with 10^{-3} K_S^0 = 18.0 M^{-1} and $K_{Br/S}$ = 76 M^{-1}.

It is important to note the occurrence of ion exchange processes between Br^-/HO^-, Br^-/PSa^- and HO^-/PSa^- in the aqueous DDABr system. But the relatively effective ion exchange process under this condition is Br^-/PSa^- (Khan *et al.*, 2000). According to **Eq. 2.1**, the ion exchange process between Br^-/PSa^- (M_vX = NaBr, thus X^- = Br^-) should change the K_S value with the increase in $[Br^-]_T$. However, the change in K_S value with increasing $[DDABr]_T$ (= 0.01 – 0.80 mM) as well as at constant [NaBr] is considered to be insignificant due to the large different in hydrophobicity of Br^- and PSa^- and a very small increase in $[Br^-]$.

The plots of **Figures 4.11** and **S6** reveal monotonic increase of δ_{ap} with increasing $[DDABr]_T$ at a constant [NaBr] and temperature. This observation is due to the decrease in $[H_2O]$ in the micellar environment of micellized PSa^- with the increase in $[DDABr]_T$ at a constant [NaBr] range 0.0 – 20 mM. However, such observations were not obtained under essentially similar conditions for the aqueous systems containing CTABr micelles. The values of δ_{ap} revealed the medium polarity of micellized PSa^- which are equivalent to the polarity of mixed CH_3CN-H_2O solvent containing ~90 – 92 % v/v CH_3CN. The values of δ_{ap} at [NaBr] = 0 are independent of $[DDABr]_T$ within its range 0.0 – 0.01 mM. Thus, the mean value of it is 1730 ± 27 $M^{-1}cm^{-1}$. From **Figure 4.11**, there are clearly two break points as indicated by the values of δ_{ap} at ~0.01 and ~0.08 mM DDABr as well as [NaBr] = 0. These breaks may be attributed to the aggregate structural transitions, cmc and cvc (critical vesicle concentration) (Grillo *et al.*, 2008; Ono *et al.*, 2005; Soltero *et al.*, 2000).

The presence of cvc in aqueous DDABr/H_2O solutions has been clearly demonstrated as in a few relatively recent reports (Grillo *et al.*, 2008; Ono *et al.*, 2005). The reported values of cmc and cvc at 25 °C were 0.046 mM and 0.73 mM, respectively (Soltero *et al.*, 2000). However, as mentioned in **Table 4.4**, the value of cmc (= 0.011 mM) which was determined by graphical method at [NaBr] = 0, is significantly lower than the reported cmc values (Grillo *et al.*, 2008; Kunitake *et al.*, 1980; Ono *et al.*, 2005; Soltero *et al.*, 2000). It is well known that the presence of 0.2 mM PSa^- in such micellar reaction mixture may resulted in cmc decrease (Khan, 2010; Khan *et al.*, 2000; Kunitake *et al.*, 1980; Yusof & Khan, 2012).

In **Figure 4.10,** the k_{obs} values obtained within 0.014 – 0.080 mM DDABr and [NaBr] = 0, were used to calculate the value of k_M (= k_M^{mr} $K_N[N]_T$) and K_S from **Eq. 4.6** by the use of nonlinear least-squares technique considering k_W (= k_W^n $[N]_T$) as a known parameter. The value of k_W is (29.9 ± 0.5) × 10^{-3} s^{-1} which was obtained as the mean value of k_{obs} obtained within $[DDABr]_T$ range 0.0 – 0.01 mM. The least-squares calculated value of K_S is 8091 ± 3763 M^{-1} with cmc = 0.012 mM, determined by graphical technique. However, the value of k_M turns out to be negative (= -1.9 ± 1.6) × 10^{-2} s^{-1} with large standard deviations associated with it, which indicates merely insignificant contribution of k_M^{mr} $K_NK_S[D_n]$ compared with k_W^n, in **Eq. 4.6**. As a result, $k_W^n >> k_M^{mr}$ $K_NK_S[D_n]$. Thus, **Eq. 4.6** is reduced to **Eq. 4.7** at cmc < [DDABr] ≤ 0.08 mM.

$$k_{obs} = \frac{k_W}{1 + K_S[D_n]} \qquad \textbf{Eq. 4.7}$$

The plots of k_W/k_{obs} versus $[DDABr]_T$ appear to be linear within $[DDABr]_T$ range 0.0 - ≤ 0.08 mM (**Figures 4.12** and **S8** (see Appendix D - **Figures S8**)) with intercept and slope value of α (= 1 – cmc K_S) and K_S, respectively. The values of α and K_S were calculated using **Eq. 4.7** by considering k_W as a known parameter. Again, the value of k_W was evaluated as the average value of k_{obs} obtained within 0.0 - < cmc. **Table 4.4** summarized the linear least-squares calculated values of α, K_S and k_W obtained at constant [NaBr]. The observed data was satisfactorily fit to the linear equation of (k_W/k_{obs} = α + $K_S[DDABr]_T$), due to the reliable values of percent residual errors, RE (= 100 × ($k_W/k_{obs\ i}$) – ($k_W/k_{cald\ i}$)/($k_W/k_{obs\ i}$) as well as standard deviations associated with the calculated values of α and K_S. The maximum and minimum values of RE are 9.8 and 0.2 %, respectively. The repeat set of kinetic runs at [NaBr] = 0 yields similar result where the calculated values of α and K_S are also shown in **Table 4.4**. It is interesting to note that the slopes of the linear segments as shown in **Figures 4.12** and **S8** decrease more rapidly in the presence of vesicles compared to WM with increasing [NaBr]. However, the k_{obs} values for the piperidinolysis of PSa^- in the presence of CTABr micelles were not sensitive to [NaBr] (Khan *et al.*, 2000).

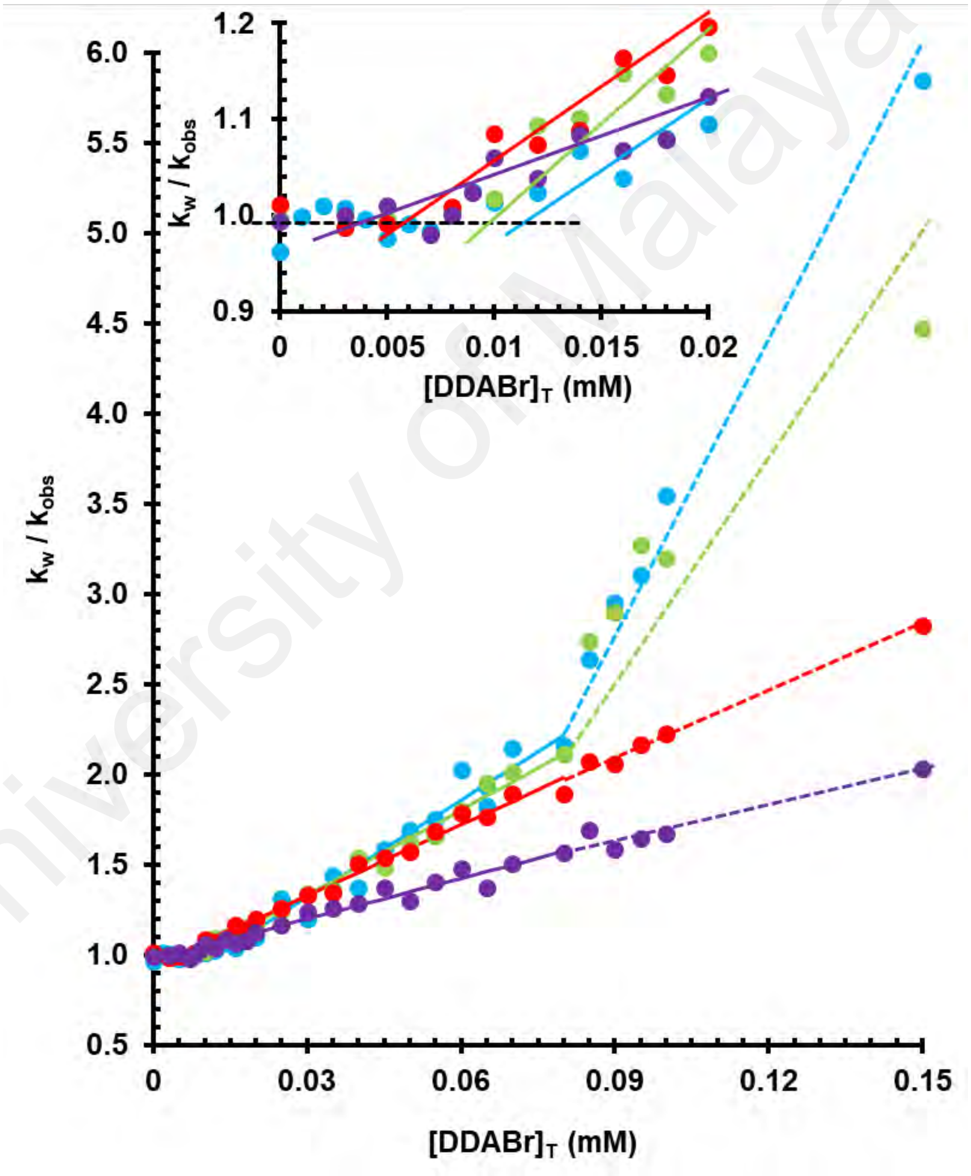

Figure 4.12: Plots showing the dependence of k_W/k_{obs} upon $[DDABr]_T$ for piperidinolysis of PSa^- at 0.2 mM PSa^-, 0.03 M NaOH, 0.1 M Pip and [NaBr] (mM) = 0 (blue), 2 (green), 5 (red) and 20 (purple) at 35 °C. The solid lines are drawn through the calculated data points from the relationship: $k_W/k_{obs} = \alpha + K_S[DDABr]_T$ with α and K_S listed in Table 4.4. Inset: The plots for the data points at the lowest values of $[DDABr]_T$ are shown at magnified scale.

The value of cvc could be determined by graphical method due to the presence of the break points in the plots of k_W/k_{obs} versus $[DDABr]_T$. However, the break points occured at $\leq$ 0.003 M NaBr only and disappeared at $\geq$ 0.005 - $\leq$ 0.020 M NaBr (**Figures 4.12** and **S8**). At [NaBr] = 0, the value of δ_{ap} in the range 2100 – 2200 $M^{-1}cm^{-1}$ corresponds to cvc in the plot of δ_{ap} versus $[DDABr]_T$ (**Figure 4.11**). In order to determine the cvc values for other [NaBr] $\geq$ 0.005 M as well, the specific values of $[DDABr]_T$ (where the values of δ_{ap} become ~2100 – 2200 $M^{-1}cm^{-1}$) were assigned as the values where the cvc occurs. In vesicle phase, the value of k_W is not possible to be determined experimentally. Thus, the kinetic data of this region were tried to fit to **Eq. 4.6** by considering k_W $(= k_W^n [N]_T)$, k_M $(= k_M^{mr} K_N[N]_T)$ and K_S as three unknown parameters. The nonlinear least-squares calculated values of these three unknown parameters, as well as cvc values at different [NaBr] are shown in **Table 4.5**. The observed data fit to **Eq. 4.6** appears to be satisfactory in terms of residual errors as evident from some representative plots of **Figure 4.13**, where solid lines are drawn through the calculated data points. However, the calculated values of k_W, k_M and K_S may be considered to be less reliable because of uncertainty associated with the values of cvc. Besides, the k_{obs} value at cvc should be equal to the corresponding calculated value of k_W using **Eq. 4.6**, but these two values differ in the range of 0.4 – 15.0 %.

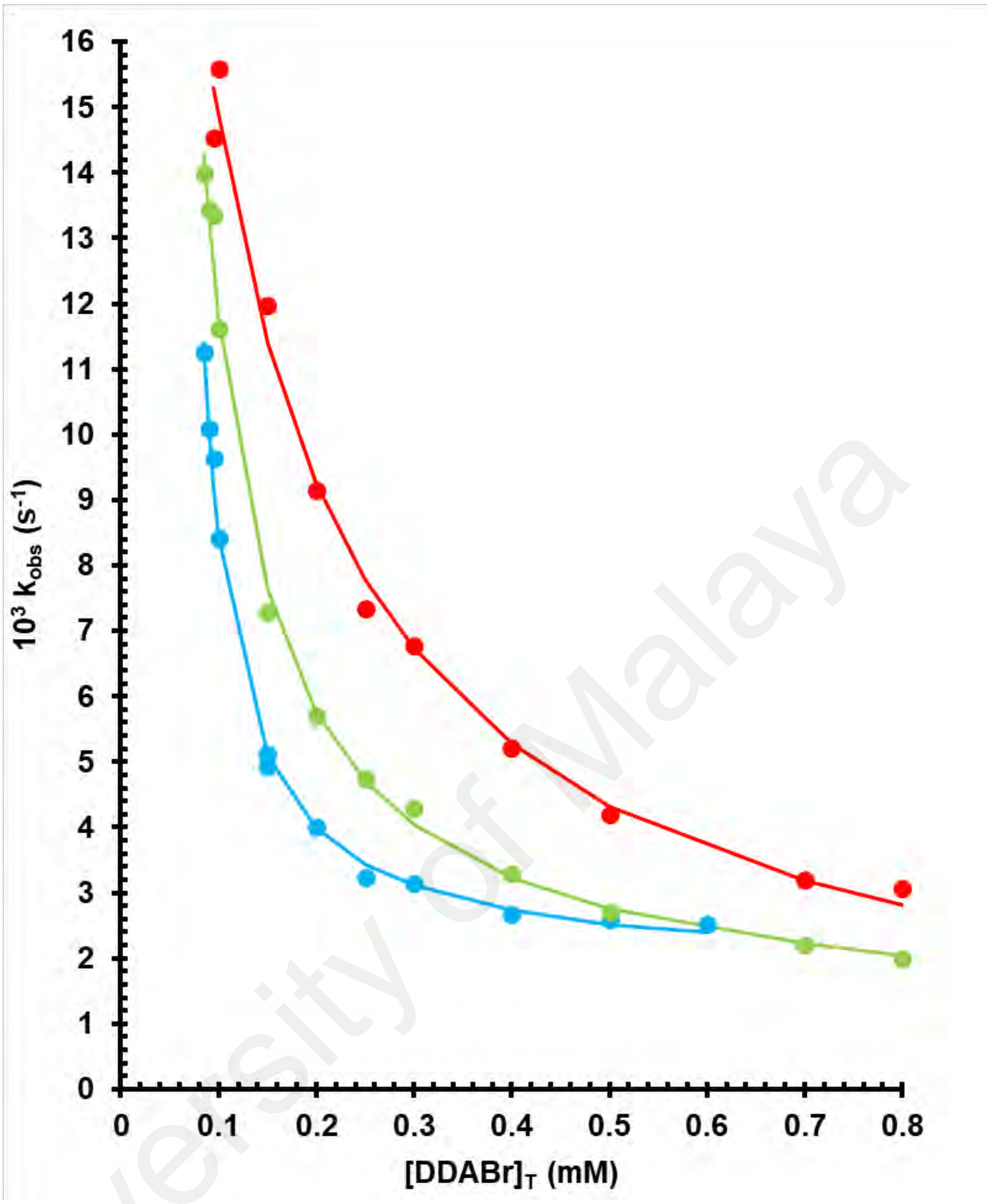

Figure 4.13: Plots showing the dependence of k_{obs} upon $[DDABr]_T$ for piperidinolysis of PSa^- at 0.2 mM PSa^-, 0.03 M NaOH, 0.1 M Pip and [NaBr] (mM) = 0 (blue), 3 (green) and 10 (red) at 35 °C. The solid lines are drawn through the calculated data points using Eq. 4.6 with k_M, K_S and k_W, listed in Table 4.5.

Table 4.5: Values of Kinetic Parameters, k_W , k_M and K_S, Calculated From **Eq. 4.6** Using k_{obs} Values Obtained at Cvc < $[DDABr]_T \le 0.80$ mM and Different Values of [NaBr].

[NaBr] (mM)	10^2 cvc [a] (mM)	$10^3 k_W$ ($10^3 k_{obs}$)[b] (s^{-1})	$10^3 k_M$ [c] (s^{-1})	$10^{-3} K_S$ (M^{-1})	$10^{-3} K_S^{cald}$ [d] (M^{-1})	10^2 $[DDABr]_T$ range (mM)
0.0		13.0 ± 0.3[e] (13.8)	1.79 ± 0.14[e]	34.2 ± 3.3[e]		9.0 – 60.0
0.0	8.0 (8.0)	13.8 ± 0.7 (12.8)	1.74 ± 0.21	33.1 ± 6.0		9.0 – 65.6
1.0	8.0 (8.0)	15.4 ± 0.4 (16.2)	1.21 ± 0.23	25.3 ± 2.9	24.4	8.0 – 80.0
2.0	6.6 (7.0)	16.5 ± 1.0 (18.8)	0.64 ± 0.25	16.1 ± 2.6	18.7	8.5 – 80.0
3.0	5.0 (6.6)	16.5 ± 0.3 (14.3)	0.94 ± 0.28	16.7 ± 1.9	15.1	8.5 – 80.0
5.0	8.0 (8.0)	21.1 ± 2.2 (19.4)	0.32 ± 0.70	11.2 ± 3.2	10.9	9.5 – 80.0
6.0	5.0	20.0 ± 2.0 (20.4)	-0.7 ± 1.0	8.40 ± 2.6	9.7	9.5 – 80.0
	4.5	21.2 ± 1.6	0.0	10.3 ± 1.6		9.5 – 80.0
10.0		20.4 ± 1.2 (19.5)	-0.1 ± 0.8	8.27 ± 1.8	6.5	9.5 – 80.0
	5.5	20.5 ± 0.8	0.0	8.37 ± 0.78		9.5 – 80.0
20.0		23.8 ± 0.4 (22.7)	-0.3 ± 0.4	5.89 ± 0.44	(3.6)[f]	9.5 – 80.0
	4.5	24.0 ± 0.3	0.0	6.17 ± 0.18		9.5 – 80.0
50.0		23.0 ± 0.3 (23.7)	-0.7 ± 0.9	2.70 ± 0.25	(1.5)	9.5 – 70.0
	2.5	23.3 ± 0.2	0.0	2.93 ± 0.7		9.5 – 80.0
100.0		24.6 ± 1.4 (24.5)	3.96 ± 1.45	4.82 ± 1.44	(0.8)	9.5 – 70.0

[a] Parenthesized values of cvc were obtained from graphical technique. [b] Parenthesized value represents k_{obs} experimentally obtained at $[DDABr]_T$ = cvc and $k_W = k_W^n [N]_T$ with $[N]_T = 0.1$ M. [c] $k_M = k_M^{mr} K_N [N]_T$ with $[N]_T = 0.1$ M. [d] Calculated from **Eq. 4.6** with $10^{-3} K_S^0 = 35.0 \ M^{-1}$ and $K_{Br/S} = 437 \ M^{-1}$ as described into the text. [e] Error limits are standard deviations. [f] Parenthesized values represent K_S^{cald} calculated from **Eq. 4.6** with $10^{-3} K_S^0 = 35.0 \ M^{-1}$ and $K_{Br/S} = 437 \ M^{-1}$.

In **Table 4.5**, the negative calculated values of k_M with large standard deviations associated with it are physicochemically meaningless due to the large contribution of k_W (i.e. $k_W >> k_M K_S[D_n]$ in **Eq. 4.6**). The k_W and K_S values were also calculated using **Eq. 4.6** by assuming the value of k_M as zero (i.e. $k_M = 0$). These calculated values of k_W and K_S for both $k_M = 0$ and $k_M \neq 0$ are not significantly different from each other. Such calculated values of k_W, k_M and K_S are shown in **Table 4.5**. The values of k_M as shown in **Table 4.5** decrease with increasing [NaBr]. However, the k_{obs} values obtained from the present study are similar to the corresponding values of k_M obtained from the aqueous solution of CTABr in the absence and presence of NaBr (Khan *et al.*, 2000). The most reliable answer for these observations may be attributed to different average locations of reactants Pip and PSa^- in SVs mixed with MLV of DDABr (Otto *et al.*, 1998).

Experimental works of a recent study (Grillo *et al.*, 2008) on DDABr/D_2O or H_2O systems provides an evidence for the presence of globular prolate micelles (i.e. WM) at $[DDABr]_T$ > cmc (= 0.046 mM) and very small vesicles (SVs) followed by large multilamellar vesicles (MLV) at $[DDABr]_T$ > cvc (= 0.73 mM DDABr). The presence of PSa^- in such micellar solution is expected to decrease the values of cmc and cvc. In view of these reports, the structure of DDABr micelles under the conditions of the present study may be considered to be WM and SVs + MLV at > 0.012 and > 0.08 mM DDABr, respectively. The flow curves of aqueous solution containing 0.06 mM DDABr/H_2O and 0.6 mM DDABr/H_2O, carried out within $\dot{\gamma}$ range 2 – 10^3 s^{-1}, reveal Newtonian flow behavior with the viscosity of water. Earlier study also had reported the similar observations (Soltero *et al.*, 2000). These observations reveal indirectly that the size of WM as well as SVs and MLV are not large enough to form entangled networks under quiescent state. The polarity of the micellar environment of micellized PSa^- in the presence of WM as well as SVs and MLV are equivalent to ~25 % and ~50 - < 94 % v/v CH_3CN of mixed CH_3CN-H_2O solvent, respectively as evident from the values of δ_{ap} obtained at different contents of CH_3CN in mixed aqueous solvents (see Appendix A -

Table S4) as well as at different values of [DDABr]$_T$ (**Figure 4.11** and see Appendix D - **Figure S6**).

The values of δ_{ap} are smaller in the presence of WM compared to that in the presence of Vs. A recent study (LóPez-BarróN *et al.*, 2012) observed the spontaneous thermoreversible formation of DDABr vesicles and WM in a protic ionic liquid. In order to find out the effects of higher temperature on the structure of DDABr aggregates, a few kinetic runs were carried out at 0.2 mM DDABr, 55 °C and within [NaBr] range 0.0 – 0.10 M. The calculated values of δ_{ap} at 55 °C were similar to those at 35 °C. Similar observations were obtained at 0.4 and 0.6 mM DDABr. The results indicate that the structures of DDABr aggregates remain unchanged with increasing temperature to 55 °C, which reveals the vesicular structure of DDABr aggregates are thermally stable under such conditions. Thus, it reveals the probable higher thermodynamic stability of DDABr aggregate structures in water than that in protic ionic liquid (LóPez-BarróN *et al.*, 2012).

The observed K_S values of aqueous DDABr solutions are described as follows: (a) In micellar phase, the calculated K_S values (**Table 4.4**) decreased nonlinearly by ~2.5-fold with increasing [NaBr] from 0 – 20 mM, and became almost independent of [NaBr] within its range 20 – 100 mM. The values of K_S were found to follow **Eq. 2.1** within [NaBr] range 1.0 – 20 mM, resulting in the calculated values of K_S^0 and $K_{Br/S}$ as ((18.0 ± 0.6) × 10^3) M^{-1} and (76 ± 10) M^{-1}, respectively. The standard deviations associated with the calculated parameters K_S^0 and $K_{Br/S}$, as well as maximum percent residual error of 6.5 % at 3 mM NaBr (**Table 4.4**) reveal directly the reliability of the data fit to **Eq. 2.1**. It is noteworthy that the value of K_S^0 obtained from **Eq. 2.1** is similar to the average value of K_S (= (18.7 ± 0.7) × 10^3 M^{-1}) obtained from the duplicate set of kinetic runs at [NaBr] = 0. The smaller values of K_S^{cald} (i.e. 1.8- and 4.2-fold smaller) than the corresponding K_S values at respective 50 and 100 mM NaBr, reveal a most probable Br-induced DDABr aggregate structural transitions from WM to most likely Vs under such reaction conditions. (b) In vesicular phase (i.e. at [DDABr] > 0.08 mM), the determined K_S values were also treated with **Eq. 2.1** for [NaBr] range 0.0 – 10 mM. The least-squares calculated values of K_S^0 and $K_{Br/S}$ are (35.0 ± 5.5) × 10^3 M^{-1} and 437 ± 141 M^{-1}, respectively. These values of K_S^0 and $K_{Br/S}$ are considered to be reliable due to the expected larger values of K_S^0 and $K_{Br/S}$ obtained in the presence of vesicles rather than that in the presence of WM. There is ~4 % larger calculated value of K_S^0 compared to the average value of K_S (= 33.7 × 10^3 M^{-1}) obtained experimentally at [NaBr] = 0 (**Table 4.5**). However, the calculated values of K_S^0 and $K_{Br/S}$ for vesicular phase are not very reliable due to moderate high standard deviations (std) associated with it (i.e. 16 % and 32 % std of respective K_S^0 and $K_{Br/S}$).

4.1.2 Determination of R_X^{Br} Value by SESp Method

4.1.2.1 Determination of K_S^0 Value of N-2-MeOPhPT$^-$ to CTABr Micelles in the Absence of M_vX (with M_vX = NaBr or Aliphatic Acids and v = 1)

Instead of SEK method, the value of K_S^0 is also needed in the use of SESp method for the determination of R_X^{Br} value. The values of initial absorbance, A_{ob} for several samples were obtained at 310 nm and 35 °C, for aqueous surfactant solution containing 0.3 mM N-2-MeOPhPT$^-$ (S^-), 10 mM NaOH and $0 \leq [CTABr]_T$ (mM) ≤ 15. The values of A_{ob} in the region lower than cmc, were almost independent upon $[CTABr]_T$. Then, increase with a monotonic trend with increasing $[CTABr]_T$ until ~3 mM CTABr, and finally became almost independent of $[CTABr]_T$. Similar observations were obtained for the system containing 0.25 mM N-2-MeOPhPT$^-$, 10 mM NaOH, $0 \leq [CTABr]_T$ (mM) ≤ 15, $\lambda = 310$ nm and 35 °C.

The substrate, N-2-MeOPhPTH, under the present study is highly nonreactive towards hydrolysis process under mild alkaline pH. The anionic probe molecule for SESp method needs to be moderately hydrophobic and fully anionic as well as nonreactive through the entire spectrophotometric measurements. It needs to be slightly hydrophobic in order to make it remains in the cationic micellar pseudophase in the absence of any inert salt. The values of the molar absorptivity of N-2-MeOPhPT$^-$, in the absence and presence of 15 mM CTABr at 310 nm, are 1250 and 2470 $M^{-1}cm^{-1}$, respectively (Khan *et al.*, 2013). Thus, a monotonic increase of A_{ob} with increasing $[CTABr]_T$ at 310 nm could be explained quantitatively in terms of PM model (Bunton, 1979; Bunton & Savelli, 1987; Khan *et al.*, 2013). A brief distribution mechanism of N-2-MeOPhPT$^-$ (i.e. S^-), in terms of PM model and under the typical spectrophotometric conditions of the present study, is expressed as,

$$S_W^- + D_n \overset{K_S^0}{\rightleftharpoons} S_M^- \qquad \textbf{Eq. 4.8}$$

where S_W^- and S_M^- represent respective N-2-MeOPhPT$^-$ in bulk water phase and micellar pseudophase, D_n represents CTABr micelles (i.e. $[D_n] = [CTABr]_T - cmc$), and $K_S^0 = K_S$ at $[M_vX] = 0$. The relationship of $A_{ob} = \delta_W[S_W^-] + \delta_M[S_M^-]$, (with δ_W and δ_M representing molar absorptivity of S^- = N-2-MeOPhPT$^-$ obtained at 310 nm in water phase and micellar pseudophase, respectively) as well as **Eq. 4.8** can lead to **Eq. 4.9** (Khan *et al.*, 2013),

$$A_{ob} = \frac{A_W + A_M K_S^0[D_n]}{1 + K_S^0[D_n]} \qquad \textbf{Eq. 4.9}$$

where $K_S^0 = K_S$ at $[M_vX] = 0$, $[D_n] = [CTABr]_T - cmc$, $A_W = \delta_W[S]_T$, $A_M = \delta_M[S]_T$ and $[S]_T = [S_W^-] + [S_M^-]$.

The observed value of A_{ob} at different $[CTABr]_T$ were treated with **Eq. 4.9**. The nonlinear least-squares calculated values of A_M and K_S^0, under the present spectrophotometric conditions and at 0.3 mM N-2-MeOPhPT$^-$, are 0.633 ± 0.089 and 3624 ± 117 M^{-1}, respectively. The value of A_W (= 0.343) was obtained experimentally in the absence of CTABr, while the cmc value, under present spectrophotometric conditions, determined by kinetic iterative technique (Khan, 2006; Khan *et al.*, 2013) is 0.26 mM. The observed data of A_{ob} versus $[D_n]$ were found to fit satisfactorily to **Eq. 4.9** as evidence from the standard deviations associated with the calculated values of A_M and K_S^0 as well as percent residual errors ($\leq$ 3.1 %) obtained at each data point within $[CTABr]_T$ range 0.0 – 0.015 M. Almost similar values of A_M and K_S^0 were obtained at 0.25 mM N-2-MeOPhPT$^-$, where the respective calculated values of A_M and K_S^0 are 0.570 ± 0.005 and 3706 ± 293 M^{-1}.

4.1.2.2 Effects of $[M_vX]$ ($\nu = 1$) on A_{ob} of Aqueous Solution Containing Constant Concentration of CTABr, NaOH and N-2-MeOPhPT$^-$ at 35 °C and $\lambda = 310$ nm

A series of spectrophotometric runs were carried out at 310 nm and 35 °C, as well as constant concentration of 0.3 mM N-2-MeOPhPTH, 0.01 M NaOH, 0.005 M CTABr and different values of $[M_vX]$, within its range 0.0 - $\leq$ 2.0 M (for M_vX = NaBr). Similar results were obtained at 0.006, 0.01 and 0.015 M CTABr under the same experimental conditions. The values of absorbance ($A_{ob}^{M_vX}$) were also obtained at 310 nm for the samples containing all mixtures except 0.3 mM N-2-MeOPhPTH due to the detectable absorption of certain $[M_vX]$ at this wavelength. Thus, the values of ΔA_{ob} (= A_{ob} - $A_{ob}^{M_vX}$) corresponds to the corrected values of absorbance due to the presence of only 0.3 mM N-2-MeOPhPT$^-$ with A_{ob} representing the absorbance value obtained due to the presence of M_vX, CTABr, NaOH and N-2-MeOPhPT$^-$ while $A_{ob}^{M_vX}$ corresponds to the absorbance value of only M_vX, CTABr and NaOH. However, the values of $A_{ob}^{M_vX}$ for M_vX = NaBr were found to be insignifant. Similar observations were obtained for several M_vX = aliphatic acids with $\nu = 1$. The observed data (ΔA_{ob} versus $[M_vX]$) are shown graphically in **Figures 4.14 – 4.17** and **Figure S9** (see Appendix E - **Figure S9**).

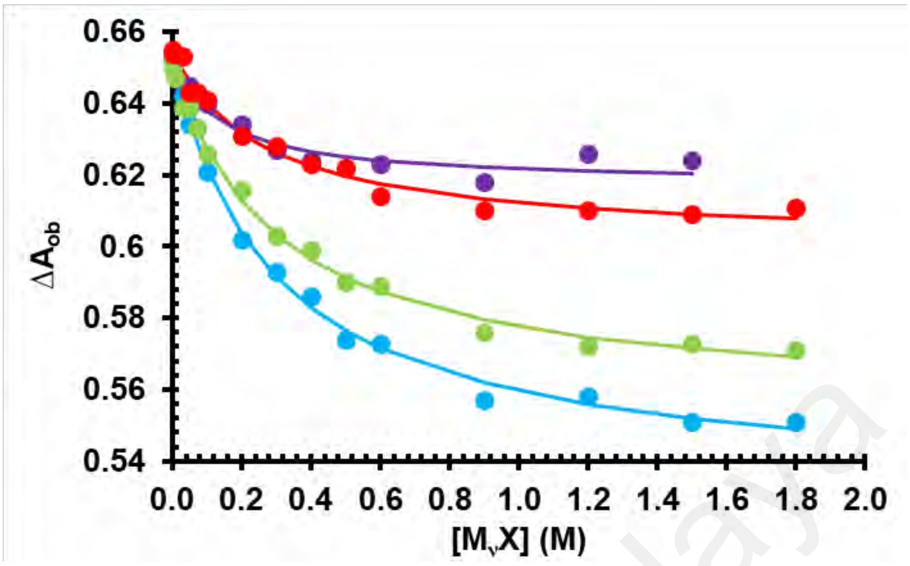

Figure 4.14: Plots showing the dependence of ΔA_{ob} upon $[M_vX]$ for M_vX = sodium acetate at 0.3 mM N-2-MeOPhPTH, 0.01 M NaOH, and [CTABr] (mM) = 5 (blue), 6 (green), 10 (red) and 15 (purple) at 35 °C. The solid lines are drawn through the calculated data points using Eq. 4.10 with θ and $K^{X/S}$ listed in Table 4.6.

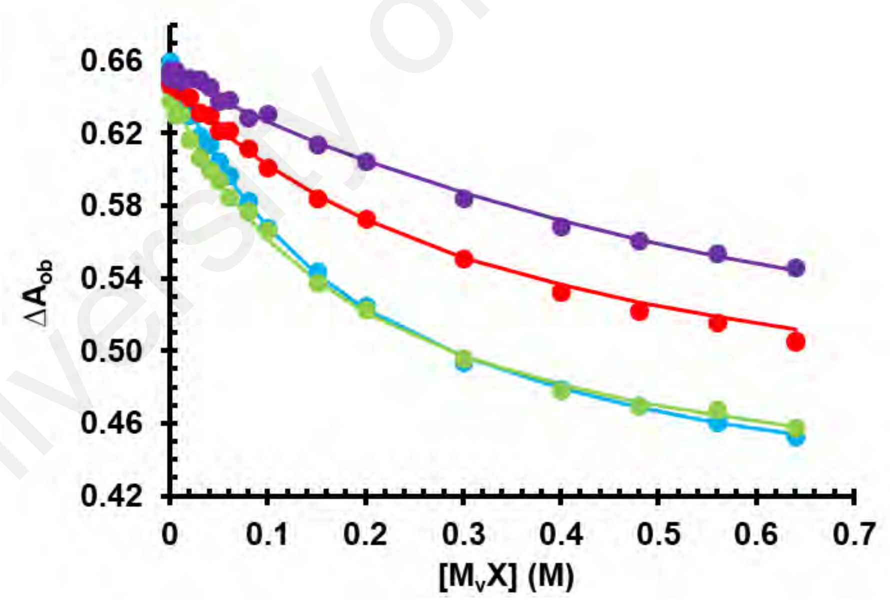

Figure 4.15: Plots showing the dependence of ΔA_{ob} upon $[M_vX]$ for M_vX = sodium butanoate at 0.3 mM N-2-MeOPhPTH, 0.01 M NaOH, and [CTABr] (mM) = 5 (blue), 6 (green), 10 (red) and 15 (purple) at 35 °C. The solid lines are drawn through the calculated data points using Eq. 4.10 with θ and $K^{X/S}$ listed in Table 4.6.

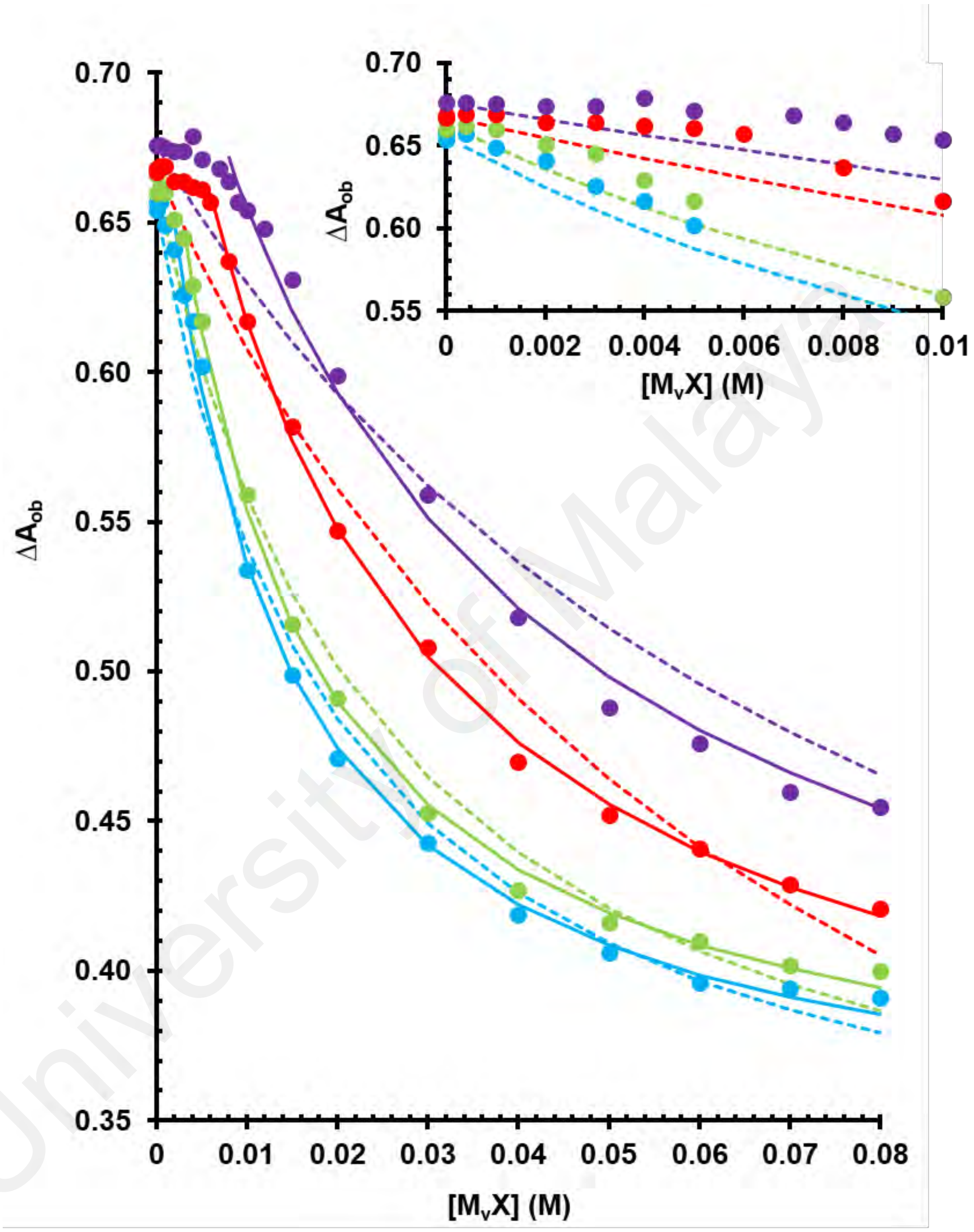

Figure 4.16: Plots showing the dependence of ΔA_{ob} upon $[M_vX]$ for M_vX = sodium heptanoate at 0.3 mM N-2-MeOPhPTH, 0.01 M NaOH, and [CTABr] (mM) = 5 (blue), 6 (green), 10 (red) and 15 (purple) at 35 °C. The solid lines are drawn through the calculated data points using Eq. 4.10 with θ and $K^{X/S}$ listed in Table 4.6.

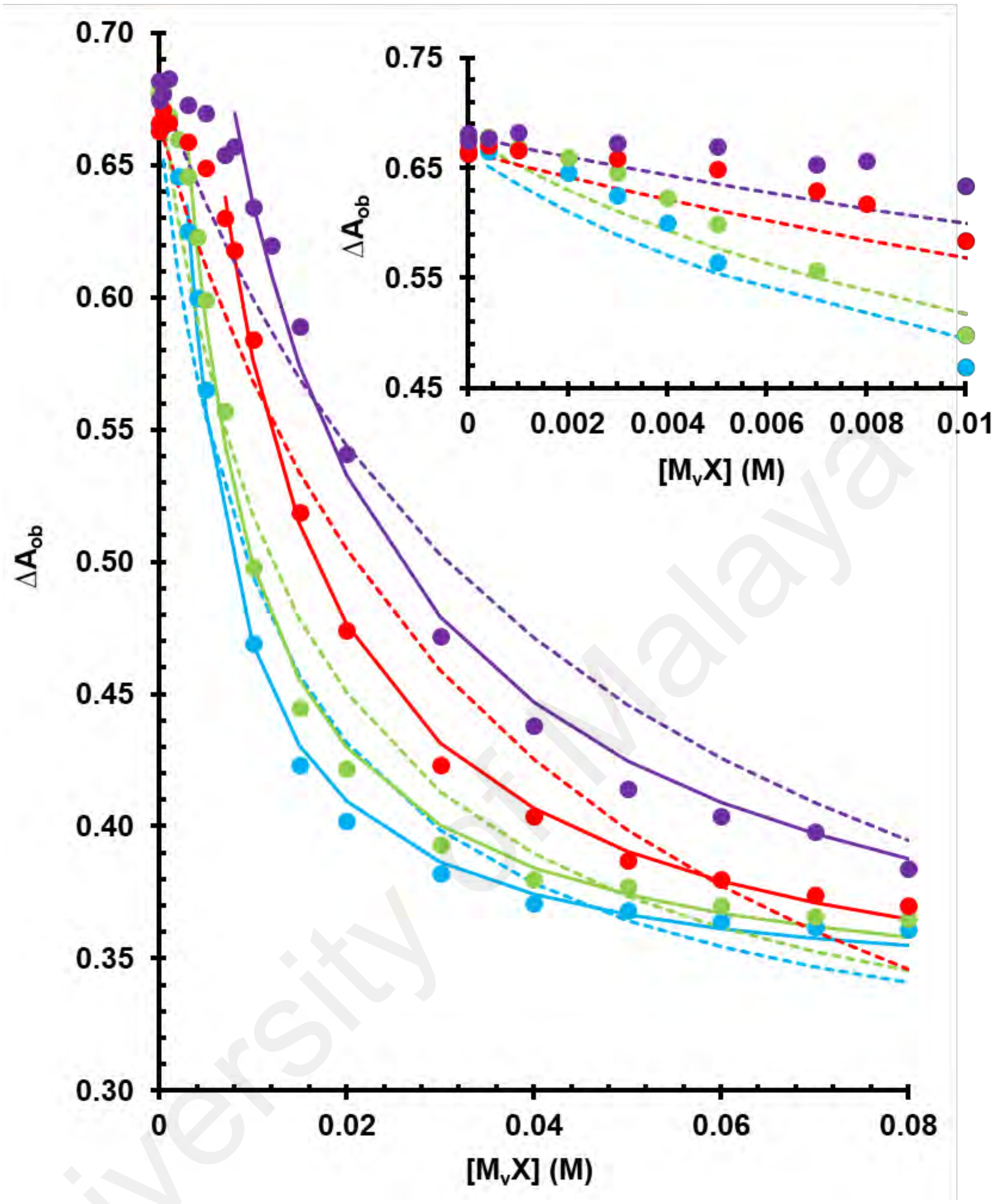

Figure 4.17: Plots showing the dependence of ΔA_{ob} upon $[M_vX]$ for M_vX = sodium octanoate at 0.3 mM N-2-MeOPhPTH, 0.01 M NaOH, and [CTABr] (mM) = 5 (blue), 6 (green), 10 (red) and 15 (purple) at 35 °C. The solid lines are drawn through the calculated data points using Eq. 4.10 with θ and $K^{X/S}$ listed in Table 4.6.

The nonlinear decrease in the plot of ΔA_{ob} with increasing $[M_vX]$ at a constant $[CTABr]_T$ and 35 °C, as exhibited by **Figures 4.14 – 4.17** and **Figure S9**, is attributed to the transfer of micellized N-2-MeOPhPT$^-$, (S^-) from the micellar pseudophase to the bulk aqueous phase through the ion exchange process X^{v-}/S^- (Khan, 2006; Khan *et al.*, 2013). This speculation has been made based on the ΔA_{ob} values, which are slightly larger in CTABr micellar pseudophase than those in bulk aqueous phase (Khan, 2006; Khan *et al.*, 2013). Early studies had reported that the ion exchange processes, as well as the most effective one which could significantly affect the value of ΔA_{ob} (i.e. X^{v-}/S^-), under the present experimental conditions, are similar to that in SEK method (Khan, 2006; Khan *et al.*, 2013).

The effective occurrence of ion exchange between X^{v-}/S^- in the related system, at a constant $[CTABr]_T$ and temperature as well as increasing $[M_vX]$ results in the decrease of K_S value (as expressed in **Eq. 2.1**) (Khan, 2006; Khan *et al.*, 2013). **Eq. 2.1** and **Eq. 4.9** (with replacement of K_S^0 by K_S) will give **Eq. 4.10**,

$$\Delta A_{ob} = \frac{A_{ob}^0 + \theta K^{X/S}[M_vX]}{1 + K^{X/S}[M_vX]} \qquad \textbf{Eq. 4.10}$$

where ΔA_{ob} (= A_{ob} - $A_{ob}^{M_vX}$), A_{ob}^0 (= ΔA_{ob} at $[M_vX] = 0$) and other empirical parameters θ, $K^{X/S}$ are expressed by the following respective **Eq. 4.12** and **Eq. 4.13**,

$$A_{ob}^0 = \frac{A_W + A_M K_S^0[D_n]}{1 + K_S^0[D_n]} \qquad \textbf{Eq. 4.11}$$

where A_W and A_M represent the absorbance value at respective $[CTABr]_T = [M_vX] = 0$, and $[CTABr]_T \neq 0$ as well as $[M_vX] = 0$. It is perhaps noteworthy that under the limiting conditions, where $A_M K_S^0$ $[D_n] >> A_W$ and K_S^0 $[D_n] >> 1$, the value of $A_M = A_{ob}^0$ (Khan *et al.*, 2013),

$$(A_M - \theta) = F_{X/S}(A_M - A_W) \qquad \textbf{Eq. 4.12}$$

where $F_{X/S}$ is an empirical constant which its value vary between > 0 - ≤ 1.0 (Khan *et al.*, 2013), and

$$K^{X/S} = K_{X/S}/(1 + K_S^0[D_n]) \qquad \textbf{Eq. 4.13}$$

It is noteworthy that the empirical constant of $K^{X/S}$ (**Eq. 4.13**) derived from SESp method (Khan *et al.*, 2013) is similar to that in SEK method (**Eq. 4.3**). From **Eq. 4.12**, it is evident that $\theta = A_W$ when $F_{X/S} = 1$. The appearance of $F_{X/S}$ in such micellar system is due to the empirical consequence, where in physical reality, the hydrophilic counterions, at $\geq$ limiting concentration of $[M_vX]$ cannot expel completely (i.e. 100 %) hydrophobic counterions from the micellar pseudophase to the bulk aqueous phase (Khan *et al.*, 2013). Such empirical approach is derived when the theoretical consequence is unable to explain partially an apparent physical reality (Khan *et al.*, 2013). One example which is similar to the present approach is the appearance of "transmission coefficient" κ in the theory of absolute reaction rates, where κ represents an empirical constant which defines the fact that not all the activated complex which reside the top of the potential energy barrier is converted into a reaction product (Khan *et al.*, 2013). It is important to note that the limiting concentration of counterions, for instance X^{v-} ions, is equal to the optimum value of $[M_vX]$, where the values of ΔA_{ob} become independent of $[M_vX]$, as in the plots of ΔA_{ob} versus $[M_vX]$.

The observed data of ΔA_{ob} versus $[M_vX]$, as exhibited from the plots of **Figures 4.14 – 4.17** and **Figure S9** were found to fit to **Eq. 4.10**. The unknown parameters of **Eq. 4.10** (θ and $K^{X/S}$) as well as Σdi^2 (where $di = \Delta A_{ob\ i} - \Delta A_{cald\ i}$, with $\Delta A_{ob\ i}$ and $\Delta A_{cald\ i}$ representing the corrected absorbance values obtained by experimental and least-squares calculated ΔA_{ob}, respectively at the ith value of $[M_vX]$) were calculated using the nonlinear least-squares technique, where A_{ob}^{0} value is considered as a known parameter determined experimentally at $[M_vX] = 0$. **Table 4.6** summarized the calculated values of θ, $K^{X/S}$ and Σdi^2 at different $[CTABr]_T$ for different M_vX. The dashed lines as exhibited from the plots of **Figures 4.16** and **4.17** are drawn through the least squares calculated absorbance (ΔA_{cald}) using **Eq. 4.10**, with the calculated values of θ, $K^{X/S}$ and Σdi^2 listed in **Table 4.6**. However, the observed data points of the plots of **Figures 4.16** and **4.17** reveal systematic positive deviations from the dashed lines at the initial lower values of $[M_vX]$. The reasons for this may be explained as follows.

Table 4.6: Values of the Empirical Constants, θ and $K^{X/S}$ Determined by SESp Method for Different M_vX in CTABr Micelles at 35 °C.[a]

$[CTABr]_T$ [b] (mM)	$10^2\ A_{ob}^{0}$ [c]	$[M_vX]_0^{op}$ (mM)	$10^2\ \theta$ (s^{-1})	$K^{X/S}$ (M^{-1})	$F_{X/S}$ [d]	$K_{X/S}$ [e] (M^{-1})	$K^{n}_{X/S}$ [f] (M^{-1})	K_X^{Br} or R_X^{Br} [g]	$[M_vX]$ [h] (mM)	$10^4\ \sum di^2$
M_vX = Sodium acetate										
5	65.3 ± 0.1	0	53.2 ± 0.26[i]	3.42 ± 0.22[i]	0.385	65.4	25.2	0.27	10 – 1800	0.7783
6	65.2 ± 0.2	0	55.6 ± 0.24	3.40 ± 0.26	0.302	77.3	23.3	0.25	10 – 1800	0.6766
10	65.5 ± 0.1	0	60.1 ± 0.22	3.84 ± 0.51	0.170	143	24.3	0.26	10 – 1800	0.6804
15	65.3 ± 0.0	0	61.8 ± 0.22	7.42 ± 1.69	0.109	411	44.8	0.47	10 – 1500	0.9271
M_vX = Sodium propanoate										
5	69.1 ± 0.5	0	50.6 ± 0.56	7.05 ± 0.59	0.546	135	73.6	0.78	10 – 640	3.5115
6	68.1 ± 0.1	0	50.1 ± 0.58	5.78 ± 0.48	0.539	131	70.9	0.75	10 – 640	2.6986
10	65.3 ± 0.2	0	52.9 ± 1.31	2.52 ± 0.51	0.391	93.8	36.7	0.39	5 – 640	2.7027
15	65.9 ± 0.3	0	57.3 ± 0.89	2.08 ± 0.39	0.265	115	30.5	0.32	5 – 640	0.7808
M_vX = Sodium butanoate										
5	65.8 ± 0.3	0	39.1 ± 0.46	5.09 ±0.21	0.832	97.3	81.0	0.86	5 – 640	1.4517
6	64.3 ± 0.5	0	40.2 ± 0.48	5.09 ± 0.25	0.768	116	88.9	0.94	5 – 640	1.6141
10	64.9 ± 0.2	0	43.5 ± 0.43	2.77 ± 0.12	0.675	103	69.6	0.74	5 – 640	0.4824
15	65.3 ± 0.2	0	39.5 ± 2.76	1.14 ± 0.18	0.809	63.1	51.1	0.54	5 – 640	1.3756
M_vX = Sodium pentanoate										
5	64.7 ± 0.4	0	35.7 ± 0.40	10.8 ± 0.35	0.939	206	194	2.05	0.4 – 320	0.9444
6	65.7 ± 0.2	0	36.0 ± 0.52	8.84 ± 0.35	0.928	201	187	1.97	0.4 – 320	1.1929
10	64.5 ± 0.1	0	32.5 ± 1.90	3.98 ± 0.41	1.020	148	151	1.60	0.4 – 320	2.8570
15	67.9 ± 0.4	0	35.3 ± 1.71	3.34 ± 0.29	0.967	185	179	1.89	1.0 – 320	1.3786
M_vX = Sodium heptanoate										
5	65.6 ± 0.2	0	30.8 ± 1.50	48.9 ± 5.86	1.10	935	1028	10.9	0.4 – 80	17.530
5	65.6 ± 0.2	1.7	33.8 ± 0.49	73.0 ± 3.76	1.01	1396	1410	14.9	2 – 80	2.5224
6	66.3 ± 0.4	0	30.1 ± 1.93	40.4 ± 5.55	1.11	919	1020	10.8	0.4 – 80	20.649
6	66.3 ± 0.4	2.3	34.3 ± 0.42	66.6 ± 2.86	0.99	1515	1492	15.8	3 – 80	1.4345

Table 4.6 continued

$[\text{CTABr}]_T$ [b] (mM)	$10^2\ A_{ob}^{0}$ [c]	$[M_vX]_0^{op}$ (mM)	$10^2\ \theta$ (s^{-1})	$K^{X/S}$ (M^{-1})	$F_{X/S}$ [d]	$K_{X/S}$ [e] (M^{-1})	$K_{X/S}^{n}$ [f] (M^{-1})	K_X^{Br} or R_X^{Br} [g]	$[M_vX]$ [h] (mM)	$10^4\ \sum di^2$
10	66.8 ± 0.1	0	15.7 ± 8.24	13.3 ± 3.59	1.55	495	768	8.11	0.4 – 80	38.161
10	66.8 ± 0.1	5.3	32.9 ± 0.63	37.5 ± 1.75	1.03	1397	1438	15.2	6 – 80	0.9755
15	67.6 ± 0.0	0	24.6 ± 5.04	12.0 ± 2.60	1.29	664	857	9.04	0.4 – 80	74.155
15	67.6 ± 0.0	7.5	33.5 ± 1.14	25.7 ± 2.10	1.02	1423	1451	15.3	8 – 80	5.7332
				M_vX = Sodium octanoate						
5	67.1 ± 0.1	0	29.3 ± 2.19	83.8 ± 16.7	1.19	1602	1907	20.1	0.4 – 80	84.149
5	67.1 ± 0.1	2.5	33.4 ± 0.43	193 ± 12.3	1.05	3696	3881	41.0	3 – 80	4.8309
6	68.5 ± 0.1	0	28.5 ± 2.19	68.8 ± 11.6	1.21	1565	1894	20.0	0.4 – 80	73.576
6	68.5 ± 0.1	2.6	32.9 ± 0.57	142 ± 9.59	1.07	3223	3448	36.4	3 – 80	7.7140
10	67.3 ± 0.2	0	18.8 ± 6.14	25.3 ± 6.88	1.50	942	1413	14.9	0.4 – 80	89.873
10	67.3 ± 0.2	6.0	31.7 ± 0.55	84.6 ± 4.77	1.10	3151	3466	36.6	7 – 80	2.7919
15	68.5 ± 0.5	0	22.9 ± 4.73	21.4 ± 4.97	1.36	1185	1611	17.0	0.4 – 80	133.04
15	68.5 ± 0.5	7.5	31.2 ± 1.06	53.2 ± 4.92	1.11	2945	3269	34.5	7 – 80	10.944

[a] $[\text{N-2MeOPhPTH}]_0$ = 0.3 mM at λ = 310 nm, and aqueous reaction mixture for each sample contanins 2 % CH_3CN. [b] Total concentration of CTABr. [c] $A_{ob}^{0} = \Delta A_{ob}$ at $[M_vX] = 0$. [d] $F_{X/S} = (A_M - \theta)/(A_M - A_W)$. [e] $K_{X/S} = K^{X/S}(1 + K_S^0\ [\text{CTABr}]_T)$. [f] $K_{X/S}^{n} = F_{X/S}K_{X/S}$. [g] K_X^{Br} or $R_X^{Br} = K_{X/S}^{n} / K_{Br/S}^{n}$. [h] Total concentration range of M_vX used in the data analysis. [i] Error limits are standard deviations.

It is noteworthy that the most effective ion exchange process occurs at the cationic micellar surface, under the present spectrophotometric conditions, is X^{v-}/S^- (where S^- represents N-2-MeOPhPT$^-$). But, the present spectrophotometric method cannot directly detect the occurrence of ion-exchange process X^{v-}/HO^- and X^{v-}/Br^- because the ΔA_{ob} values, at 310 nm are independent to $[HO^-]$ and $[Br^-]$. However, the occurrence of ion-exchange process X^{v-}/HO^- and X^{v-}/Br^- can affect the ion exchange process between X^{v-}/S^- by decreasing the effective concentration of M_vX, i.e. $[M_vX]_S^{ef}$. According to PM model, the micellar binding process of different counterions is independent of each other. As a result, the magnitudes of the micellar binding constant of different counterion will be independent of each other as well. The ratio of the micellar binding constant of exchanging counterions is used to determine the value of ion exchange constant. Therefore, different ion exchange constant values resulted from various counterionic exchange processes, should also be independent of each other. In the present spectrophotometric system, the hydrophobicity of counterions X^{v-}, Br^- and HO^- varies in the order: $X^{v-} > Br^- > HO^-$. The addition of X^{v-} ions to the present system will cause HO^- ions (which is the most hydrophilic one) to be expelled first from the micellar pseudophase to the bulk aqueous phase. A further increase in $[M_vX]$ has no effect on ion exchange process between X^{v-}/HO^- when $[M_vX] = [M_vX]_{OH}^{op}$ (where $[M_vX]_{OH}^{op}$ represents the saturated decreasing effects of $[M_vX]$ on $[HO_M^-]$ at the optimum value of $[M_vX]$) but it will certainly cause the second most hydrophilic counterions, Br^- to be expelled from the micellar pseudophase to the aqueous phase. Thus, the effective concentration of $[M_vX]$ that could affect the ion exchange process between X^{v-}/Br^- is represented as $[M_vX]_{Br}^{ef} = [M_vX] - [M_vX]_{OH}^{op}$ (Khan *et al.*, 2013). A further increase in $[M_vX]$ has no effect on ion exchange process between X^{v-}/Br^- when $[M_vX] = [M_vX]_{OH}^{op} + [M_vX]_{Br}^{op}$ (where $[M_vX]_{Br}^{op}$ represents the saturated decreasing effects of $[M_vX]$ on $[Br_M^-]$ at the optimum value of $[M_vX]$). Thus, the effective concentration of $[M_vX]$ that could affect the ion exchange process between X^{v-}/S^- is represented as,

$$[M_vX]_S^{ef} = [M_vX] - ([M_vX]_{OH}^{op} + [M_vX]_{Br}^{op}) \qquad \textbf{Eq. 4.14}$$

where $[M_vX]_S^{ef} \approx [M_vX]$ when $[M_vX] >> [M_vX]_0^{op}$ (with $[M_vX]_0^{op} = [M_vX]_{OH}^{op} + [M_vX]_{Br}^{op}$) (Khan *et al.*, 2013). However, the magnitudes of $[M_vX]_0^{op}$ are no longer negligible when the observed values of ΔA_{ob} (as shown in **Figures 4.16** and **4.17**) show significant positive deviations from the dashed lines at the lower values of $[M_vX]$. These values of $[M_vX]_0^{op}$ were determined by an iterative technique (Khan, 2010; Khan *et al.*, 2013), and these values of $[M_vX]_0^{op}$ are shown in **Table 4.6**. The treatments of the data by using **Eq. 4.10** is more compatible at $[M_vX]_0^{op} \neq 0$ compared with that at $[M_vX]_0^{op} = 0$. The reliability of the data could be seen from the standard deviations associated with the calculated kinetic parameters, θ and $K^{X/S}$ as well as from the values of Σdi^2.

The appearance of an empirical parameter, $F_{X/S}$ in micellar system is reliable in the sense that: (i) its value is used to measure the fraction of micellized couterions (S_M^-) transferred to the bulk aqueous phase through ion exchange X^{v-}/S^- (Khan, 2010; Khan *et al.*, 2013) and (ii) its value is used to measure the micellar penetration of counterions X^{v-} relative to S^- (where S^- has larger hydrophobicity than X^{v-}) in terms of multistate/multiple micellar pseudophase model (Khan, 2006, 2010; Khan *et al.*, 2013). **Eq. 4.12** has been used to calculate the values of $F_{X/S}$, which are shown in **Table 4.6** where the values of A_M, A_W and θ are shown in **Table 4.6** as well. It is also evidence from **Table 4.6** as well as **Eq. 4.12** that the calculated values of θ are almost independent of $[CTABr]_T$.

It is noteworthy that the definition of empirical parameter, $K^{X/S}$ in the present method is similar to that in SEK method. The $K^{X/S}$ values, calculated from **Eq. 4.10** were decreased with increasing $[CTABr]_T$. The values of $K_{X/S}$ were calculated by using **Eq. 4.3** or **Eq. 4.13** with the experimentally calculated value of K_S^0 as (3624 M^{-1}). These values at different [CTABr]$_T$ are shown in **Table 4.6**. The K_S^0 value of S = N-2-MeOPhPT$^-$ is ~2-fold smaller than that with S = PSa$^-$. This observation reveals that the hydrophobicity of PSa$^-$ is greater than S = N-2-MeOPhPT$^-$. From the **Table 4.6**, the values of $K_{X/S}$ as well as $K_{X/S}^n$ (= $F_{X/S}K_{X/S}$) within [CTABr]$_T$ range 5 – 15 mM were found to be almost the same, which is a requirement for the validity of **Eq. 2.1** (Khan *et al.*, 2013). The values of K_X^{Br} or R_X^{Br} were calculated by using the relationship K_X^{Br} or R_X^{Br} = $K_{X/S}^n / K_{Br/S}^n$, where the value of $K_{Br/S}^n$ at 35 °C and in the presence of SM is 94.7 M^{-1}. It is noteworthy that the values of K_X^{Br} or R_X^{Br} are determined based on the values of both $K_{X/S}^n$ and $K_{Br/S}^n$, whether their values are obtained in the presence of similar or different structural features of micellar aggregates. These calculated values of R_X^{Br} are essentially independent of [CTABr]$_T$ at a constant temperature (**Table 4.6**). Thus, the mean values of R_X^{Br} at different temperatures are shown in **Table 4.7**.

Table 4.7: Mean Values of $F_{X/S}$ and R_X^{Br}, Determined by SESp Method for Different M_vX Used in the Presence of CTABr Micelles at 35 °C.

M_vX	$[M_vX]_0^{op}$	10^2 $F_{X/S}$ [a]	R_X^{Br} [b]
Acetic acid (CH_3COOH)	Nonzero	24 ± 13[c]	0.31 ± 0.1[c]
Propanoic acid (C_2H_5COOH)	Nonzero	44 ± 13	0.56 ± 0.2
Butanoic acid (C_3H_7COOH)	Nonzero	77 ± 7	0.77 ± 0.2
Pentanoic acid (C_4H_9COOH)	Nonzero	97 ± 4	1.88 ± 0.2
Heptanoic acid ($C_6H_{13}COOH$)	Nonzero	101 ± 2	15.3 ± 0.4
Octanoic acid ($C_7H_{15}COOH$)	Nonzero	108 ± 3	37.1 ± 2.8

[a] Mean values of $F_{X/S}$ obtained at 5, 6, 10 and 15 mM CTABr. [b] Mean values of R_X^{Br} obtained at 5, 6, 10 and 15 mM CTABr. [c] Error limits are standard deviations.

Early study had reported the use of SEK and SESp methods for the determination of K_X^{Br} or R_X^{Br} values, where the values obtained from those methods are not significantly different from each other for the same X (Khan *et al.*, 2013). Besides, Khan in his early report did mentioned that the values of K_X^{Br} or R_X^{Br} are independent of anionic probe molecules (S^-) as well as the use of methods to derive K_S values at different [M_vX] (Khan *et al.*, 2013). Similarly, Khan et. al had reported the determined values of K_X^{Br} for X = Cl^- and 2,6-$Cl_2C_6H_3CO_2^-$ using SESp method, are comparable to those obtained by the use of other physicochemical methods (Khan *et al.*, 2013). Hence, the empirical definition of $K_{Br/S}$ and $K_{X/S}$ may lead to the following relationship: $K_{Br/S} = \Omega_S K_{Br}/K_S$ and $K_{X/S} = \Omega_S K_X/K_S$, respectively. The empirical definition of Ω_S, along with its characteristics behavior has been discussed in details in SEK method.

4.1.3 SEK Versus SESp Methods: Advantages and Disadvantages

It is very common that any physical techniques developed by humans might exhibit its relative advantages and disadvantages. The same goes to the present methods (SEK and SESp) where their relative advantages and disadvantages are described as follows (Khan *et al.*, 2013): One need to spend more time using SEK method compared to SESp method, because kinetic measurements requires difficulties in some aspects compared to that in SESp method. Moreover, SEK method highly demands on relatively large number of requirements to maintain its use. Other than that, SEK and SESp methods require secondary and primary data, respectively in order to determine the empirical constants which lead to the determination of the final value of K_X^{Br} or R_X^{Br}. The more reliable empirical parameters may be obtained in the use of SEK method rather than that in SESp method due to the significantly larger range of variation of variable experimental data. In relation to that, larger number of assumptions could be seen in SEK method rather than SESp method. The new anionic probe molecule is perhaps easy to find for SEK method compared to SESp method. Other than that, the probe molecules used in SEK method are chemically reactive than that used in SESp method, where its molecules are almost inert under the conditions of the present method. Lastly, SEK and SESp methods are not suitable at respective pH < ~11 and < ~6.

4.2 Rheological Observations of Aqueous Solutions of Mixed CTABr/M_vX

4.2.1 Rheological Measurements and Morphological Transitions of Aqueous CTABr/M_vX System Containing 15 mM CTABr and Different [M_vX] (ν = 1, 2) with M_vX = 4-MeO- and 3-Me-, 4-MeSaNa$_v$

Flow test measurements of aqueous solutions containing constant concentration of 0.2 mM PSaH, 30 mM NaOH, 100 mM Pip, 15 mM CTABr and varying values of [M_vX], within its range between 0.0 – 300 mM, were carried out at a constant temperature (T = 25, 35, 40, 45 and 55 °C). The observed viscosity, η data versus shear rate, $\dot{\gamma}$ for different [M_vX] with (M_vX = 4-MeO- and 3-Me-, 4-MeSaNa$_v$ and ν = 2) are shown in **Figures 4.18 –4.31**. Similar flow curves were obtained for the system containing 4-MeO- and 3-Me-, 4-MeSaNa$_v$ (ν = 1, 2) at 25 and 35 °C. The plots are shown in **Figures S10 – S18** (see Appendix F - **Figures S10 – S18**). Some of the flow curves at typical values of [M_vX] complicate to each other, thus are not shown in the figures.

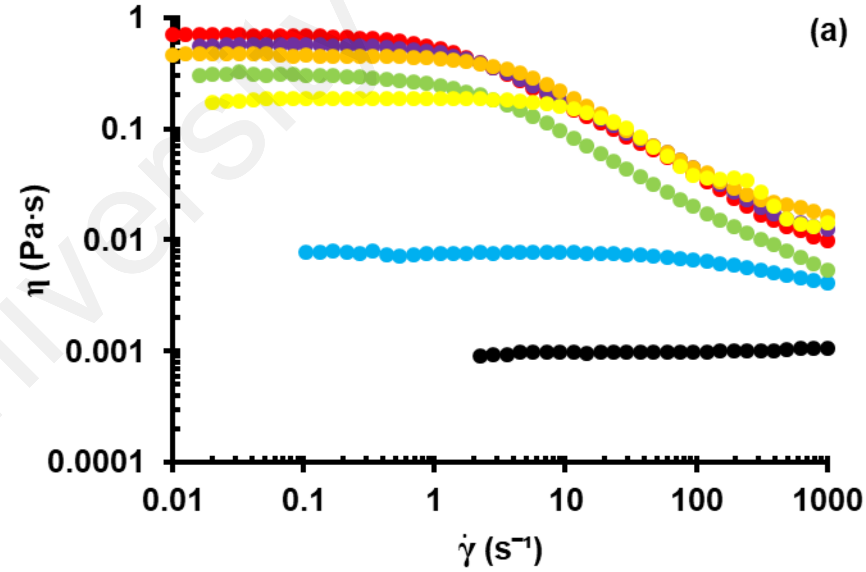

Figure 4.18: Plots showing the dependence of η upon $\dot{\gamma}$ for piperidinolysis of PSa$^-$ at 0.2 mM PSa$^-$, 0.1 M Pip, 15 mM CTABr and [4-MeOSaNa$_v$] (mM) with ν = 2 at (a): 5 (black), 10 (blue), 12 (green), 14 (red), 15 (purple), 17 (orange) 20 (yellow) and (b): 40 (blue), 70 (green), 100 (red), 150 (purple), 200 (orange) and 300 (yellow) at 25 °C.

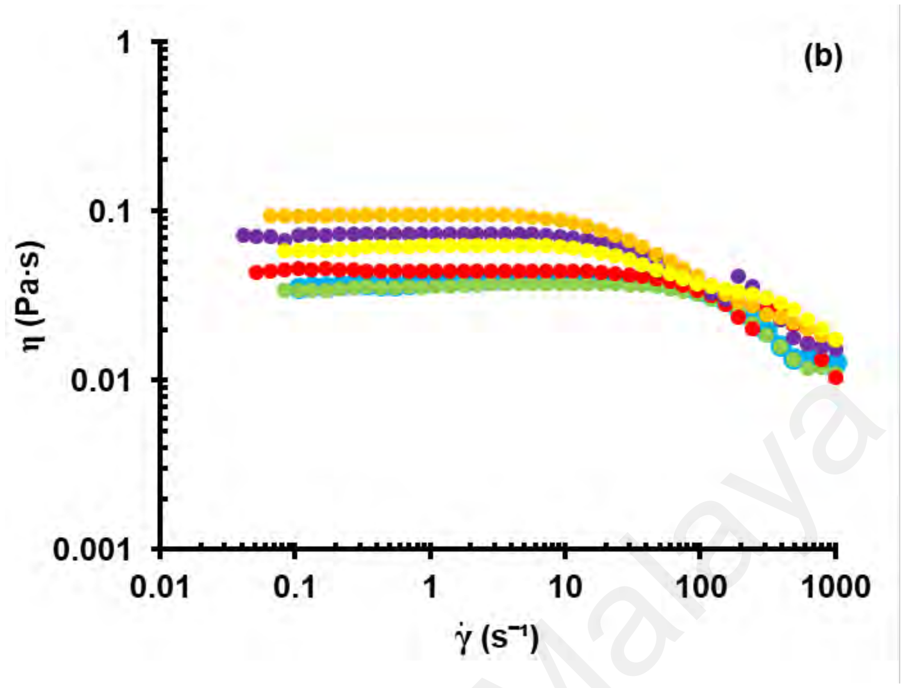

Figure 4.18, continued

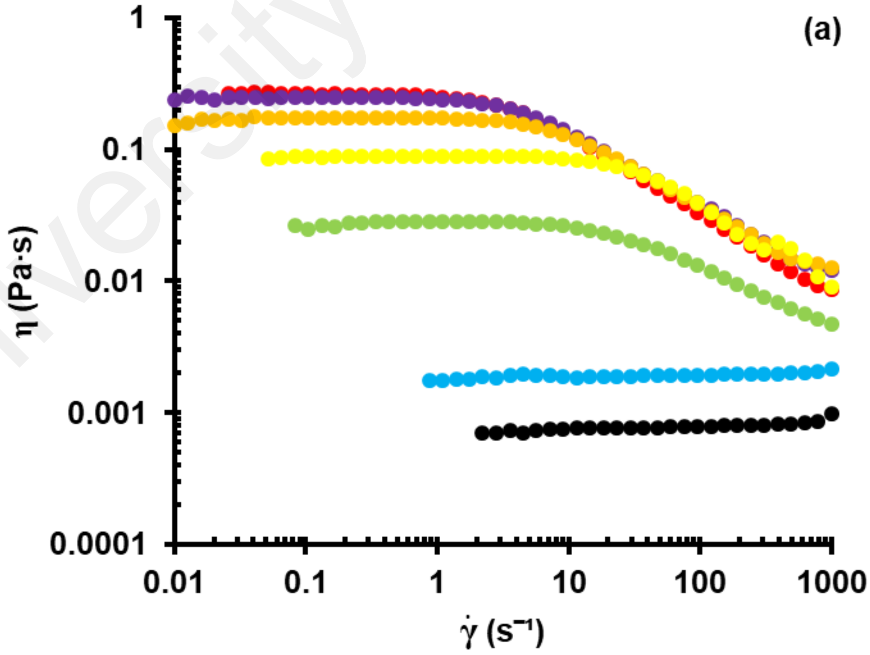

Figure 4.19: Plots showing the dependence of η upon $\dot{\gamma}$ for piperidinolysis of PSa$^-$ at 0.2 mM PSa$^-$, 0.1 M Pip, 15 mM CTABr and [4-MeOSaNa$_v$] (mM) with ν = 2 at (a): 5 (black), 10 (blue), 12 (green), 14 (red), 15 (purple), 17 (orange) 20 (yellow) and (b): 40 (blue), 70 (green), 100 (red), 150 (purple), 200 (orange) and 300 (yellow) at 35 °C.

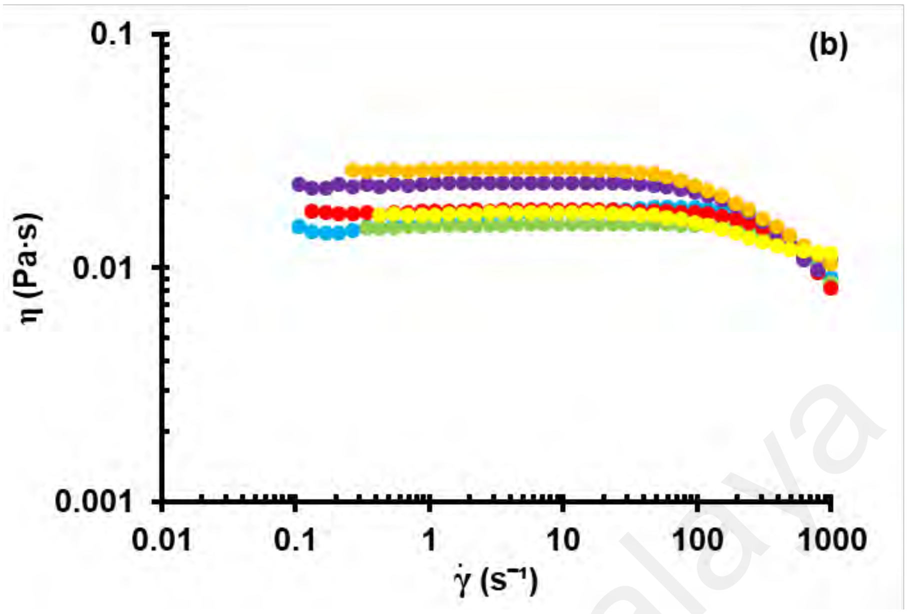

Figure 4.19, continued

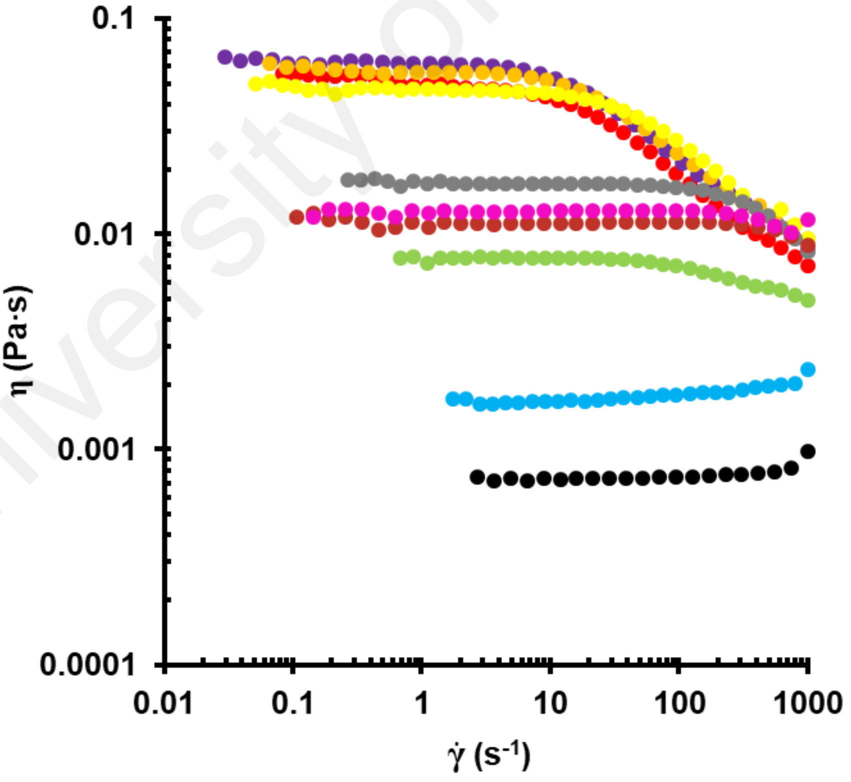

Figure 4.20: Plots showing the dependence of η upon $\dot{\gamma}$ for piperidinolysis of PSa^- at 0.2 mM PSa^-, 0.1 M Pip, 15 mM CTABr and [$4\text{-}MeOSaNa_v$] (mM) with ν = 2 at 5 (black), 10 (blue), 12 (green), 13 (red), 14 (purple), 15 (orange) 20 (yellow), 30 (grey), 70 (brown) and 100 (pink) at 40 °C.

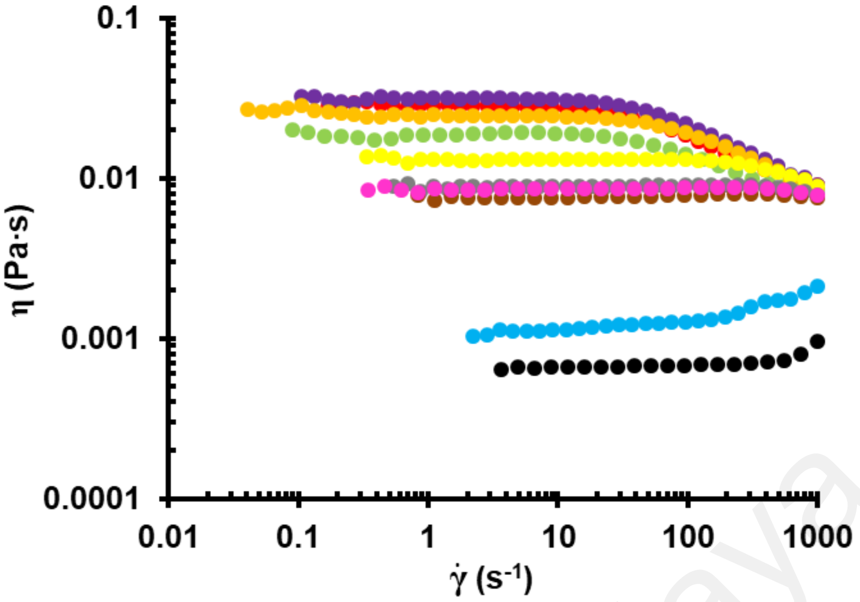

Figure 4.21: Plots showing the dependence of η upon $\dot{\gamma}$ for piperidinolysis of PSa^- at 0.2 mM PSa^-, 0.1 M Pip, 15 mM CTABr and [4-MeOSaNa$_v$] (mM) with ν = 2 at 5 (black), 10 (blue), 15 (green), 17 (red), 19 (purple), 20 (orange) 30 (yellow), 40 (grey), 70 (brown) and 100 (pink) at 45 °C.

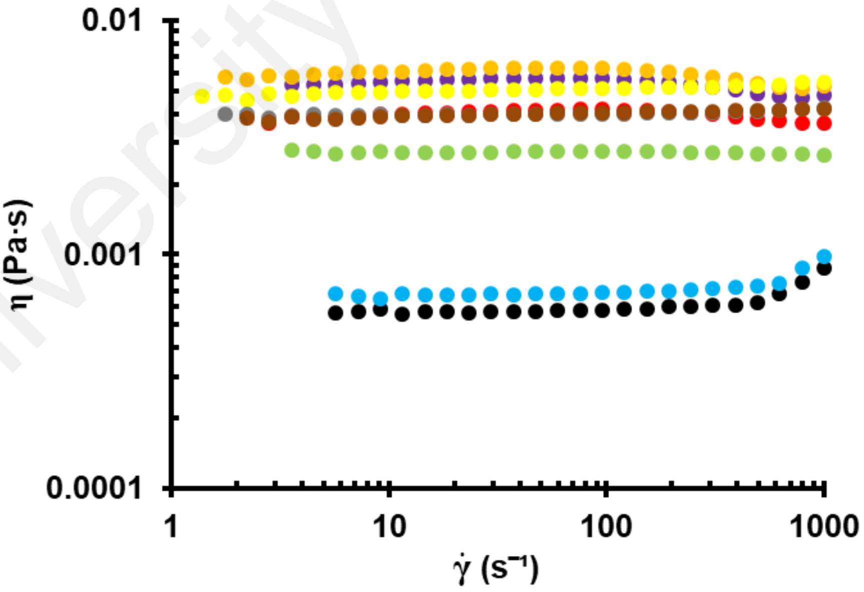

Figure 4.22: Plots showing the dependence of η upon $\dot{\gamma}$ for piperidinolysis of PSa^- at 0.2 mM PSa^-, 0.1 M Pip, 15 mM CTABr and [4-MeOSaNa$_v$] (mM) with ν = 2 at 5 (black), 10 (blue), 15 (green), 17 (red), 19 (purple), 20 (orange), 40 (yellow), 70 (grey) and 100 (brown) at 55 °C.

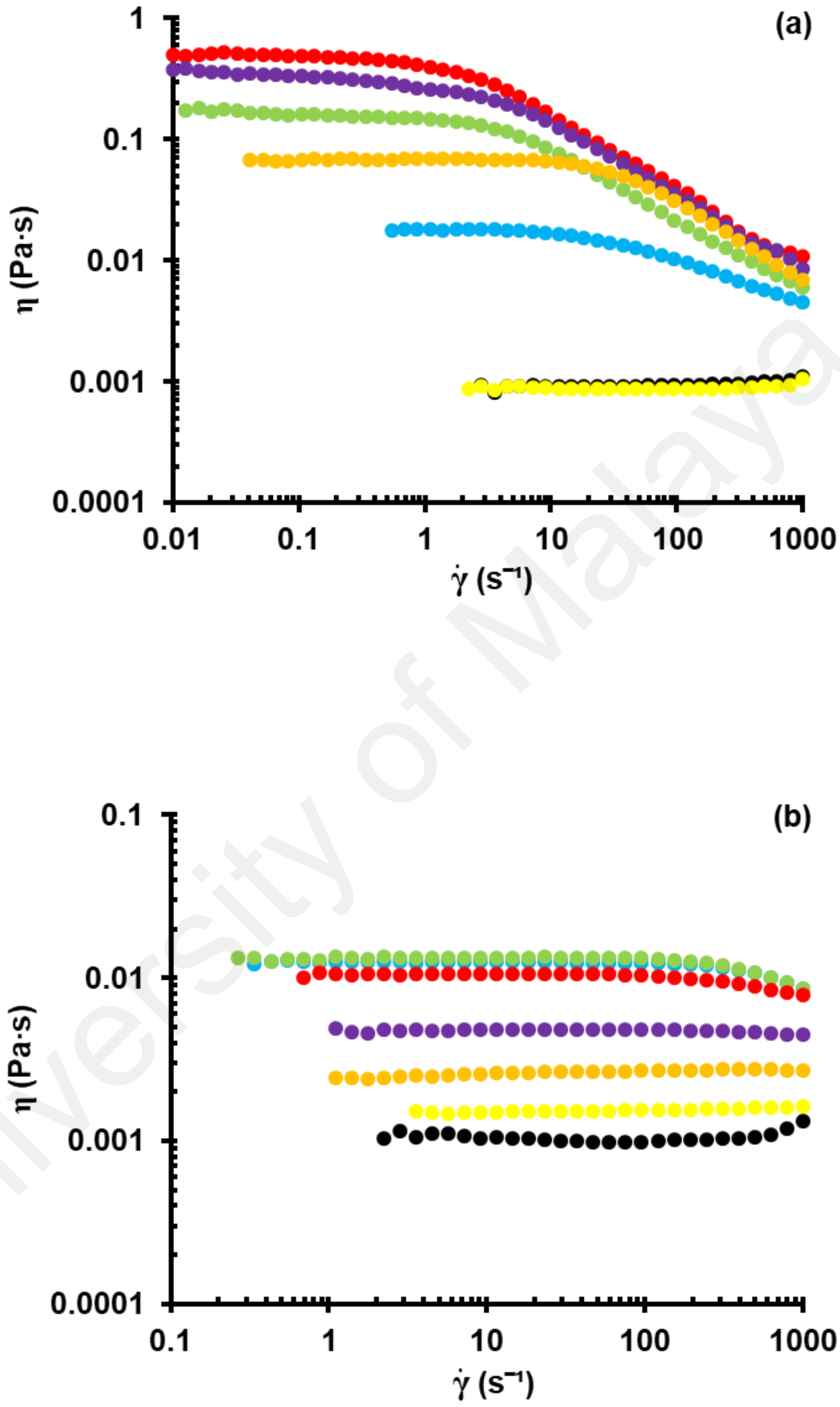

Figure 4.23: Plots showing the dependence of η upon $\dot{\gamma}$ for piperidinolysis of PSa^- at 0.2 mM PSa^-, 0.1 M Pip, 15 mM CTABr and [3-MeSaNa$_v$] (mM) with ν = 2 at (a): 7 (black), 10 (blue), 11 (green), 12 (red), 13 (purple), 15 (orange), 30 (yellow) and (b): 40 (black), 80 (blue), 100 (green), 150 (red), 200 (purple), 250 (orange) and 300 (yellow) at 35 °C.

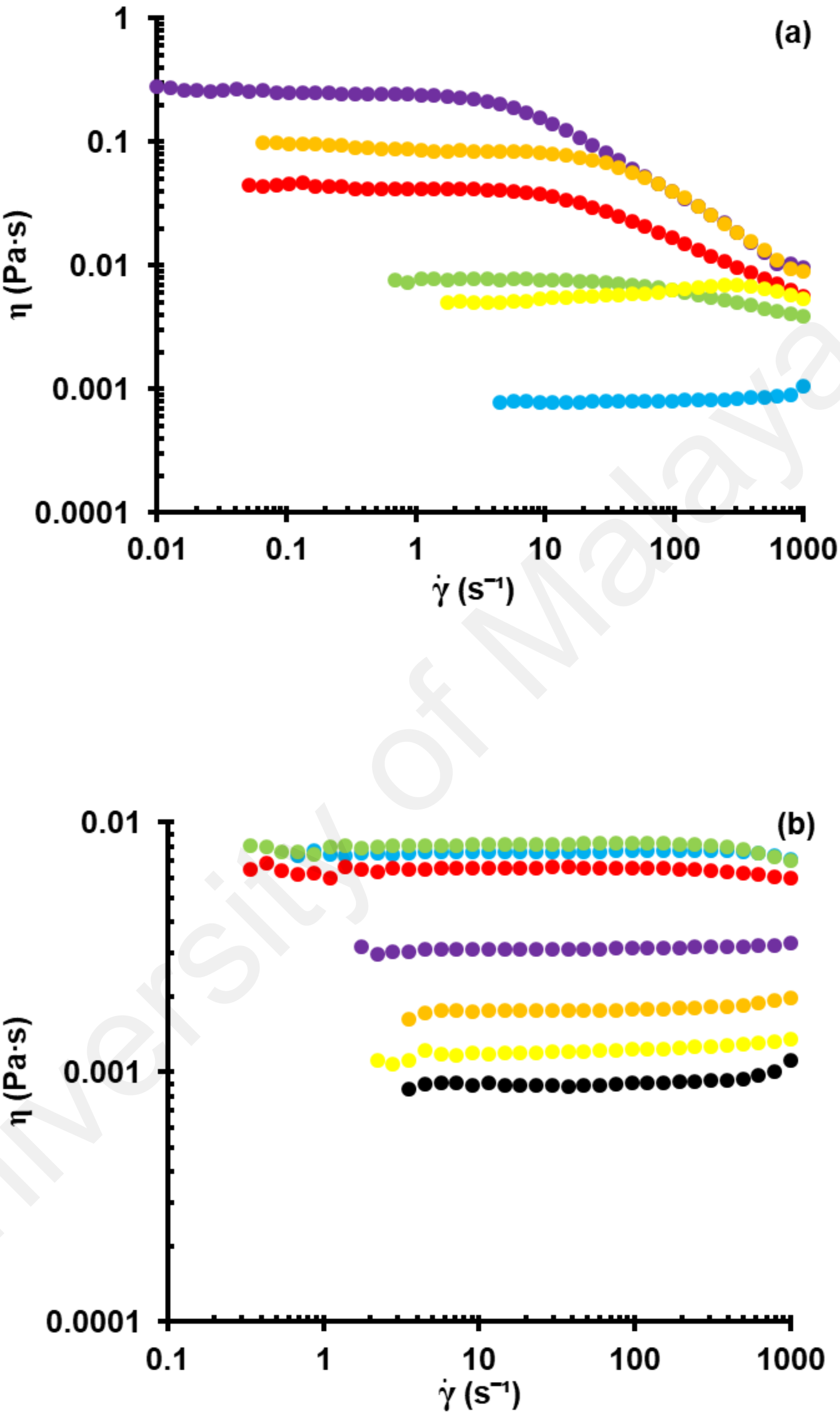

Figure 4.24: Plots showing the dependence of η upon $\dot{\gamma}$ for piperidinolysis of PSa$^-$ at 0.2 mM PSa$^-$, 0.1 M Pip, 15 mM CTABr and [3-MeSaNa$_v$] (mM) with $\nu = 2$ at (a): 7 (blue), 10 (green), 11 (red), 13 (purple), 15 (orange), 20 (yellow) and (b): 40 (black), 60 (blue), 100 (green), 150 (red), 200 (purple), 250 (orange) and 300 (yellow) at 40 °C.

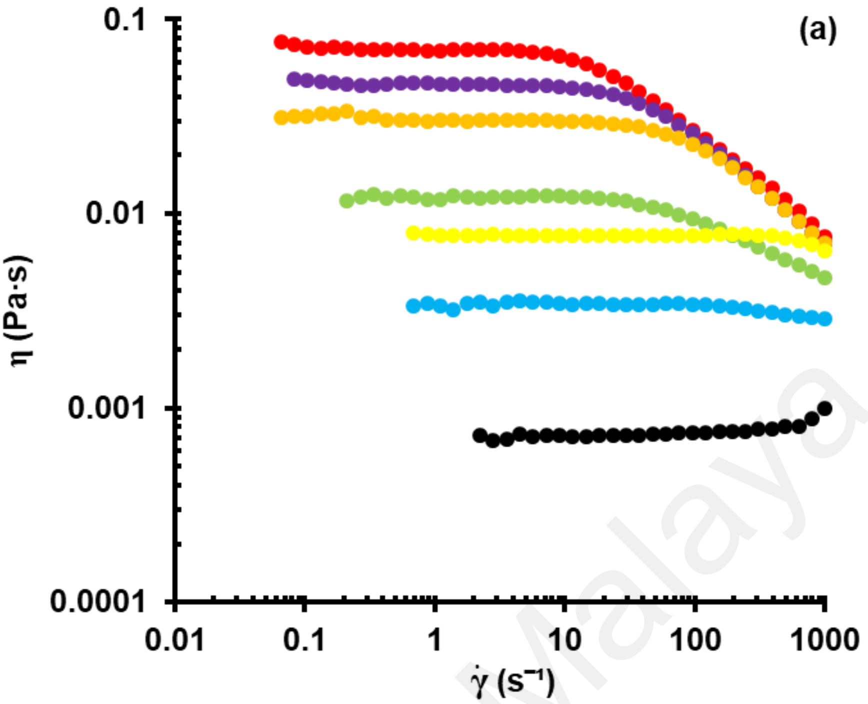

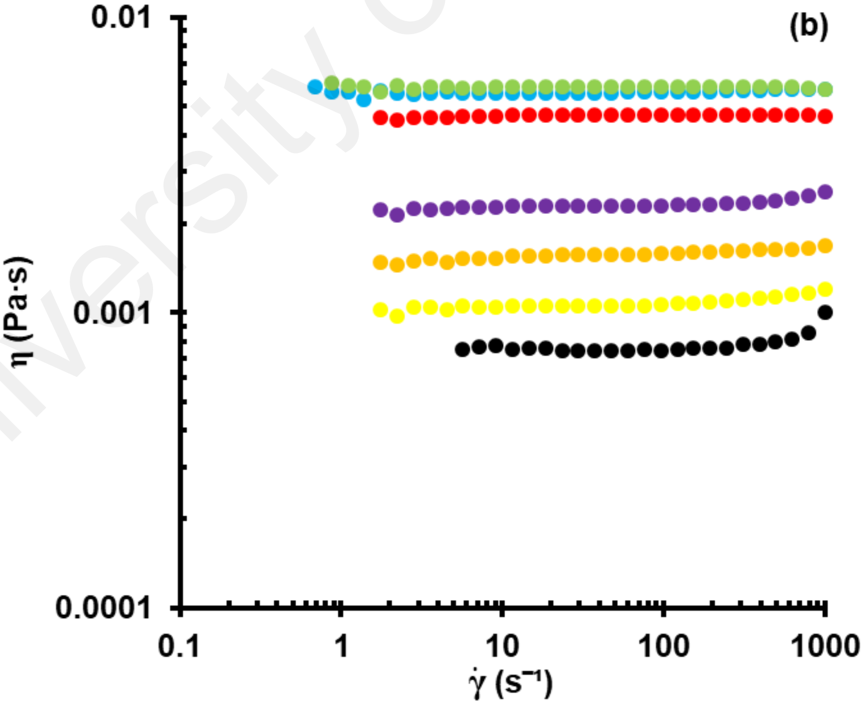

Figure 4.25: Plots showing the dependence of η upon $\dot{\gamma}$ for piperidinolysis of PSa^- at 0.2 mM PSa^-, 0.1 M Pip, 15 mM CTABr and [3-$MeSaNa_v$] (mM) with ν = 2 at (a): 7 (black), 10 (blue), 11 (green), 13 (red), 14 (purple), 15 (orange), 20 (yellow) and (b): 40 (black), 80 (blue), 100 (green), 150 (red), 200 (purple), 250 (orange) and 300 (yellow) at 45 °C.

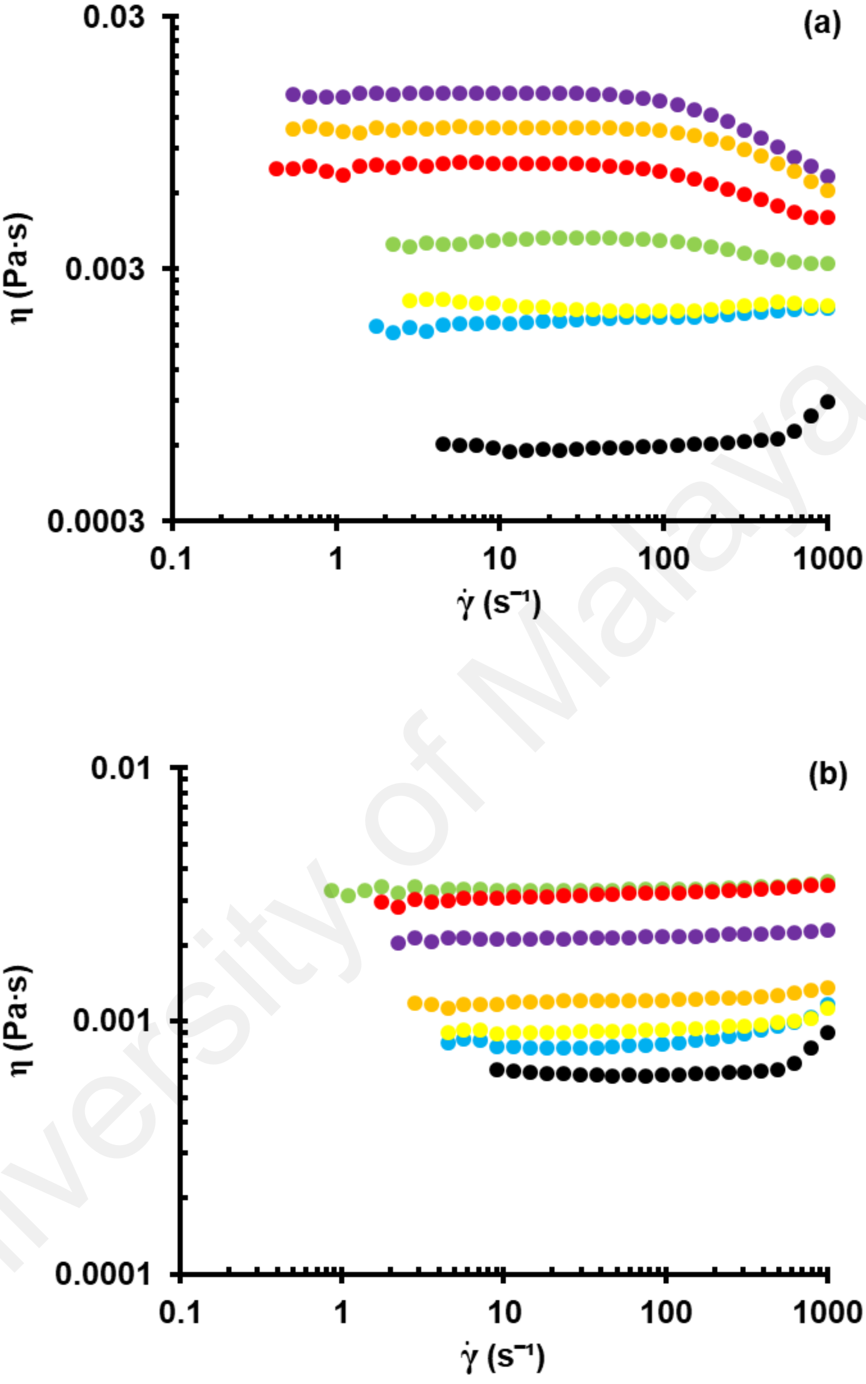

Figure 4.26: Plots showing the dependence of η upon γ̇ for piperidinolysis of PSa^- at 0.2 mM PSa^-, 0.1 M Pip, 15 mM CTABr and [3-$MeSaNa_v$] (mM) with ν = 2 at (a): 7 (black), 10 (blue), 11 (green), 12 (red), 14 (purple), 15 (orange), 20 (yellow) and (b): 40 (black), 60 (blue), 100 (green), 150 (red), 200 (purple), 250 (orange) and 300 (yellow) at 55 °C.

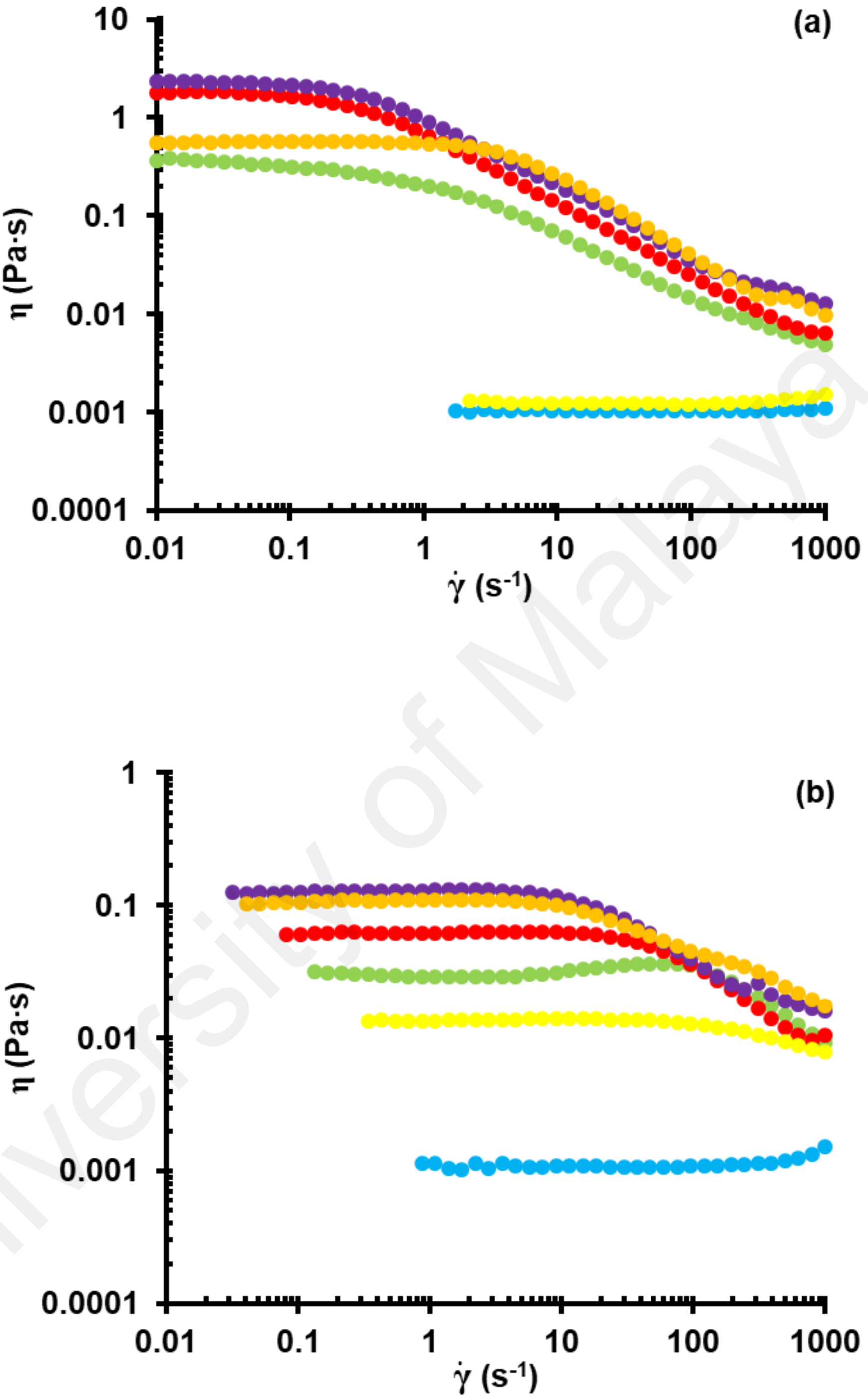

Figure 4.27: Plots showing the dependence of η upon $\dot{\gamma}$ for piperidinolysis of PSa^- at 0.2 mM PSa^-, 0.1 M Pip, 15 mM CTABr and [4-MeSaNa$_v$] (mM) with ν = 2 at (a): 5 (blue), 10 (green), 11 (red), 12 (purple), 15 (orange), 20 (yellow) and (b): 40 (blue), 60 (green), 100 (red), 150 (purple), 200 (orange) and 300 (yellow) at 25 °C.

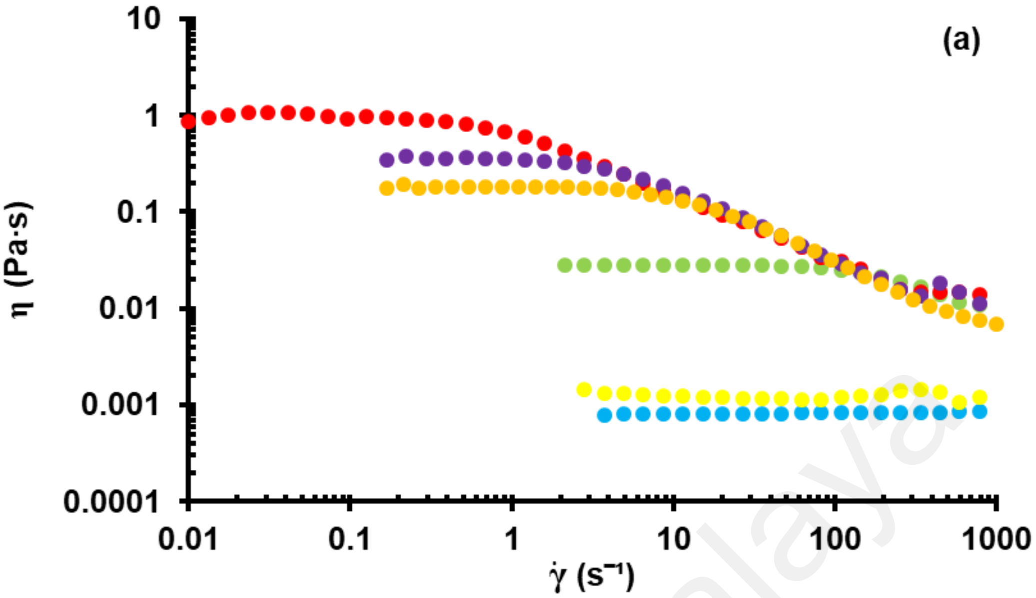

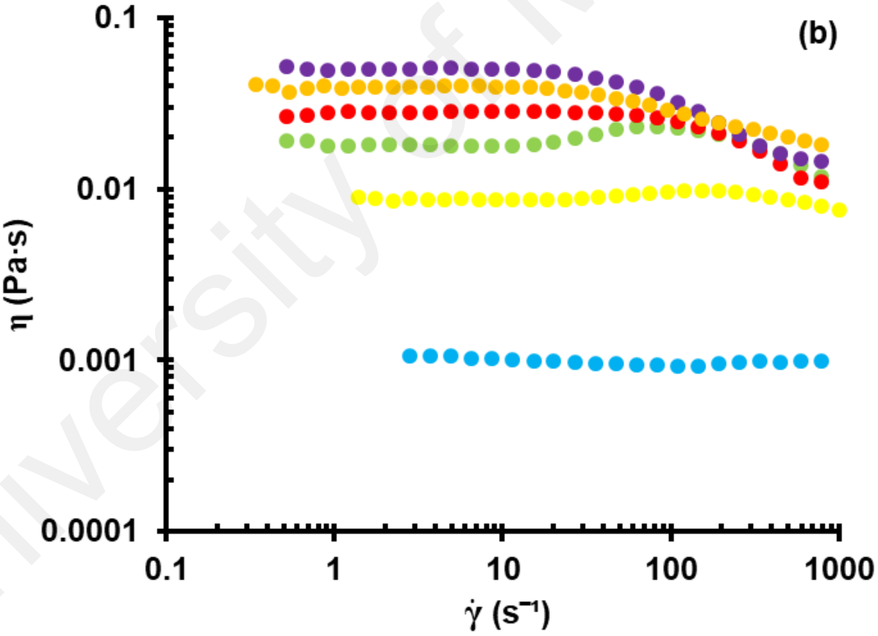

Figure 4.28: Plots showing the dependence of η upon $\dot{\gamma}$ for piperidinolysis of PSa$^-$ at 0.2 mM PSa$^-$, 0.1 M Pip, 15 mM CTABr and [4-MeSaNa$_v$] (mM) with ν = 2 at (a): 5 (blue), 10 (green), 12 (red), 14 (purple), 15 (orange), 21 (yellow) and (b): 40 (blue), 60 (green), 100 (red), 150 (purple), 200 (orange) and 300 (yellow) at 35 °C.

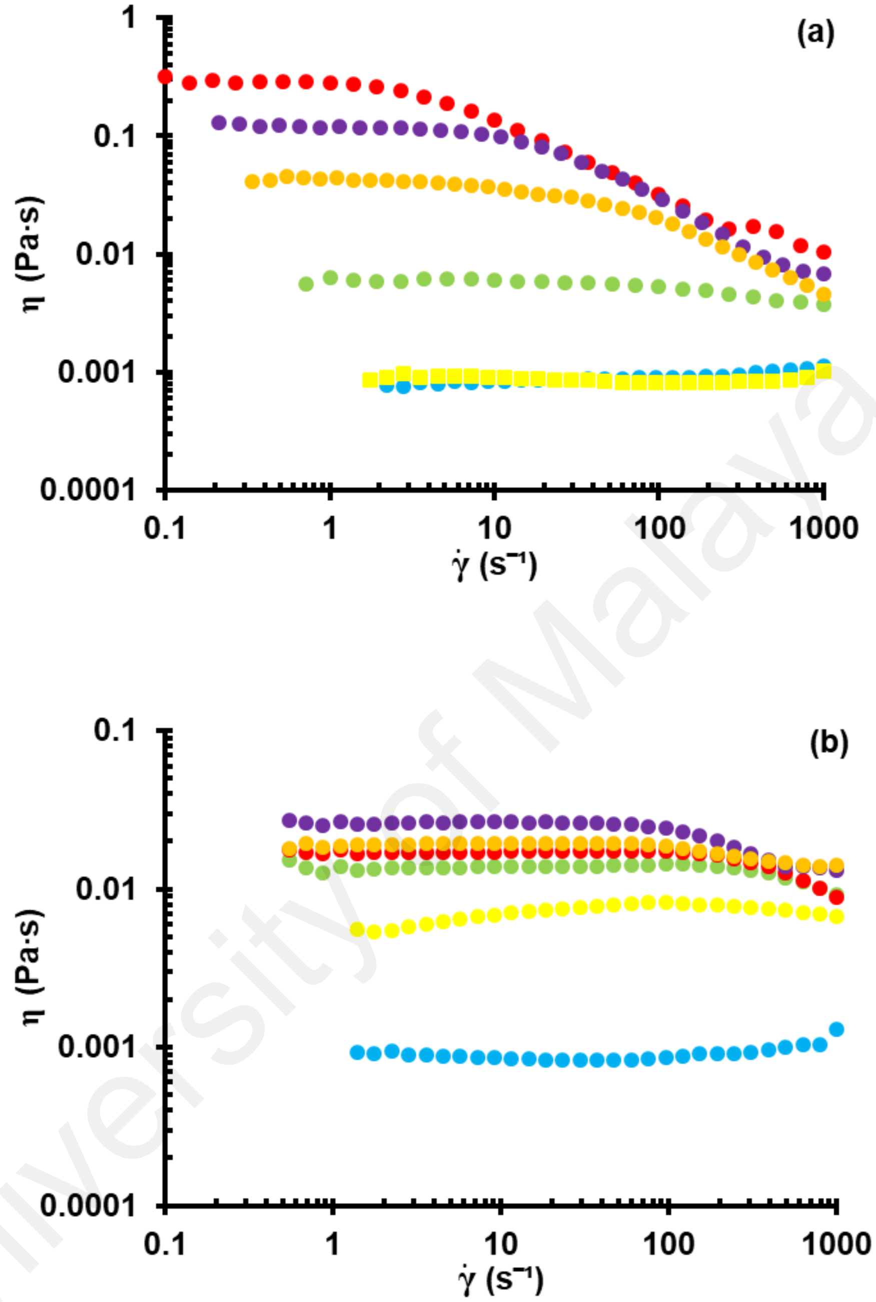

Figure 4.29: Plots showing the dependence of η upon $\dot{\gamma}$ for piperidinolysis of PSa$^-$ at 0.2 mM PSa$^-$, 0.1 M Pip, 15 mM CTABr and [4-MeSaNa$_v$] (mM) with ν = 2 at (a): 7 (blue), 10 (green), 13 (red), 15 (purple), 18 (orange), 30 (yellow) and (b): 50 (blue), 70 (green), 100 (red), 150 (purple), 200 (orange) and 300 (yellow) at 40 °C.

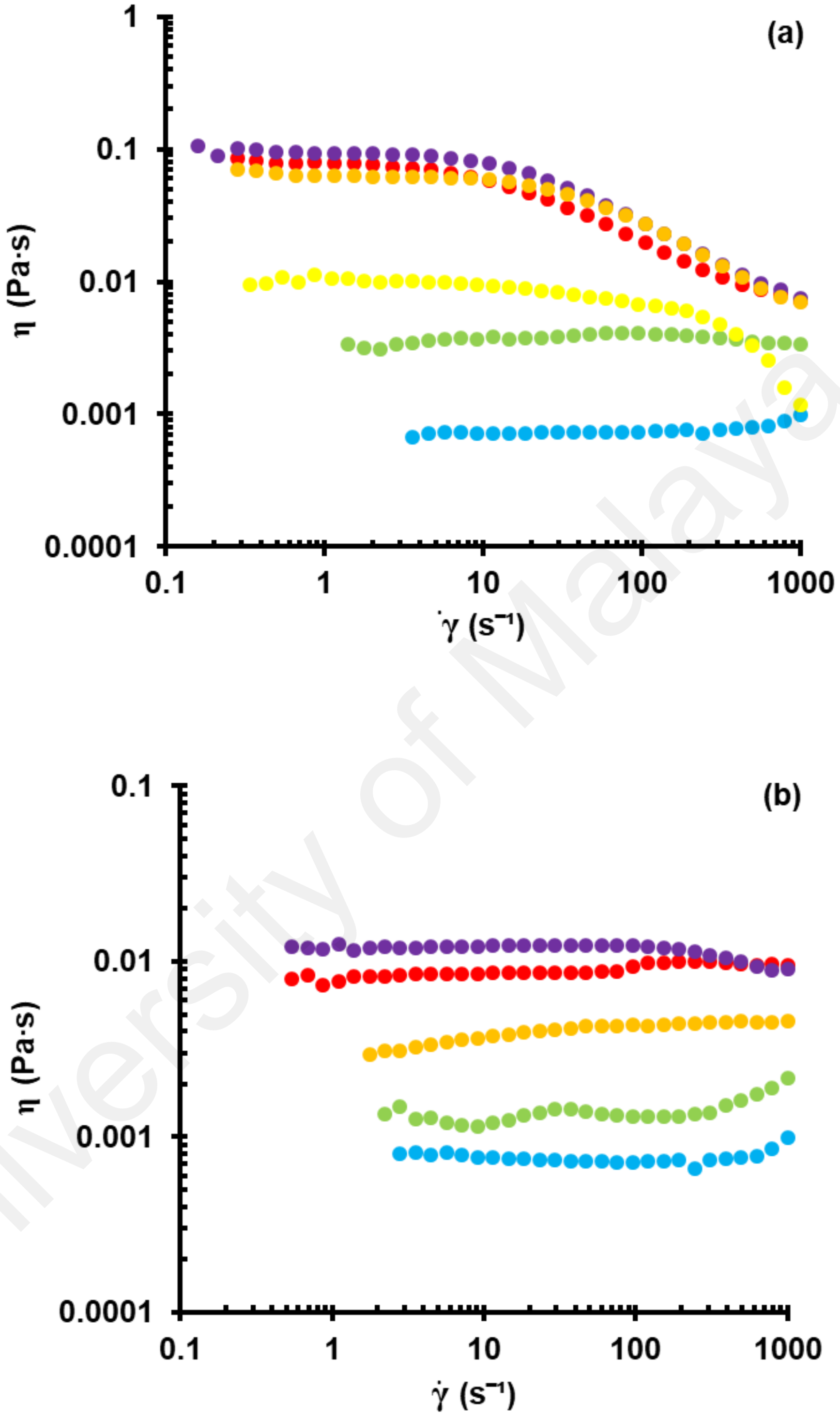

Figure 4.30: Plots showing the dependence of η upon $\dot{\gamma}$ for piperidinolysis of PSa$^-$ at 0.2 mM PSa$^-$, 0.1 M Pip, 15 mM CTABr and [4-MeSaNa$_\nu$] (mM) with $\nu = 2$ at (a): 7 (blue), 10 (green), 12 (red), 14 (purple), 15 (orange), 21 (yellow) and (b): 30 (blue), 60 (green), 70 (red), 150 (purple) and 300 (orange) at 45 °C.

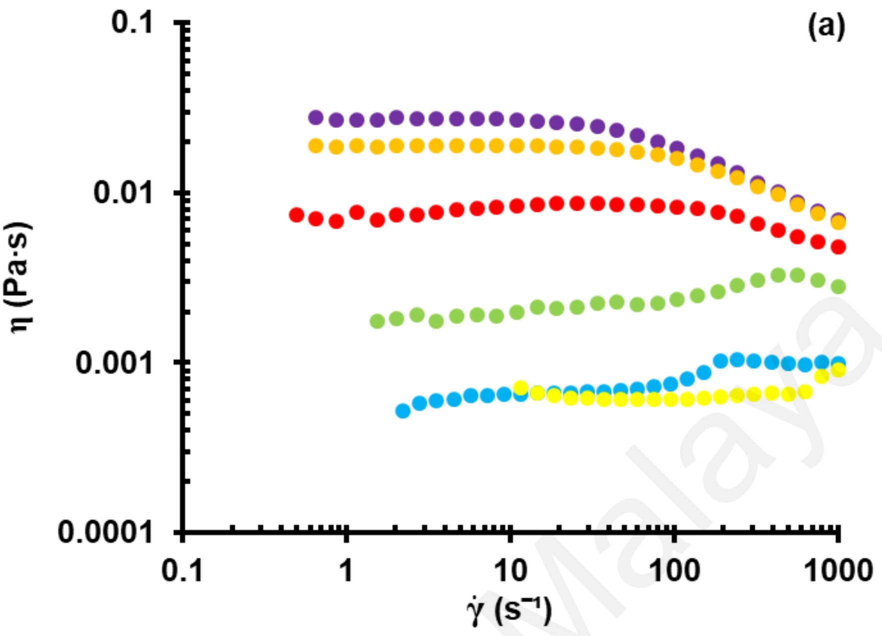

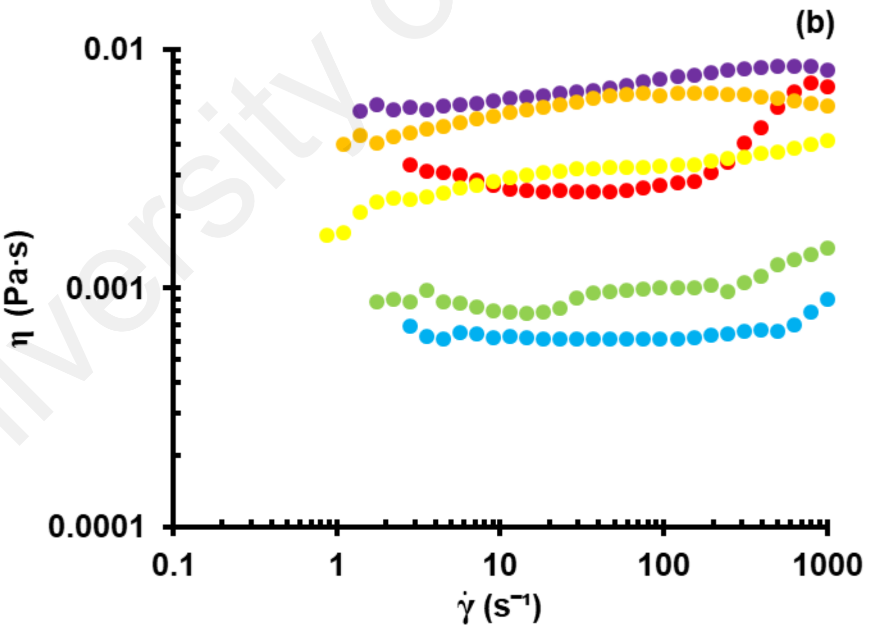

Figure 4.31: Plots showing the dependence of η upon $\dot{\gamma}$ for piperidinolysis of PSa^- at 0.2 mM PSa^-, 0.1 M Pip, 15 mM CTABr and [4-MeSaNa$_v$] (mM) with ν = 2 at (a): 7 (blue), 10 (green), 12 (red), 14 (purple), 15 (orange), 21 (yellow) and (b): 50 (blue), 70 (green), 80 (red), 150 (purple), 200 (orange) and 300 (yellow) at 55 °C.

The distinctive nature of flow curves for M_vX = 4-MeOSaNa$_v$ may be expressed as follows: (a) For M_vX = 4-MeOSaNa$_v$ (ν = 1): (i) The flow curves show only Newtonian behavior with the η values similar to that of water at 5 mM M_vX (25 and 35 °C) and slightly higher than viscosity of water at 10 mM M_vX (35 °C). (ii) At initial lower values of $\dot{\gamma}$, the flow curves show the behavior of Newtonian fluid, then continued by shear thinning behavior at higher $\dot{\gamma}$ values at ~10 mM < [M_vX] < 300 mM at 25 as well as 12 mM < [M_vX] < 300 mM at 35 °C (b) For M_vX = 4-MeOSaNa$_v$ (ν = 2): (i) The flow curves come out with Newtonian fluid behavior at the initial lower values of $\dot{\gamma}$, followed by shear thinning behavior at higher values of $\dot{\gamma}$ at ~10 mM < [M_vX] < 300 mM at 25 and 35 as well as 12 mM < [M_vX] < 100 mM at 40 °C. Similar observations were obtained at 15 mM < [M_vX] < 40 mM and 19 mM < [M_vX] < 20 mM at 45 and 55 °C, respectively. (ii) There is only Newtonian fluid behavior exhibited by the flow curves at 10 mM M_vX (35, 40 and 45 °C), as well as $\geq$ 40 - $\leq$ 100 mM M_vX (55 °C). At 5 mM M_vX (25 – 55 °C), the flow curves show only Newtonian behavior with the η values of water. (c) For M_vX = 4-MeOSaNa$_v$ (ν = 2): (i) The flow curves showed similar behavior to that of M_vX = 4-MeOSaNa$_v$ (ν = 1), for the [M_vX] range between 5 – 300 mM.

On the other hand, the observable behavior of flow curves for M_vX = 4-MeSaNa$_v$ are described as follows: (a) For M_vX = 4-MeSaNa$_v$ (ν = 1): (i)The flow curves show only Newtonian behavior with the η values similar to that of water at 5, 20 – 40 mM M_vX (25 °C) as well as 5, and 40 mM M_vX (35 °C). (ii) Newtonian behavior was shown at lower values of $\dot{\gamma}$, then followed by shear thinning behavior at higher $\dot{\gamma}$ values at > 10 mM - < 20 mM and > 40 mM - $\leq$ 300 mM (25 °C) as well as > 10 mM - < 40 mM and > ~80 mM - $\leq$ 300 mM (35 °C). (b) For M_vX = 4-MeSaNa$_v$ (ν = 2): (i) The flow curves consist of initial Newtonian fluid behavior followed by shear thinning at > ~10 mM - < 30 mM and > ~70 mM - $\leq$ 300 mM (25, 35, 40 °C) as well as > ~12 mM - < 30 mM (45 °C) and ~12 mM - < 21 mM (55 °C). (ii) Values of η were not different from η of water at [M_vX] $\leq$ 7 mM and 30 mM < [M_vX] < 50 mM (35 – 55 °C). (c) For M_vX = 4-MeSaNa$_v$ (ν = 2): (i) The flow curves showed similar behavior to that of M_vX = 4-MeSaNa$_v$ (ν = 1), for the [M_vX] range between 5 – 300 mM. The distinctive nature exhibited by the flow curves of 3-MeSaNa$_v$ (ν = 1, 2) are almost similar to those for 4-MeSaNa$_v$ (ν = 1, 2). It is relevant to note that the flow curves of aqueous CTABr/M_vX solution, which exhibit Newtonian behavior at lower $\dot{\gamma}$ as well as shear thinning behavior at higher $\dot{\gamma}$ values are indicative of the presence of wormlike micelles (WM) or large unilamellar/multilamellar vesicles (ULV/MLV) (Gradzielski, 2011; Razak *et al.*, 2016). In contrast, the flow curves with Newtonian fluid behavior and η of pure water show indirectly the presence of spherical micelles (SM) or small ULV/MLV (Carver *et al.*, 1996; Davies *et al.*, 1996; Fagge *et al.*, 2016).

Oscillatory rheometry were carried out at a constant concentration of [M_vX] (M_vX= 4-MeO- and 3-Me-, 4-MeSaNa$_v$) at which the maximum zero shear viscosity (η_0^{max}) occurs in the plot of zero shear viscosity (η_0) versus [M_vX], as shown in **Figures 4.32** – **4.34** for respective M_vX= 4-MeO- and 3-Me-, 4-MeSaNa$_v$ (ν = 2). The reaction conditions were kept similar as in steady shear rheological measurements and 35 °C. The observed oscillatory rheograms are shown in **Figures 4.35 (a)**, **(b)**, and **(c)**, **(d)** for 4-MeO-, 3-Me-, and 4-MeSaNa$_v$ (ν = 2), respectively. The presence of loop in the plots of elastic modulus (G'), viscous viscosity (G") versus oscillatory shear frequency (ω) reveal indirectly the presence of network structures of WM (Carver *et al.*, 1996; Koshy *et al.*, 2010). Aqueous CTABr solution containing 150 mM 4-MeSaNa$_v$ (ν = 2) (**Figure 4.35 (d)**) shows dominant viscous behavior within range 0.1 – 40 rad s^{-1}, which may be attributed to the presence of stabilized dispersion (Macosko & Larson, 1994) or short rodlike micelles (Ketner *et al.*, 2007).

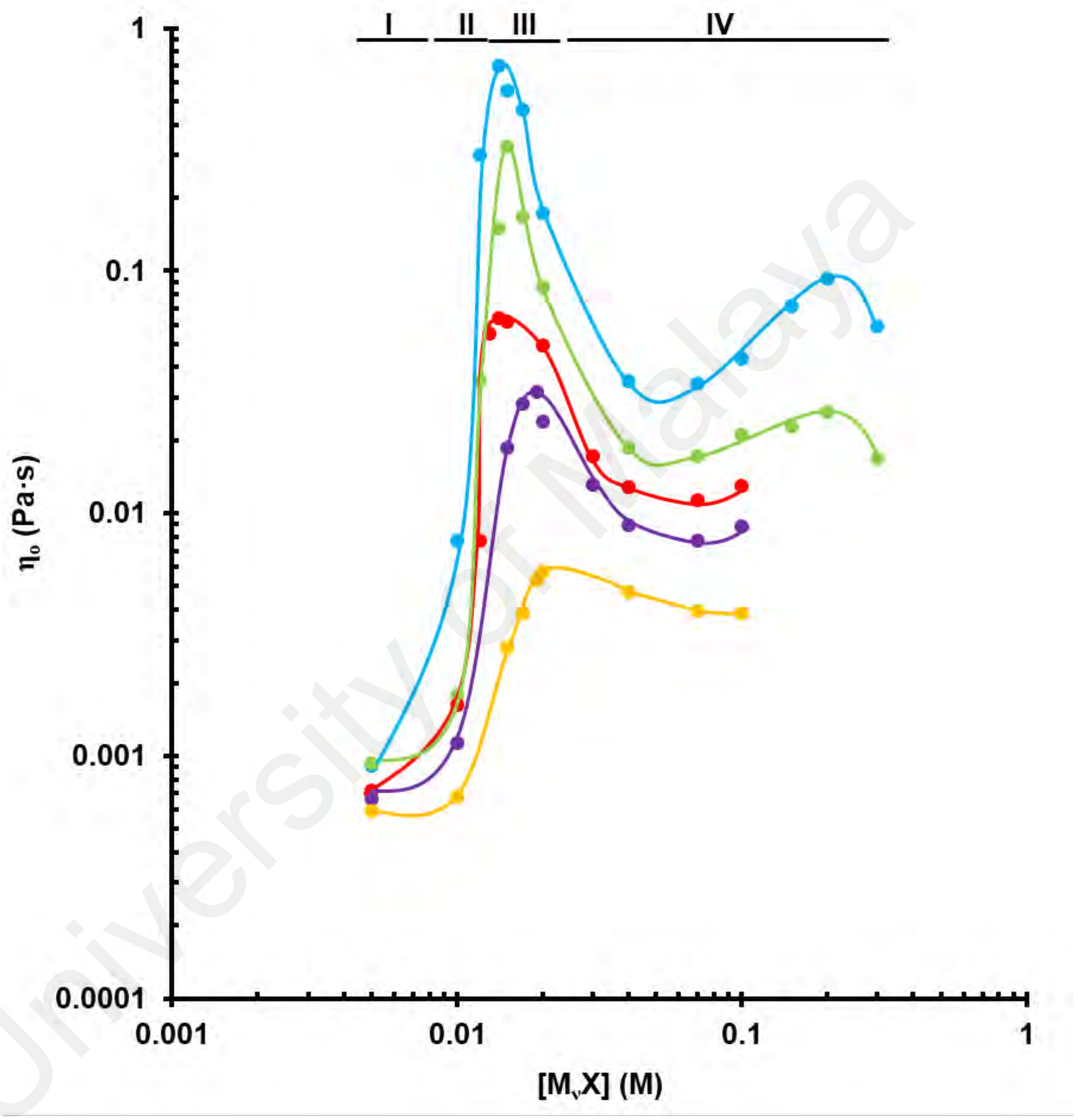

Figure 4.32: Plots showing the dependence of η_0 upon $[M_\nu X]$ ($M_\nu X$ = 4-MeOSaNa$_\nu$ with $\nu = 2$) for piperidinolysis of PSa$^-$ at 0.2 mM PSa$^-$, 0.1 M Pip and 15 mM CTABr at 25 (blue), 35 (green), 40 (red), 45 (purple) and 55 (orange) °C.

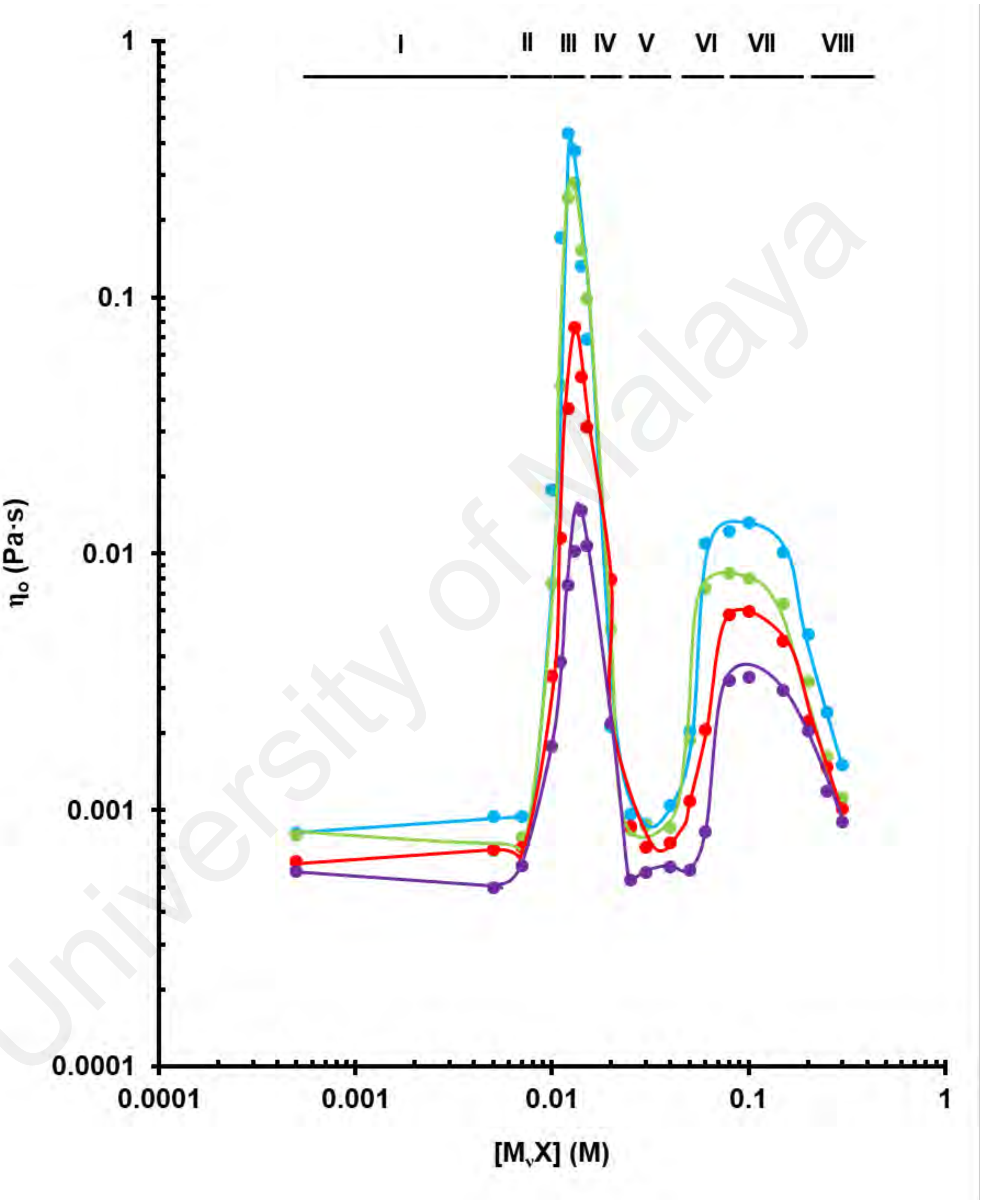

Figure 4.33: Plots showing the dependence of η_0 upon [$M_\nu X$] ($M_\nu X$ = 3-MeSaNa$_\nu$ with ν = 2) for piperidinolysis of PSa$^-$ at 0.2 mM PSa$^-$, 0.1 M Pip and 15 mM CTABr at 35 (blue), 40 (green), 45 (red), and 55 (purple) °C.

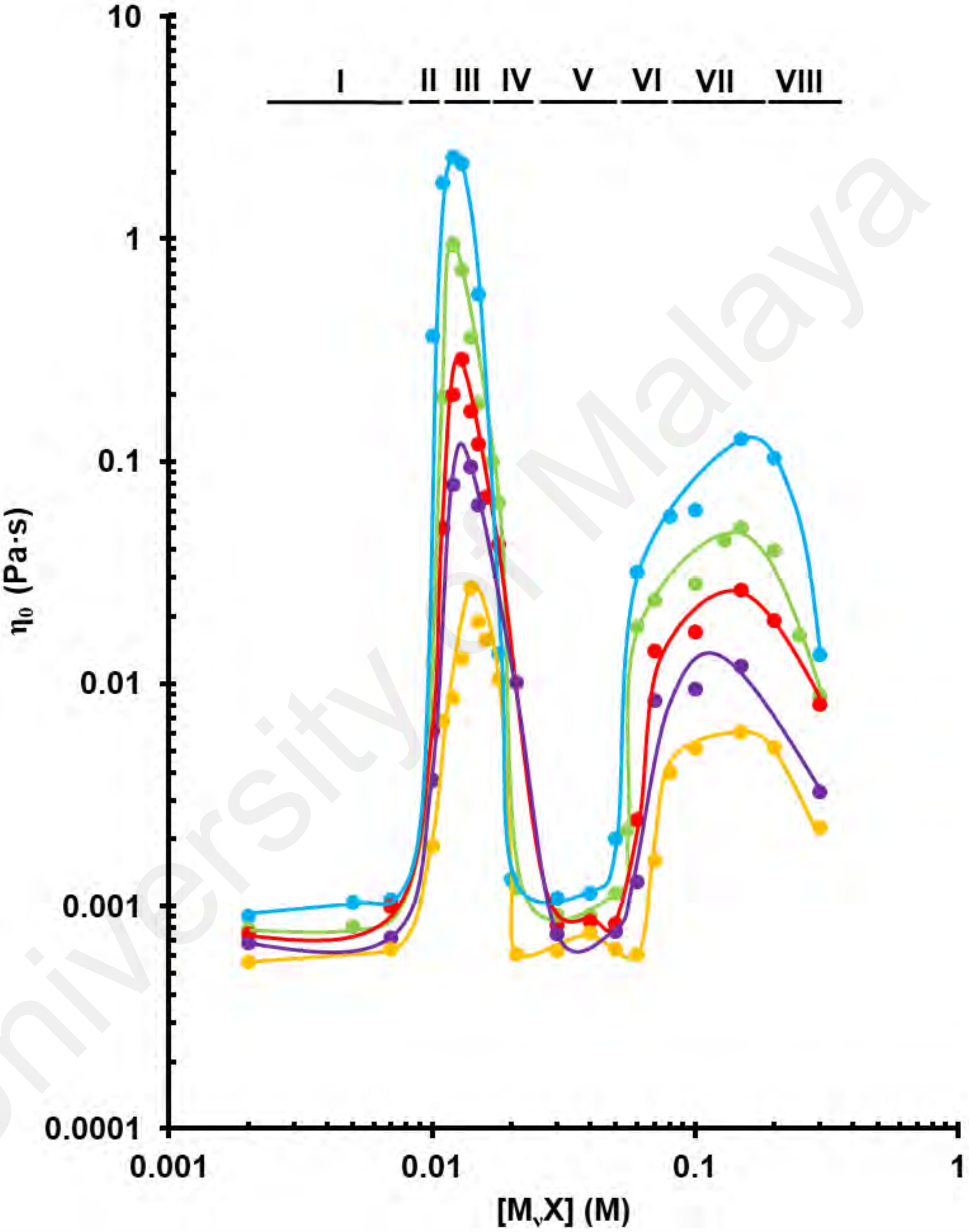

Figure 4.34: Plots showing the dependence of η_0 upon [$M_\nu X$] ($M_\nu X$ = 4-MeSaNa_ν with $\nu = 2$) for piperidinolysis of PSa^- at 0.2 mM PSa^-, 0.1 M Pip and 15 mM CTABr at 25 (blue), 35 (green), 40 (red), 45 (purple) and 55 (orange) °C.

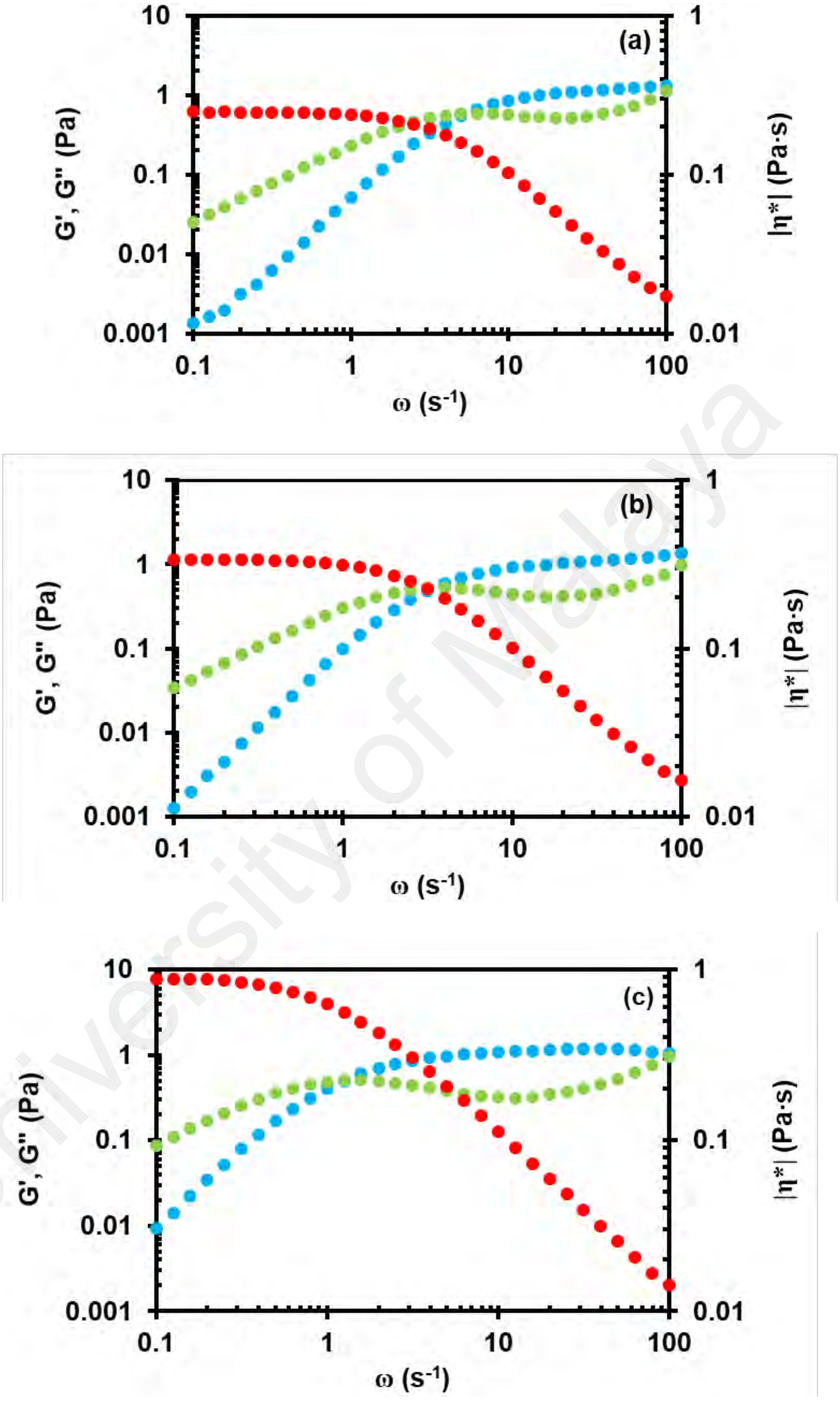

Figure 4.35: Elastic modulus, G' (blue), viscous modulus, G" (green) and complex viscosity, η^* (red) upon oscillatory shear frequency (ω) at a constant [$M_\nu X$] ($\nu = 2$), 15 mM CTABr, 0.2 mM PSaH, 0.03 M NaOH, 0.1 M Pip and 35 °C where (a): [M_2X] = 15 mM 4-MeOSaNa$_2$; (b): [M_2X] = 12 mM 3-MeSaNa$_2$; (c): [M_2X] = 12 mM 4-MeSaNa$_2$; (d): [M_2X] = 150 mM 4-MeSaNa$_2$.

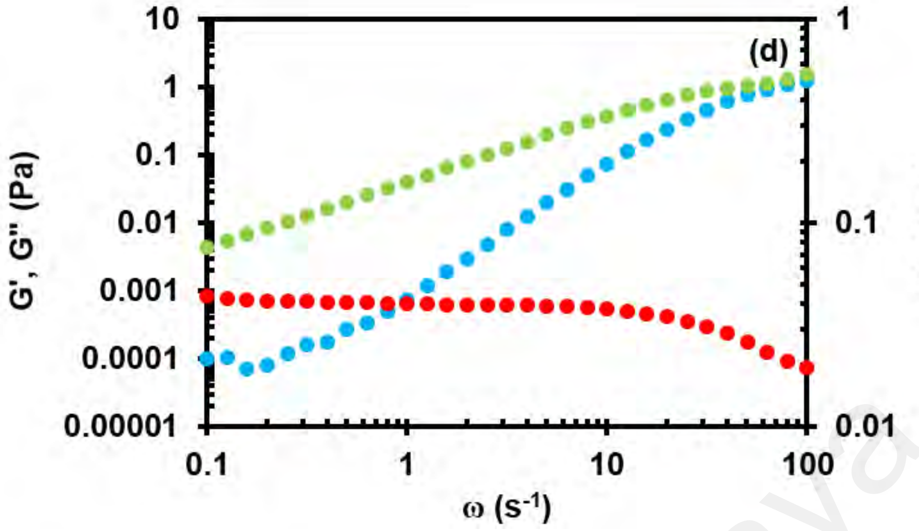

Figure 4.35, continued

The plots of zero shear viscosity (η_0) versus [$M_\nu X$] are shown in **Figures 4.32 – 4.34** for respective $M_\nu X$= 4-MeO- and 3-Me-, 4-MeSaNa$_\nu$ (ν = 2). Similar observations were obtained for $M_\nu X$= 4-MeO- and 3-Me-, 4-MeSaNa$_\nu$ (ν = 1, 2), which are shown in **Figures S19** – **S21** (see Appendix F - **Figures S19 – S21**). The values of η_0 were obtained from the initial plateau regions of flow curves, η versus $\dot{\gamma}$ at a constant [$M_\nu X$] and temperature. The visibility of a maximum in the plots of η_0 versus [$M_\nu X$] (**Figures 4.32 – 4.34** and **Figures S19 – S21**) at each temperature decreases with increasing temperature. However, the plots of **Figures 4.33** and **4.34** for respective $M_\nu X$= 3-Me- and 4-MeSaNa$_\nu$ (ν = 2), represent double maxima at each temperature, where the η_0 of first maximum is several fold larger than that at second maximum. Similar observations were obtained for $M_\nu X$= 3-Me- and 4-MeSaNa$_\nu$ (ν = 1, 2) which are shown in **Figures S20** and **S21** as well. It is noteworthy that the theoretical interpretation of such viscosity maximum plots is lacking (Davies *et al.*, 2006; Fagge *et al.*, 2016; Ziserman *et al.*, 2009) despite being no longer unusual for the aqueous ionic surfactant solutions containing counterionic salt (Dreiss, 2007; Raghavan *et al.*, 2002; Rehage & Hoffmann, 1991). It is relevant to note that the appearance of first viscosity maximum in the plots of η_0 versus [$M_\nu X$] (**Figures 4.33 –**

4.34, **Figures S20 – S21**) is indicative of the presence of linear WM, which is evidence from the occurrence of shear thinning behavior in the plots of η versus $\dot{\gamma}$ (**Figures 4.18 – 4.31**, **S10 – S18**). Hypothesis had been made in an attempt to explain the characteristic of micelles beyond this peak. One hypothesis favors linear WM transformed into branched WM while another favors the decrease in the length of WM with increasing values of C_S/C_D (Ziserman *et al.*, 2009). However, such viscosity maximum plots which are indicative of the presence of linear, entangled and branched WM has been established by the use of various physical techniques (Fagge *et al.*, 2016; Rehage & Hoffmann, 1991; Ziserman *et al.*, 2009).

In this study, the aqueous solution of CTABr/M_vX systems for different types of M_vX studied exhibit micro-structural transitions. The rheological results of aqueous solution containing increasing [M_vX] (M_vX = 4-MeOSaNa$_v$ (v = 1, 2)) indirectly indicates the morphological changes from SM-to-WM-to-branched micelles (**Figures 4.32** and **S19**). In these figures, each plot at different temperatures is divided into four different regions. The microstructural transitions for each region are described as follows: (i) Region I which corresponds to [M_vX] < ~5 mM contains only spherical/spheroidal/ellipsoidal micelles (SM). This prediction was supported indirectly from the observable flow curve of 5 mM M_vX which shows Newtonian fluid behavior with η not different from that of water (**Figures S18** and **S22** as well as **Figures S10** – **S13**) (see Appendix F). It is also relevant to note that this conclusion is drawn from the reported data which show the presence of only SM at 15 mM CTAX with X = Br^- (Romsted, 2007) and 2,6-$Cl_2C_6H_3CO_2^-$ (Carver *et al.*, 1996). (ii) Region II which corresponds to [M_vX] in the range > 5 mM - < 15 mM reveals the presence of short and long linear WM. This conclusion was made due to the presence of Newtonian flow behavior with the η value higher than that of water and this region also corresponds to the initial stage of structural transformation from SM to highly entangled WM. (iii) Region III which shows the maximum viscosity contains the network structural/entangled WM (EWM) while region IV is the region where branched micelles density increases with increasing [M_vX]. It is noteworthy to highlight the presence of a second weak maximum at 200 mM of M_vX. However, it is believed that this observation, at this concentration range is not the same as those for both M_vX = 3- and 4-MeSaNa$_v$.

An attemp has been made to support this prediction, where several kinetic runs were carried out under the reaction conditions as follows: (a) 10 mM NaOH, 100 mM Pip, 0.2 mM PSaH, 35 °C, 370 nm and varying CH_3CN content from 2 – 92 % v/v in mixed CH_3CN-H_2O solvent, as well as (b) 30 mM NaOH, 100 mM Pip, 0.2 mM PSaH, 35 °C, 370 nm and different [M_vX] = (M_vX = 4-Me- and 4-MeOSaNa$_v$ (ν = 2)). The calculated values of kinetic parameter, δ_{ap} of those kinetic runs were summarized in **Table S4** and **S5** (see Appendix A - **Table S5**), and are described as follows: The values of δ_{ap} increase nonlinearly from 1750 to 4350 $M^{-1}cm^{-1}$ with the increase in CH_3CN content which reveals medium polarity changes of that reaction mixtures. On the other hand, the values of δ_{ap} are almost independent of [4-MeOSaNa$_v$] within its range 0 - ~15 mM and then reveals a monotonic decrease with increasing [4-MeOSaNa$_v$] within its range ~30 – 300 mM. The values of δ_{ap} are almost independent of [4-MeSaNa$_v$] within its range 0 - ~50 mM. After this concentration, the δ_{ap} values show a sharp decrease with increasing [4-MeSaNa$_v$] until 70 mM and then become almost independent of [4-MeSaNa$_v$] within its range ~70 – 300 mM. From these observations, it can be concluded that [M_vX]-induced CTABr/M_vX aggregates structural transition, within [M_vX] range 50 – 300 mM, is not the same for 4-MeOSaNa$_v$ and 4-MeSaNa$_v$. The observed plots (**Figures 4.32** and **S19**) appear to be similar to those obtained for 5-MeOSaNa$_v$ under essentially similar conditions (Yusof & Khan, 2012).

The rheological results of aqueous CTABr solutions with increasing [M_vX] (M_vX = 4-MeSaNa$_v$ (ν = 1, 2)) indirectly indicate the morphological changes from SM-to-WM-to-small vesicles (SVs)/planar bilayer sheets (PBLS)-to-multilamellar vesicles (MLV) (**Figure 4.34**). In this figure, there are eight different regions exhibited by each plot at different temperatures. The microstructural transitions for each region are described as follows: (i) Regions I – IV which is in the [M_vX] range 2 – 18 mM are almost similar to the corresponding regions I – IV of **Figure 4.32**, except that: (i) the formation of short WM and long WM exhibited by the flow curves at respective 10 mM 4-MeOSaNa$_v$ and 3-, 4-MeSaNa$_v$. (ii) the decrease in η_0 with the increase in [3-, 4-MeSaNa$_v$] from 12 to 18 mM is ~10^3-fold compared to that of 4-MeOSaNa$_v$ which is only ~17-fold (Region IV). Thus, this observation indicates that region V for [M_vX] range ~21 – 50 mM may not contain branched micelles. It needs to be highlighted that region V reveals the turbid region within [M_vX] range > 25 - < 50 mM (**Figure 4.34**). Sreejith et. al in their report had detected (by the use of cryo-TEM) the presence of PBLS and Vs (Sreejith *et al.*, 2010) on related but not identical systems, where η_0 plots, similar to those in **Figure 4.33** and **Figure 4.34** were obtained. Another report had highlighted the existence of a precipitate/turbid phase which is due to the presence of PBLS (Kawasaki *et al.*, 2002). In view of these studies (Abdel-Rahem & Hoffmann, 2007; Kawasaki *et al.*, 2002; Zheng *et al.*, 2000), it may be reasonable to propose that regions V and VI – VIII contain most likely SVs/PBLS and MLV, respectively.

However, it should be bear in mind that this is a speculative claim only for aqueous solution of CTABr/4-MeSaNa$_v$ as well as CTABr/3-MeSaNa$_v$. Besides, the exact structure of micelles, for instance between small SM, SVs and PBLS as well as WM/ BWM and MLV cannot be easily differentiated by rheological measurements.

4.2.2 Rheological Measurements and Morphological Transitions of Aqueous CTABr/M$_v$X System Containing 15 mM CTABr and Different [M$_v$X] (v = 1) with M$_v$X = 2,3-, 2,4-, 2,5-, 2,6-, 3,4- and 3,5-Cl$_2$BzNa

In order to determine the values of η of aqueous CTABr/M$_v$X (M$_v$X = 2,3-, 2,4-, 2,5-, 2,6-, 3,4- and 3,5-Cl$_2$BzNa) solution, a steady-shear rheological measurements were carried out at different $\dot{\gamma}$ range (0.01 – 1000 s^{-1}) and 35 °C. The aqueous CTABr solution contains 0.2 mM PSaH, 100 mM Pip, 0.03 < 0.045 M NaOH, 15 mM CTABr and different values of [M$_v$X] range 10 – 340 mM. The plots of η versus $\dot{\gamma}$ at different [M$_v$X] values are shown in **Figures 4.36 – 4.41**.

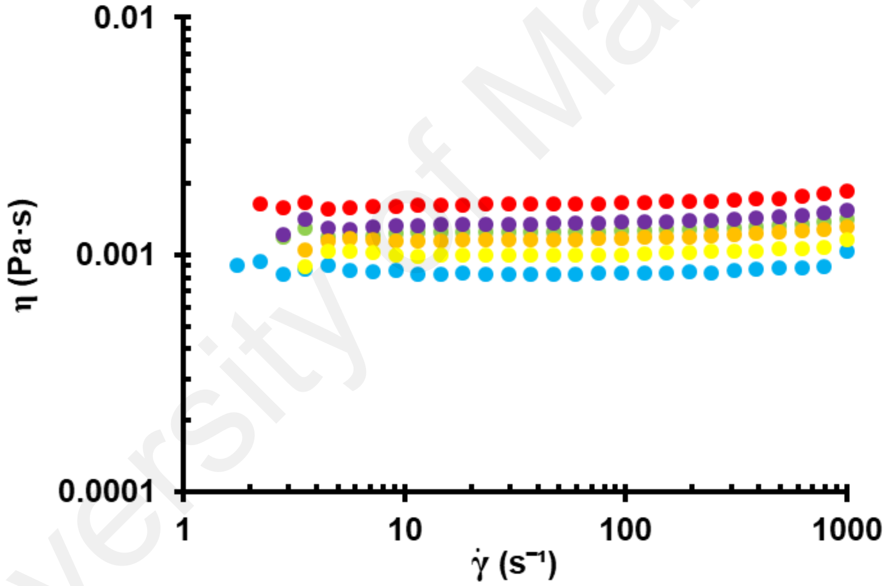

Figure 4.36: Plots showing the dependence of η upon $\dot{\gamma}$ for piperidinolysis of PSa$^-$ at 0.2 mM PSa$^-$, 0.1 M Pip, 15 mM CTABr and [M$_v$X] = [2,3-Cl$_2$BzNa$_v$] (mM) with v = 1 at 10 (blue), 20 (green), 40 (red), 70 (purple), 100 (orange) and 340 (yellow) at 35 °C.

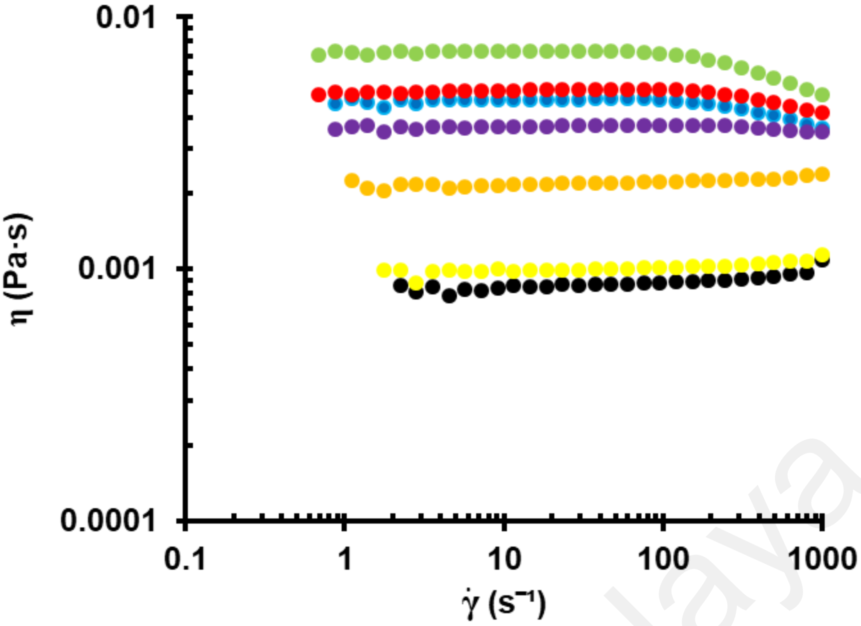

Figure 4.37: Plots showing the dependence of η upon γ̇ for piperidinolysis of PSa⁻ at 0.2 mM PSa⁻, 0.1 M Pip, 15 mM CTABr and $[M_vX] = [2,4\text{-}Cl_2BzNa_v]$ (mM) with ν = 1 at 10 (black), 20 (blue), 30 (green), 40 (red), 70 (purple), 100 (orange) and 340 (yellow) at 35 °C.

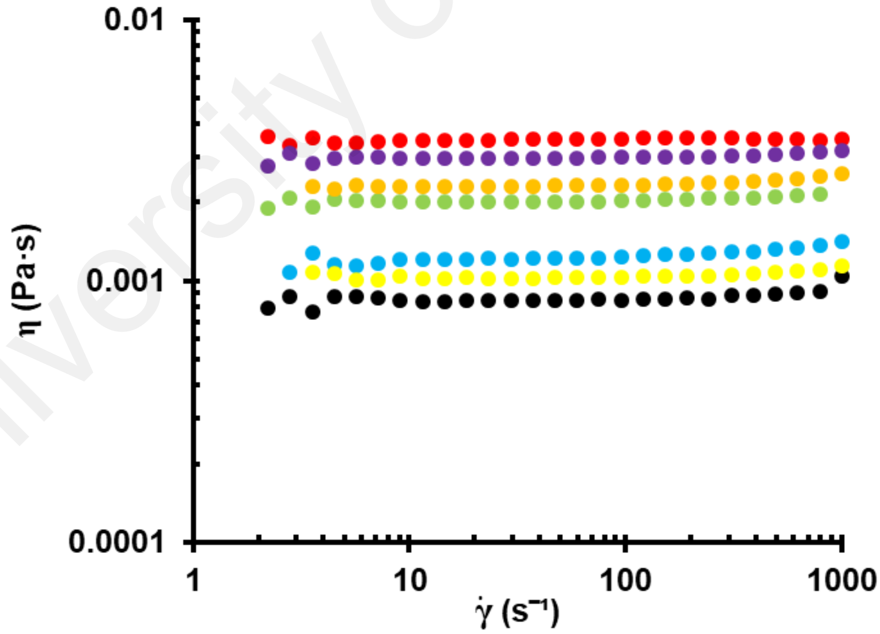

Figure 4.38: Plots showing the dependence of η upon γ̇ for piperidinolysis of PSa⁻ at 0.2 mM PSa⁻, 0.1 M Pip, 15 mM CTABr and $[M_vX] = [2,5\text{-}Cl_2BzNa_v]$ (mM) with ν = 1 at 10 (black), 15 (blue), 20 (green), 40 (red), 70 (purple), 100 (orange) and 340 (yellow) at 35 °C.

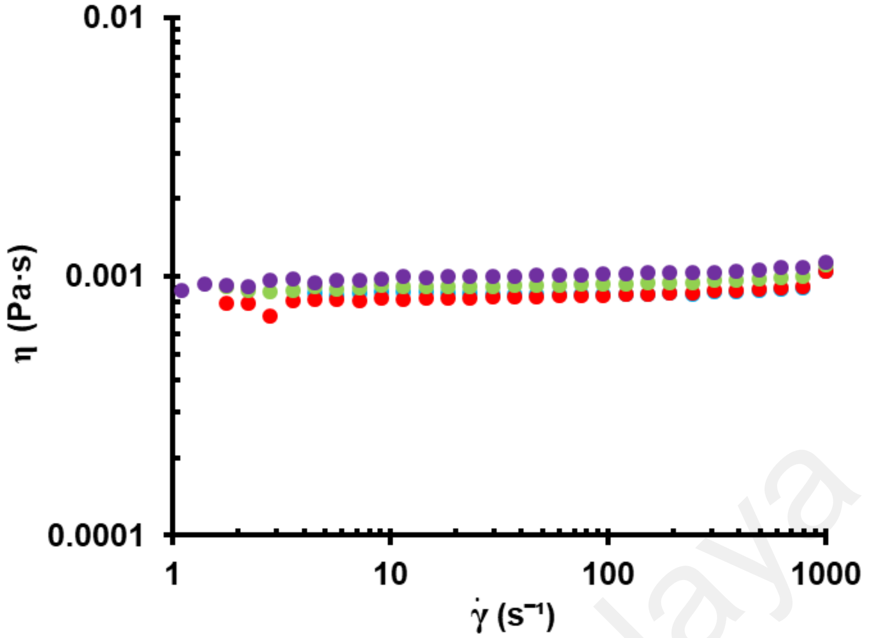

Figure 4.39: Plots showing the dependence of η upon $\dot{\gamma}$ for piperidinolysis of PSa$^-$ at 0.2 mM PSa$^-$, 0.1 M Pip, 15 mM CTABr and [M_vX] = [2,6-Cl_2BzNa_v] (mM) with ν = 1 at 10 (blue), 40 (green), 100 (red) and 340 (purple) at 35 °C.

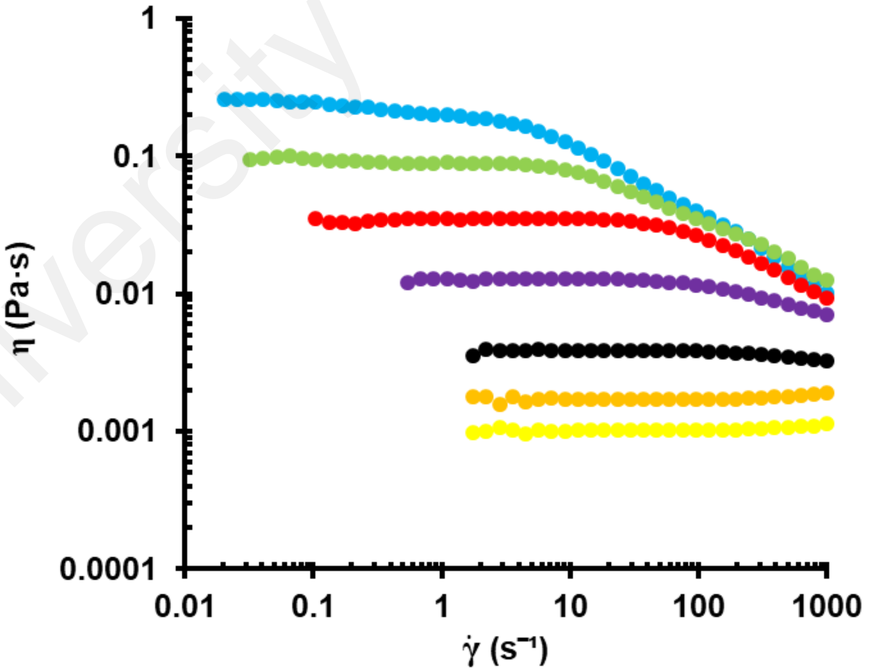

Figure 4.40: Plots showing the dependence of η upon $\dot{\gamma}$ for piperidinolysis of PSa$^-$ at 0.2 mM PSa$^-$, 0.1 M Pip, 15 mM CTABr and [M_vX] = [3,4-Cl_2BzNa_v] (mM) with ν = 1 at 10 (black), 13 (blue), 15 (green), 20 (red), 60 (purple), 100 (orange) and 340 (yellow) at 35 °C.

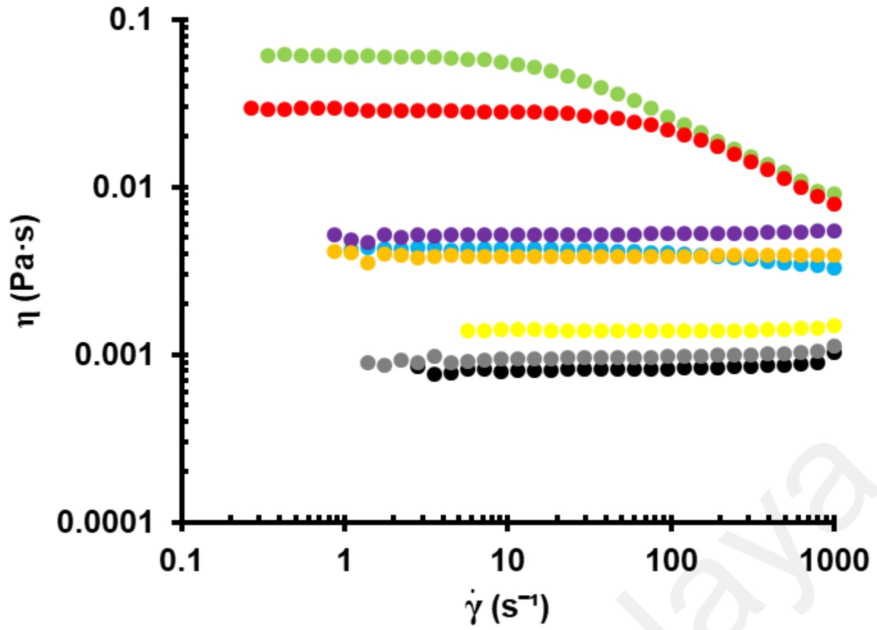

Figure 4.41: Plots showing the dependence of η upon $\dot{\gamma}$ for piperidinolysis of PSa^- at 0.2 mM PSa^-, 0.1 M Pip, 15 mM CTABr and $[M_vX]$ = $[3,5\text{-}Cl_2BzNa_v]$ (mM) with ν = 1 at 5 (black), 10 (blue), 13 (green), 15 (red), 40 (purple), 80 (orange), 120 (yellow) and 300 (grey) at 35 °C.

The observed results are described as follows: (a) For M_vX (= 2,4-, 3,4- and 3,5-Cl_2BzNa) (**Figures 4.37, 4.40** and **4.41**): The lowest value of $[M_vX]$ (= 10 mM) show only Newtonian fluid behavior with the viscosity not different from that of water i.e. ~0.001 Pa·s which is indicative of the presence of SM (Carver *et al.*, 1996; Fagge *et al.*, 2016; Romsted, 2007; Yusof *et al.*, 2013). The viscosity starts to increase within $[M_vX]$ range 15 to 30 mM (2,4-Cl_2BzNa), ~12 to 13 mM (3,4-Cl_2BzNa) and ~10 to 13 mM (3,5-Cl_2BzNa) until the highest viscosity value is achieved. The characteristic behavior of these flow curves show Newtonian behavior at the initial segments of flow curves (lower range of $\dot{\gamma}$), followed by shear thinning behavior (at higher range of $\dot{\gamma}$). It is noteworthy that the occurrence of such shear thinning in the plots of η versus $\dot{\gamma}$ reveals the presence of WM in such micellar solutions (Lin *et al.*, 2009a; Raghavan & Kaler, 2001; Yusof *et al.*, 2013). The network structure of WM is deformed by a higher shear. Thus, results in the formation of shear thinning which is due to the alignment of wormlike aggregates under flow. Shear thinning could be observed when the deformation is faster than the time required regaining equilibrium network structure. With increasing network density, the relaxation becomes slower, i.e. shear thinning begins at lower $\dot{\gamma}$ (Yusof *et al.*, 2013). (b) For M_vX (= 2,3-, 2,5- and 2,6-Cl_2BzNa) (**Figures 4.36, 4.38** and **4.39**), all the flow curves of these M_vX show only Newtonian flow behavior. For M_vX = 2,3- and 2,5-Cl_2BzNa, the viscosity values increase slightly from (~0.001 - ~0.002 Pa·s) within [M_vX] range >10 – 30 mM and then decrease with the increase in [M_vX] at this concentration. The η values for 2,6-Cl_2BzNa exhibit the values similar to that of water for the entire rheological runs covered within [M_vX] range 10 – 340 mM. These observations reveal the presence of merely SM only in that system. This conclusion was made based on the earlier rheological and cryo-TEM studies carried out under slightly different conditions (Carver *et al.*, 1996; Yusof *et al.*, 2013).

Figure 4.42 shows the plots of η_0 versus [M_vX] for different M_vX = 2,3-, 2,4-, 2,5-, 2,6-, 3,4- and 3,5-Cl_2BzNa. Each plot exhibit a maximum, except for 2,6-Cl_2BzNa and 3,5-Cl_2BzNa which show the respective absence of maximum and presence of double maxima. However, the presence of non-symmetrical maxima were noticed for 2,4-, 3,4- and 3,5-Cl_2BzNa. Early study had reported the η_0 versus [MX] plots for 0.05 M cetylpyridinium chloride (CPyCl) and MX systems (MX = 2-, 3- and 4-CH_3BzNa, 4-C_2H_5BzNa, 4-C_3H_7BzNa and 4-$C_5H_{11}BzNa$), where broad maxima exist for MX = 3- and 4-CH_3BzNa (similar to those for M_vX = 2,3- and 2,5-Cl_2BzNa) and nearly symmetrical double maxima for MX = 4-C_2H_5BzNa, 4-C_3H_7BzNa and 4-$C_5H_{11}BzNa$ (Rehage & Hoffmann, 1991; Yusof *et al.*, 2013). The observed plots of η_0 versus [M_vX] for both M_vX = 3,4- and 3,5-Cl_2BzNa are almost similar to those obtained for M_vX = 4-MeOSaNa_v. However, the origin of these maxima is not fully understood at the molecular level (Davies *et al.*, 2006; Dreiss, 2007; Yusof *et al.*, 2013; Ziserman *et al.*, 2009). It is well known that the characteristic behavior of such viscosity maximum in the plots of η_0

versus [M_vX] are indicative of the presence of long linear, entangled and branched WM in the aqueous solution of surfactant/MX solutions (Abdel-Rahem, 2008; Ait-Ali & Makhloufi, 1997; Ali & Makhloufi, 1999; Davies *et al.*, 1996; Dreiss, 2007; Razak *et al.*, 2016; Rehage & Hoffmann, 1991; Schubert *et al.*, 2004; Yusof *et al.*, 2013).

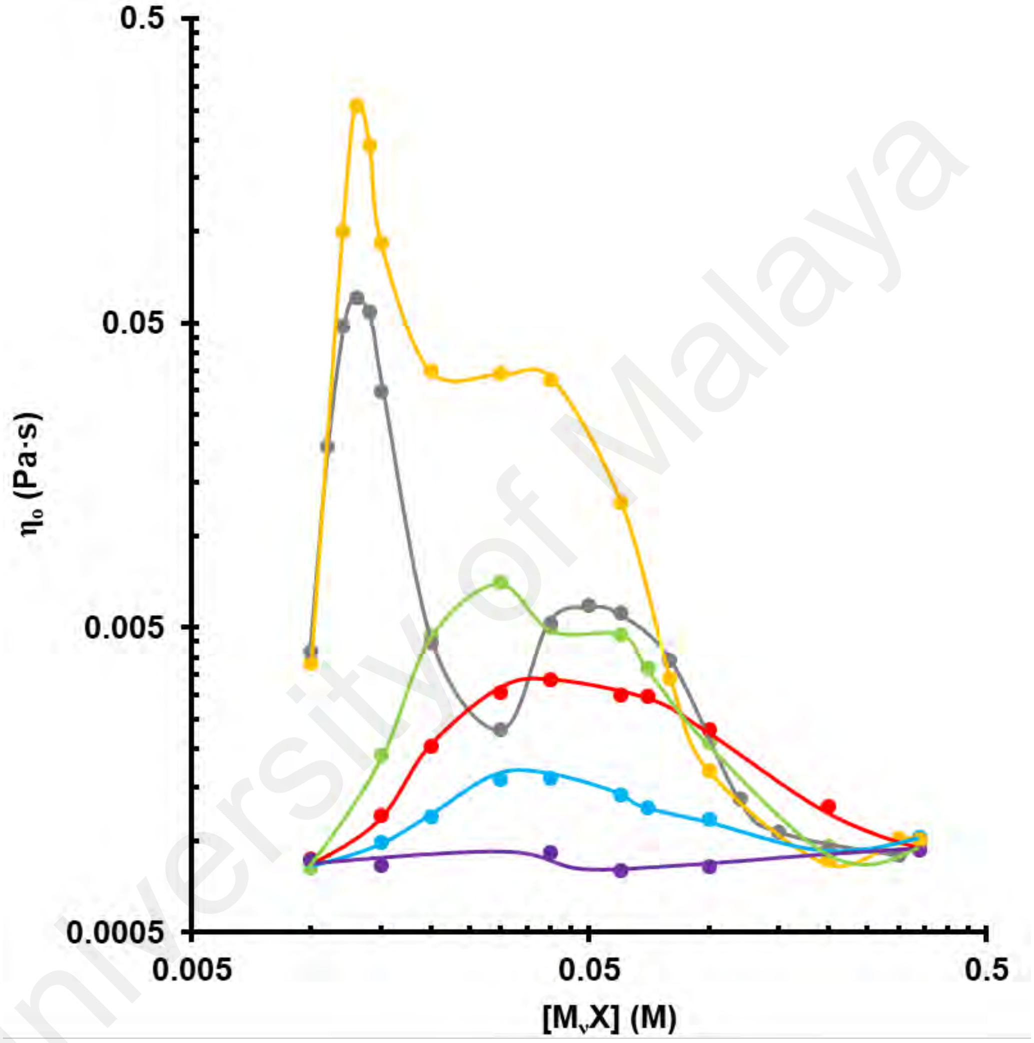

Figure 4.42: Plots of η_0 versus [M_vX] for piperidinolysis of PSa^- at 0.2 mM PSa^-, 0.1 M Pip, 15 mM CTABr and M_vX (v = 1): 2,3-$Cl_2BzCOONa$ (blue), 2,4-$Cl_2BzCOONa$ (green), 2,5-$Cl_2BzCOONa$ (red), 2,6-$Cl_2BzCOONa$ (purple), 3,4-$Cl_2BzCOONa$ (orange) and 3,5-$Cl_2BzCOONa$ (grey) at 35 °C.

In order to support the rheological results of X-induced micellar structure of aqueous CTABr/M_vX solution, turbidity measurements were carried out at 0.2 mM PSaH, 0.03 M NaOH, 100 mM Pip, 15 mM CTABr and different [M_vX] range from 1 – 300 mM (for M_vX = 2,3-, 2,4-, 2,5-, 2,6-, 3,4- and 3,5-Cl_2BzNa) (Razak & Khan, 2013; Yusof *et al.*,

2013) in which their counterion affinity to CTABr micelles have been quantified. The plots of turbidity for each dichlorobenzoate substituted benzoate salts in the present study are shown in **Figure 4.43**. It is necessary to remind that, although the surfactant solution looks clear to the naked eye, it might contains small unilamellar vesicles like the reported one in the earlier study, where the surfactant solution shows turbidity of ~0.1 absorbance units at 500 nm (Davies *et al.*, 2006; Razak & Khan, 2013). Turbidity of the present study was expressed in absorbance units (A_{ob}) which represents the corrected absorbance due to the presence of CTABr/M_vX aggregates only. The characteristics behavior of each plot in **Figure 4.43** are described as follows: (i) The presence of A_{ob} maxima were observed at a range of ~70, ~50 and ~100 mM for M_vX = 2,3-, 2,4- and 3,4-Cl_2BzNa, respectively while such maxima are absent for M_vX = 2,6-Cl_2BzNa with an average value of A_{ob} = 0.003. (ii) For M_vX = 3,5-Cl_2BzNa, a maximum value of A_{ob} (= 0.11) was observed at 25

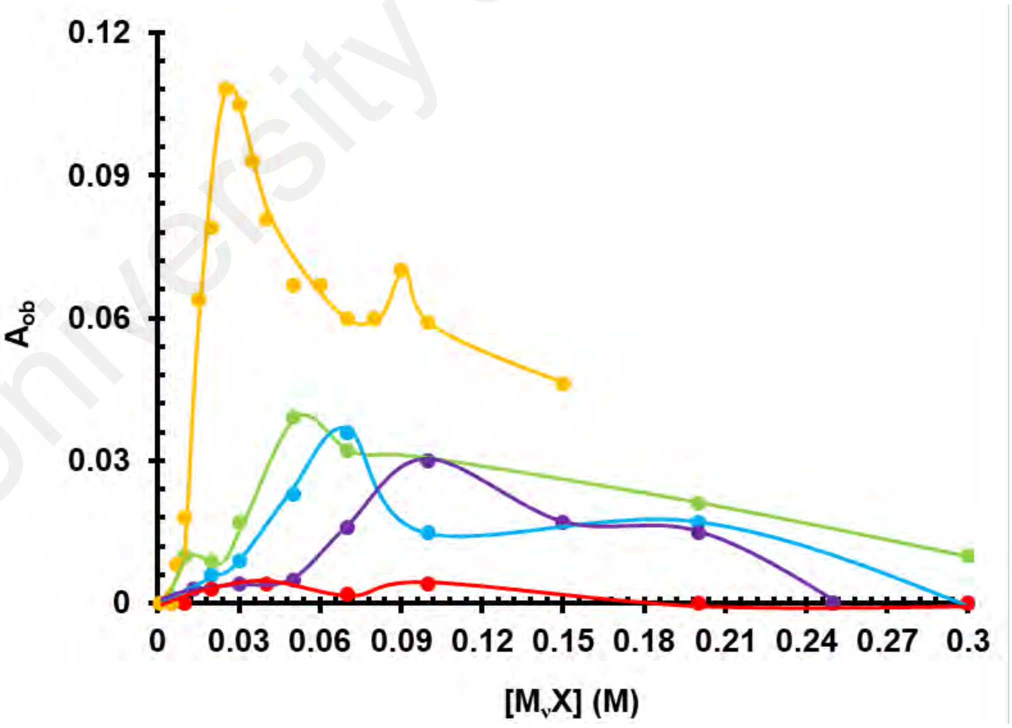

Figure 4.43: Effects of $[M_vX]$ on corrected absorbance at 600 nm, A_{ob}, (i. e. absorbance due to presence of CTABr/M_vX aggregates) of aqueous solutions containing 15 mM CTABr, 0.1 M Pip, 0.03 M NaOH and 0.2 mM PSaH at 35 °C where M_vX = 2,3-$Cl_2BzCOONa$ (blue), 2,4-$Cl_2BzCOONa$ (green), 2,6-$Cl_2BzCOONa$ (red), 3,4-$Cl_2BzCOONa$ (purple) and 3,5-$Cl_2BzCOONa$ (orange).

mM 3,5-Cl_2BzNa. The plot of viscosity for 3,5-Cl_2BzNa shows the presence of double maxima, each at 13 mM (with η_0^{max} = 0.061 Pa·s) and 40 – 60 mM (with η_0^{max} = 0.006 Pa·s) 3,5-Cl_2BzNa.

Davies et. al (2006) and Razak & Khan (2013) reported the presence of small unilamellar vesicles in aqueous CTABr/M_vX solution with absorbance units of ~0.1 at 500 nm. Perhaps it is noteworthy to conclude that the aqueous solution of CTABr/M_vX (M_vX = 3,5-Cl_2BzNa) contains significant concentration of Vs. Carver et. al (Carver *et al.*, 1996) had reported the maximum value of A_{ob} (= ~0.03 – 0.04) obtained at $\geq$ 50 mM MX (MX = 2,3-, 2,4- and 3,4-Cl_2BzNa) contain only rodlike or WM. However, the values of A_{ob} obtained from the present study for M_vX = 2,3- and 2,4-Cl_2BzNa are $\leq$ 0.009 at $\leq$ 20 mM while for M_vX = 3,4-Cl_2BzNa, the $A_{ob} \leq 0.005$ at $\leq$ 50 mM. Earlier studies (Carver *et al.*, 1996; Lin *et al.*, 2001; Magid *et al.*, 1990) reveal that the presence of long linear and entangled WM as well as branched micelles are the characteristic behavior of first sharp viscosity maximum as exhibited by **Figure 4.42**, where the presence of such aggregates in the aqueous solution of CTABr/M_vX did not show any turbidity. It is interesting to note that, for M_vX = 3,5-Cl_2BzNa, the viscosity plot of minimum value corresponds to the turbidity plot of maximum value. It has been shown by the earlier study (Sreejith *et al.*, 2010) on closely related systems where the turbid region is indicative of the planar bilayer sheets and Vs. It is reported that the existence of precipitate/turbid phase are attributed to the presence of planar bilayer sheets (Kawasaki *et al.*, 2002; Razak & Khan, 2013). On the other hand, the viscosity values similar to that of water were obtained for CTABr/MX solutions that contain unilamellar vesicles (Yusof & Khan, 2012).

4.2.3 Rheological Measurements and Morphological Transitions of Aqueous CTABr/M$_v$X System Containing 15 mM CTABr and Different [M$_v$X] ($\nu = 1$) with M$_v$X = Sodium Acetate, Sodium Propanoate, Sodium Butanoate, Sodium Pentanoate, Sodium Heptanoate and Sodium Octanoate

In order to determine the η values of aqueous CTABr/M$_v$X system, a steady-shear rheological measurements were carried out on aqueous solution of different [M$_v$X] (M$_v$X = sodium acetate, sodium propanoate, sodium butanoate, sodium pentanoate, sodium heptanoate and sodium octanoate), as well as at different $\dot{\gamma}$ range (0.01 – 1000 s^{-1}) and 35 °C. The aqueous CTABr solution contains 0.3 mM N-2MeOPhPTH, 10 mM NaOH, 15 mM CTABr and different values of [M$_v$X] range 1 – 1000 mM. The plots of η versus $\dot{\gamma}$ for all aliphatic salts studied except octanoate salt showed the presence of only Newtonian behavior with the η value similar to η of water. However, the observed η of that system on octanoate salt is slightly higher than the η of water which is ~0.002 Pa·s. The plots of η versus $\dot{\gamma}$ of those salts are shown in **Figure S22**. The rheological results of these systems were summarized in **Figure 4.44**, where the values of η_0 at different [M$_v$X] values are shown.

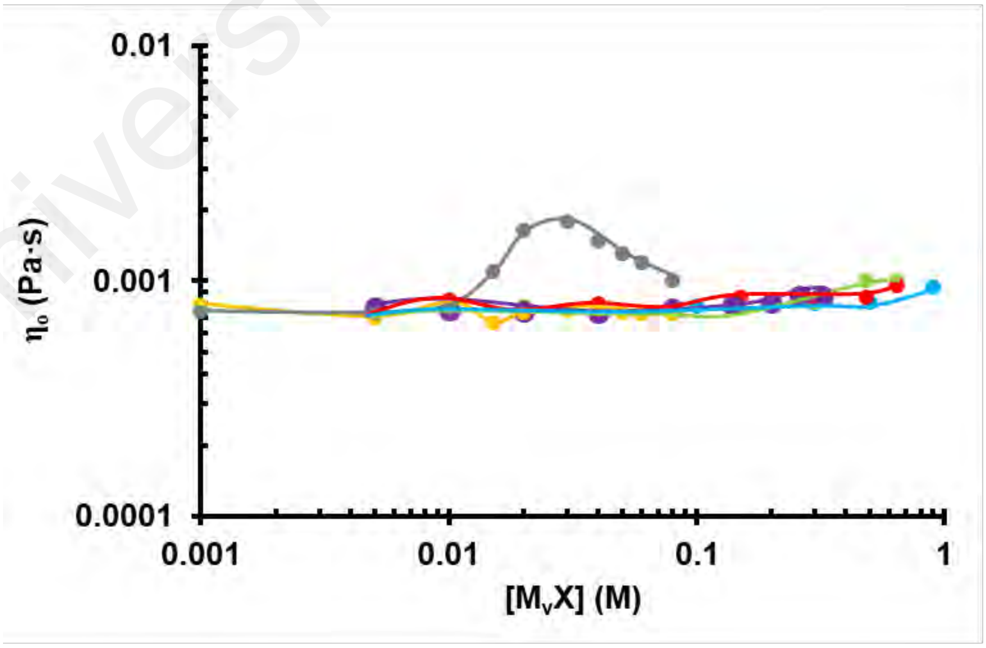

Figure 4.44: Plots of η_0 versus [M$_v$X] for aqueous solution mixture containing 0.3 mM N-2-MeOPhPTH, 0.01 M NaOH, 15 mM CTABr and M$_v$X ($\nu = 1$): sodium acetate (blue), sodium propanoate (green), sodium butyrate (red), sodium pentanoate (purple), sodium heptanoate (orange) and sodium octanoate (grey) at 35 °C.

The observed results are described as follows: (a) The η values at different [M_vX] (M_vX = sodium acetate, sodium propanoate, sodium butanoate, sodium pentanoate and sodium heptanoate) exhibit the values of η similar to that of water for the entire rheological runs covered within [M_vX] range 1 – 1000 mM. These observations reveal the presence of merely SM only in the systems. This conclusion was made based on the earlier rheological and cryo-TEM studies carried out under slightly different conditions (Carver *et al.*, 1996; Yusof *et al.*, 2013). (b) For M_vX (= sodium octanoate), the lower value of [M_vX], range 1 to 15 mM show only Newtonian fluid behavior with the viscosity comparable to that of water i.e. ~0.001 Pa·s which is indicative of the presence of SM (Carver *et al.*, 1996; Fagge *et al.*, 2016; Romsted, 2007; Yusof *et al.*, 2013). The viscosity values increase slightly from (~0.001 - ~0.002 Pa·s) within [M_vX] range ~20 to 30 mM and then decrease with the increase in [M_vX] beyond this concentration.

Figure 4.44 shows the plots of η_0 versus [M_vX] for different M_vX = sodium acetate, sodium propanoate, sodium butanoate, sodium pentanoate, sodium heptanoate and sodium octanoate. Each plot showed an absence of maximum, except for octanoate salt which showed the presence of broad maxima. However, the presence of this maximum was in the range of ~0.002 Pa·s. Early study had reported the presence of broad maxima in the plots of η_0 versus [MX] for 0.05 M cetylpyridinium chloride (CPyCl) and MX systems (MX = 3- and 4-CH_3BzNa) (Rehage & Hoffmann, 1991; Yusof *et al.*, 2013). It is well known that the characteristic behavior of such viscosity maximum in the plots of η_0 versus [M_vX] are indicative of the presence of long linear, entangled and branched WM in the aqueous solution of surfactant/MX solution (Abdel-Rahem, 2008; Ait-Ali & Makhloufi, 1997; Ali & Makhloufi, 1999; Davies *et al.*, 1996; Dreiss, 2007; Razak *et al.*, 2016; Rehage & Hoffmann, 1991; Schubert *et al.*, 2004; Yusof *et al.*, 2013) It is relevant to note that the aqueous solution of CTABr/M_vX system, for (M_vX = sodium acetate, sodium propanoate, sodium butanoate, sodium pentanoate, sodium heptanoate and sodium octanoate), did not show any turbidity development for the entire rheological runs. Thus, it indicates the absence of probable unilamellar vesicles in those systems.

4.2.4 Determination of Flow Activation Energy, E_a by Using Arrhenius-Type Empirical Relationship, of Aqueous CTABr/M_vX Systems with Various Aggregate Structures

The value of E_a could be determined by knowing at least, the values of η_0 obtained at different temperature ranges. In this study, the values of η_0 for different [M_vX] as well as [M_vX]$_{sc}$ (where [M_vX]$_{sc}$ represents a specific value of [M_vX] at which the viscosity maximum occurs in the plot of η_0 versus [M_vX]) were obtained within temperature range of 20 – 55 °C for M_vX = 4-MeOSaNa$_v$ and 3-, 4-MeSaNa$_v$ as well as M_vX = 2,3-, 2,4-, 2,5-, 2,6-, 3,4- and 3,5-Cl_2BzNa. The value of η_0 were found to fit to an Arrhenius-type of empirical relationship, **Eq. 4.15**,

$$\eta_0 = \mathrm{A}\exp(\mathrm{E_a}/\mathrm{RT}) \qquad \textbf{Eq. 4.15}$$

where A is pre-exponential factor, E_a represents flow activation energy, T is absolute temperature in Kelvin (K) and R is the universal gas constant (= 8.314 J $mol^{-1}K^{-1}$). The calculated values of A and E_a at different [M_vX] (for M_vX = 4-MeOSaNa$_v$ and 3-, 4-MeSaNa$_v$) are shown in **Table 4.8**.

Similarly, those values at [M_vX]$_{sc}$ for M_vX = 2,3-, 2,4-, 2,5-, 2,6-, 3,4- and 3,5-Cl_2BzNa are also shown in **Table 4.8**. The [M_vX]$_{sc}$ of 2,6-Cl_2BzNa was selected at ~40 mM 2,6-Cl_2BzNa, which is similar to those for 2,3-, 2,4-, 2,5-, 3,4- and 3,5-Cl_2BzNa. It is due to the absence of such viscosity maximum in the plot of η_0 versus [2,6-Cl_2BzNa]. The observed data fit to **Eq. 4.15** was satisfactory in terms of residual errors (RE = 100 × $(\ln \eta_0 - \ln \eta_0^{\mathrm{cald}})/\ln \eta_0$)) (**Table 4.8**) and standard deviations associated with the calculated parameters, ln (A) and E_a. The solid lines in the plots of **Figure 4.45** were drawn through the calculated data points. However, the solid line drawn at 40 mM 3-MeSaNa$_v$ (ν =2) and T range 20 – 55 °C was not perfectly linear but certainly reveal linear plots within T

Table 4.8: Values of ln A and E_a, Calculated from **Eq 4.15** at Different [M_vX].

M_vX	[M_vX] (mM)	CTABr-M_vX aggregate Structure [a]	Region [b]	- ln A (Pa·s)	E_a (kJ mol^{-1})	RE [c] (%)
4-MeOSaNa$_v$	10	SWM [d]	II	20.5 ± 2.0[e]	36.3 ± 5.3[e]	-1.71
	15	EWM [f]	III	69.5 ± 7.3	174 ± 19	-22.3
	20	EWM + BWM [g]	IV	44.6 ± 2.8	108 ± 7	4.36
	40	BWM	IV	24.8 ± 0.5	53.2 ± 1.3	0.55
	70	BWM	IV	27.0 ± 0.4	58.5 ± 1.1	0.49
	100	BWM	IV	28.0 ± 0.6	61.8 ± 1.6	-0.54
4-MeSaNa$_v$	10	LWM [h]	II	35.0 ± 2.4	78.1 ± 6.2	-1.89
	12	EWM	III	75.3 ± 2.5	192 ± 7	-55.7
	14	EWM + BWM	IV	43.1 ± 1.0	108 ± 3	-2.35
	15	EWM + BWM	IV	39.1 ± 3.5	96.0 ± 9.2	-6.64
	18	EWM + BWM	IV	32.7 ± 2.1	76.7 ± 5.5	-2.40
	> 25 - < 50	SVs/PBLS [i]	V	13.2 ± 0.3	15.9 ± 0.8	0.20
	100	MLV [j]	VI	32.6 ± 1.7	74.2 ± 4.5	2.01
	150	MLVM [k]	VII	39.4 ± 3.1	93.1 ± 8.0	3.87
	300	MLV	VIII	28.3 ± 6.1	60.6 ± 16.0	-5.66
3-MeSaNa$_v$ [l]	12	EWM	III	67.6 ± 1.3	171 ± 3	28.4
	> 25 - < 50	SVs/PBLS	V	22.1 ± 2.3	39.6 ± 6.0	-4.66
				(33.0 ± 0.8)[n]	(66.7 ± 1.9)[n]	0.40
				(14.1 ± 0.8)[o]	(18.3 ± 2.0)[o]	-0.41
	80	MLV	VI	32.0 ± 1.6	71.2 ± 4.0	-5.82
2,3-Cl$_2$BzNa$_v$ [p]	40	SWM		23.3 ± 1.7	43.4 ± 4.3	-4.40

Table 4.8 continued

M_vX	$[M_vX]$ (mM)	CTABr-M_vX aggregate structure [a]	Region [b]	- ln A (Pa·s)	E_a (kJ mol^{-1})	RE [c] (%)
				(31.3 ± 2.4)[n]	(63.5 ± 6.0)[n]	1.1
				(18.6 ± 0.2)[o]	(31.0 ± 0.5)[o]	0.1
2,4-Cl_2BzNa_v [p]	30	EWM + BWM		51.0 ± 5.0	119 ± 13	-30
				(73.2 ± 2.2)[n]	(175 ± 5)[n]	3.5
				(32.8 ± 1.7)[o]	(71.3 ± 4.6)[o]	-1.4
2,5-Cl_2BzNa_v [p]	40	SWM		32.6 ± 3.5	69.8 ± 9.0	-12
				(48.4 ± 3.0)[n]	(109 ± 7)[n]	1.9
				(21.4 ± 2.0)[o]	(40.1 ± 5.4)[o]	1.4
2,6-Cl_2BzNa_v [p]	40	SM		14.0 ± 0.7	17.7 ± 1.9	1.5
3,4-Cl_2BzNa_v [p]	13	EWM		67.9 ± 2.8	169 ± 7	38
	40			46.8 ± 2.7	111 ± 7	-25
3,5-Cl_2BzNa_v [p]	13	EWM + Vs		38.4 ± 1.9	90.5 ± 4.8	-9.0
	40			27.6 ± 1.4	57.2 ± 3.7	3.7
	30			16.7 ± 1.2	26.9 ± 3.0	-2.5

[a] Approximate structure of CTABr-M_vX aggregate and unless mentioned, the values of –ln A and E_a were obtained from observed data obtained within temperature range 35 – 55 °C. [b] Micro aggregate structural regions based upon the plots of **Figures 4.32** – **4.34** and **Figure 4.42**. [c] Maximum absolute value of RE obtained in the data treatment with logarithmic form of **Eq. 4.15**. [d] SWM = short linear wormlike micelles. [e] Error limits are standard deviations. [f] EWM = entangled WM. [g] BWM = branched WM. [h] LWM = long linear WM. [i] SVs = small vesicles, PBLS = planar bilayer sheets. [j] MLV = multilamellar vesicles. [k] MLVM = MLV of maximum mean size. [l] Values of –ln A and E_a were calculated from **Eq. 4.15** using observed data obtained within temperature range 20 – 55 °C. [m] Parenthesized values were calculated from **Eq. 4.15** using observed data obtained within: [n] T range 20 – 35 °C and [o] T range 35 – 55 °C. [p] The values of –ln A and E_a were obtained from published paper by Razak & Khan (2013).

range 20 – 35 °C as well as 35 – 55 °C (which were represented by the dotted lines in **Figure 4.45**). Similar plots were obtained for M_vX = 2,3-, 2,4- and 2,5-Cl_2BzNa. In contrast, M_vX = 3,4- and 3,5-Cl_2BzNa reveal linear plots within the temperature range of 20 – 55 °C (**Figure 4.46**).

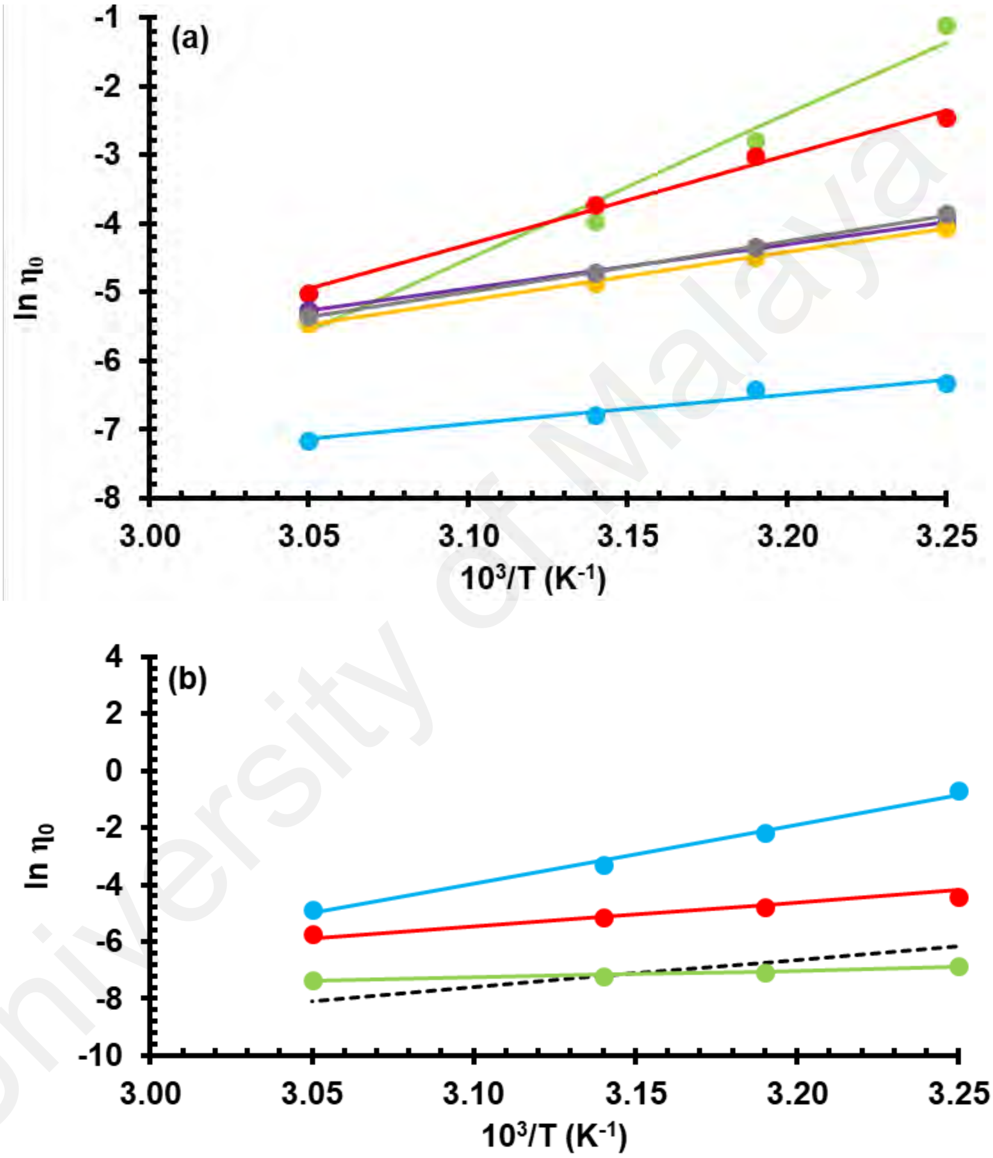

Figure 4.45: Plots showing the dependence of ln η_0 upon 1/T for samples containing 0.2 mM PSa^-, 0.1 M Pip, 15 mM CTABr and various concentrations of M_vX where (a): [4-MeOSaNa$_v$]/mM ($\nu = 2$): 10 (blue), 15 (green), 20 (red), 40 (purple), 70 (orange), and 100 (grey); (b): [3-MeSaNa$_v$]/mM (ν = 2): 12 (blue), 40 (green), 80 (red); and (c): [4-MeSaNa$_v$]/mM (ν = 2): 10 (black), 12 (blue), 14 (green), 15 (red), 30-40 (purple), 100 (orange), 150 (grey), 300 (pink) at temperature range of 20 – 55 °C. The solid lines are drawn drawn through the calculated data points using Eq. 4.15 with ln A and E_a listed in Table 4.8.

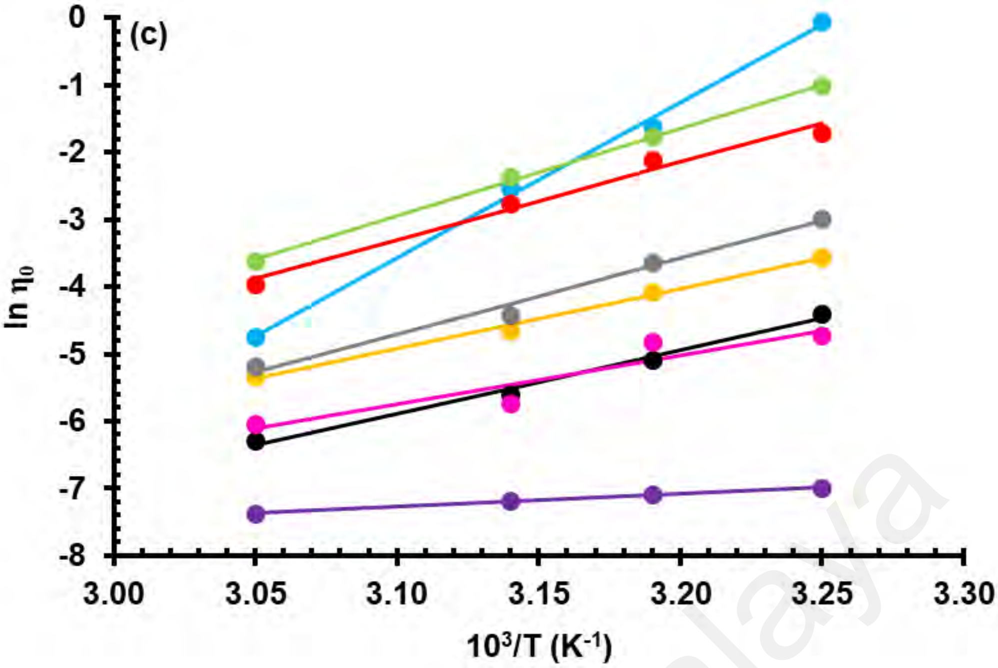

Figure 4.45, continued

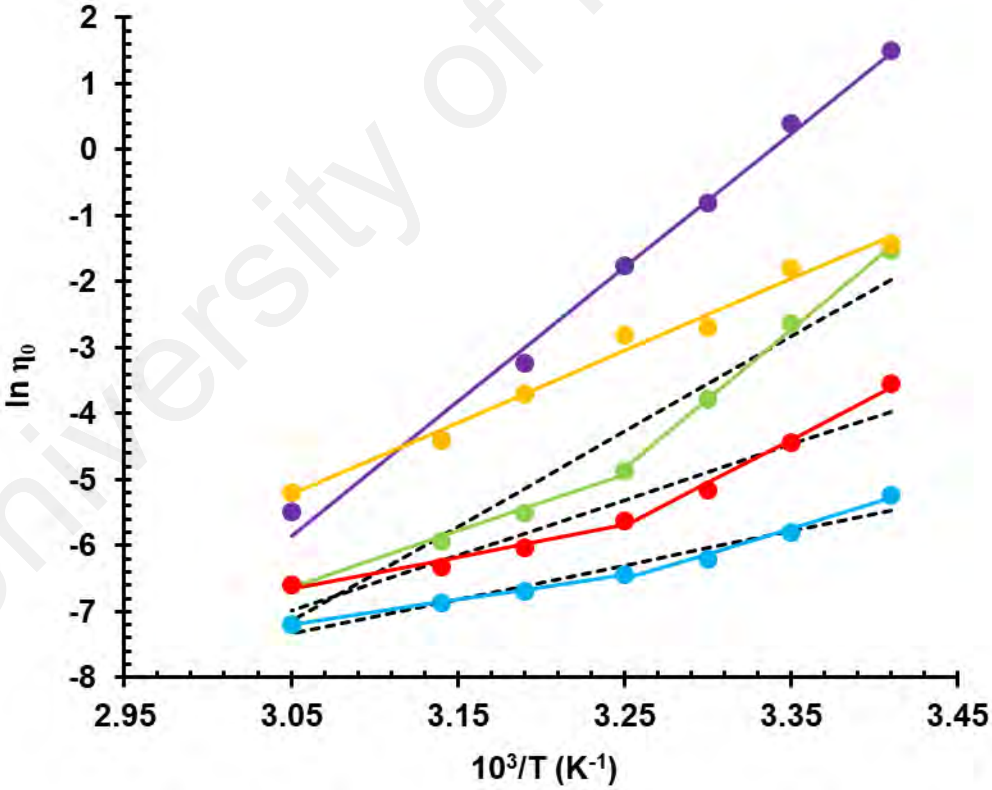

Figure 4.46: Plots showing the dependence of ln η_0 upon 1/T for samples containing 0.2 mM PSa^-, 0.1 M Pip, 15 mM CTABr and various concentrations of M_vX where $[M_vX]$ (v = 1): 40 mM 2,3-Cl_2BzNa (blue), 30 mM 2,4-Cl_2BzNa (green), 40 mM 2,5-Cl_2BzNa (red), 130 mM 3,4-Cl_2BzNa (purple) and 130 mM 3,5-Cl_2BzNa (orange) at temperature range of 20 – 55 °C. The solid lines are drawn through the calculated data points using Eq. 4.15 with ln A and E_a listed in Table 4.8.

The nonlinear plots of ln η_0 versus 1/T, as exhibited by M_vX = 2,3-, 2,4- and 2,5-Cl_2BzNa as well as 3-$MeSaNa_v$ were almost similar to the reported one (Candau *et al.*, 1989; Kern *et al.*, 1994; Razak & Khan, 2013), where two different slopes were obtained at different temperature ranges. However, the slope values of the Arrhenius plots of M_vX = 2,3-, 2,4- and 2,5-Cl_2BzNa as well as 3-$MeSaNa_v$ are higher within the temperature range of 20 – 35 °C, compared to that at 35 – 55 °C (Razak & Khan, 2013). The probable reasons for this observation may be described as follows: the plots of ln η_0 versus 1/T appear to be linear when the E_a value remains essentially constant, which reveals indirectly that the structures of aqueous CTABr/M_vX aggregates remain unchanged (Razak & Khan, 2013). Recently, it has been shown that the temperature increase from 35 to 55 °C resulted in several fold decrease in the value of R_X^{Br} (Razak & Khan, 2013; Yusof & Khan, 2012). These values of R_X^{Br} were determined only in the presence of similar structures of aqueous CTABr/M_vX aggregates. The significantly high values of R_X^{Br} at 35 °C, (i.e. R_X^{Br} = 119 and 206 for respective 3,4- and 3,5-Cl_2BzNa) (Razak & Khan, 2013; Yusof *et al.*, 2013) may not result in the decrease of R_X^{Br} value at 55 °C to as low as $\leq$ ~6. Thus, it reveals the presence of aggregates of similar structures (SM or WM or Vs) in the system (i.e. E_a remains constant). On the other hand, the reported R_X^{Br} values at 35 °C for 2,3-, 2,4- and 2,5-Cl_2BzNa are 25, 45 and 25, respectively, which may result in the formation of different CTABr/M_vX aggregate structures at higher temperature (i.e. 55 °C) (Razak & Khan, 2013; Yusof *et al.*, 2013). The presence of RM at 35 °C (i.e. R_X^{Br} = ~25) will probably change to SM at 55 °C (Razak & Khan, 2013).

It had been reported elsewhere (Raghavan & Kaler, 2001) that the values of E_a of various aqueous cationic surfactant solutions containing WM vary in the range 70 – 300 kJ mol^{-1}. For 3- and 4-$MeSaNa_v$ (ν = 2), the value of E_a (=15.9 kJ mol^{-1}) as exhibited by region V is similar to the reported value of E_a (=15.3 – 17.6 kJ mol^{-1}) for aqueous isotropic liquid containing 2 % poly(ethylene glycol) and ≤ 2 % Laponite RD (clay) (Morariu & Bercea, 2011) where small aggregates formed by several clay discs suspended in water. Davies et. al and Zhang et. al had reported the turbidity appearance of ~0.10 – 0.15 absorbance units due to the presence of ULV (Davies *et al.*, 2006; Zhang & Liu, 2011). There are also several papers (Davies *et al.*, 2006; Sreejith *et al.*, 2010; Yusof & Khan, 2012) which report the effects of temperature on reversible conversion of Vs-to-WM. It is relevant to note that the observed turbidity maximum of aqueous CTABr/$M_{\nu}X$ for 25 mM $M_{\nu}X$ = 3-MeSaNa_{ν} (ν = 1) and 30 mM 4-MeSaNa_{ν} (ν = 2) are 0.193 and 0.481, respectively which are much higher than those in the earlier reports (Davies *et al.*, 2006; Sreejith *et al.*, 2010; Yusof & Khan, 2012; Zhang & Liu, 2011). It has been noted also that the viscosity of region V decreases with an increase in temperature. From the comparison made to the earlier reports (Davies *et al.*, 2006; Morariu & Bercea, 2011; Sreejith *et al.*, 2010; Yusof & Khan, 2012; Zhang & Liu, 2011), it is perhaps relevant to conclude that region V contains most likely small planar bilayer aggregates rather than ULV due to highly insolubility of planar bilayer aggregates in water (Kawasaki *et al.*, 2002; Stuart & Boekema, 2007) as well as contradictory of viscosity value to those in the reports which reveals the structural transitions of ULV-to-WM with increasing temperatures (Davies *et al.*, 2006; Sreejith *et al.*, 2010; Yusof & Khan, 2012).

The aqueous solution of CTABr/$M_{\nu}X$ (with $M_{\nu}X$ = 2,6-Cl_2BzNa) contains only SM where the R_X^{Br} = 4.7 (Razak & Khan, 2013; Yusof *et al.*, 2013). The significantly low value of R_X^{Br} as well as the lowest value of E_a (= 17.7 kJ mol^{-1}) obtained in this study of aqueous CTABr/2,6-Cl_2BzNa may be considered as a characteristic behavior of SM. The E_a values obtained for 2,5-Cl_2BzNa, within 20 – 35 °C and 35 – 55 °C are 1.7- and 1.3-fold larger, respectively than those for 2,3-Cl_2BzNa. It is noteworthy that the R_X^{Br} values (Yusof *et al.*, 2013) obtained for both salts are the same (i.e. 25). On the other hand, the values of E_a obtained for 2,4-Cl_2BzNa, within 20 – 35 °C and 35 – 55 °C are significantly larger than those obtained for 2,3- and 2,5-Cl_2BzNa, which relate mutually with the R_X^{Br} values for these counterions. The values of E_a within temperature range of 35 – 55 °C are $\geq$ 2-fold smaller than those at 20 – 35 °C for M_vX = 2,3-, 2,4- and 2,5-Cl_2BzNa due to probable shorter length of WM at temperature range of 35 – 55 °C compared to those at 20 – 35 °C. Similarly, the values of E_a are significantly higher at 13 mM 3,4-Cl_2BzNa (due to the presence of highly entangled WM) than that at 40 mM 3,4-Cl_2BzNa (which contains branched micelles). The values of E_a appear to be larger at both concentration values, 13 and 40 mM 3,4-Cl_2BzNa compared to those of 3,5-Cl_2BzNa, but the R_X^{Br} value for 3,5-Cl_2BzNa is ~1.7-fold larger than that for 3,4-Cl_2BzNa. These observations reveals indirect perception that the aqueous solutions of 3,4-Cl_2BzNa contain only WM while such aqueous solutions of 3,5-Cl_2BzNa contain the mixture of WM and Vs.

4.3 The Significant Correlation Between the Theory of X-Induced Micellar Growth of Aqueous CTABr/M_vX System and the Values of R_X^{Br}

A strong counterion binding to ionic surfactant aggregates have been discussed only qualitatively, but the quantitative correlation of this is rare (Brianáborak, 2010; Davies *et al.*, 2006; Murgia *et al.*, 2011; Oelschlaeger *et al.*, 2010; Rao *et al.*, 1987; Yusof & Khan, 2010). One assumption had been made, where the value of the maximum viscosity of aqueous surfactant solution (η_0^{max}) should be proportional to the mean length of WM. Thus, the increase in η_0^{max} values should increase the values of R_X^{Br} as well. However, the validity of this assumption is determined by the proportionality between R_X^{Br} and the mean length of WM where the increase in R_X^{Br} values causes the increase in the mean length of WM. This correlation is described as: η_0 α mean length of WM α R_X^{Br}.

In **Figure 4.47**, the values of R_X^{Br} and η_0^{max} show a nonlinear decrease with increasing temperature (35 – 55 °C) for both M_vX = 4-MeO- and 4-MeSaNa_v (ν = 2). Almost similar plots were obtained by Yusof and Khan, in their report, where the R_X^{Br} values decrease by several fold with increasing temperatures (Yusof & Khan, 2010). These observations reveal, although indirectly, a quantitative correlation between the magnitudes of R_X^{Br} and η_0^{max} upon temperature as well as micellar structural transition. These quantitative correlations are described as follows: the structural aggregates of aqueous CTABr/M_vX will remain spherical/spheroidal micelles (SM), rodlike/wormlike (RM/WM) or unilamellar vesicles (Gamboa *et al.*, 1989) if the R_X^{Br} values $\leq$ ~6, $\geq$ ~6 - $\leq$ ~150 and ~700 – 800, respectively (Razak & Khan, 2013). The R_X^{Br} values should be ~120 and > ~150 in the presence of respective WM and Vs. This correlation has been made based upon the values of R_X^{Br}, where in the presence of WM, R_X^{Br} is 119 for M_vX = 3,4-Cl_2BzNa. The minimum value of R_X^{Br} with the presence of Vs is concluded to be > ~150 (Razak & Khan, 2013).

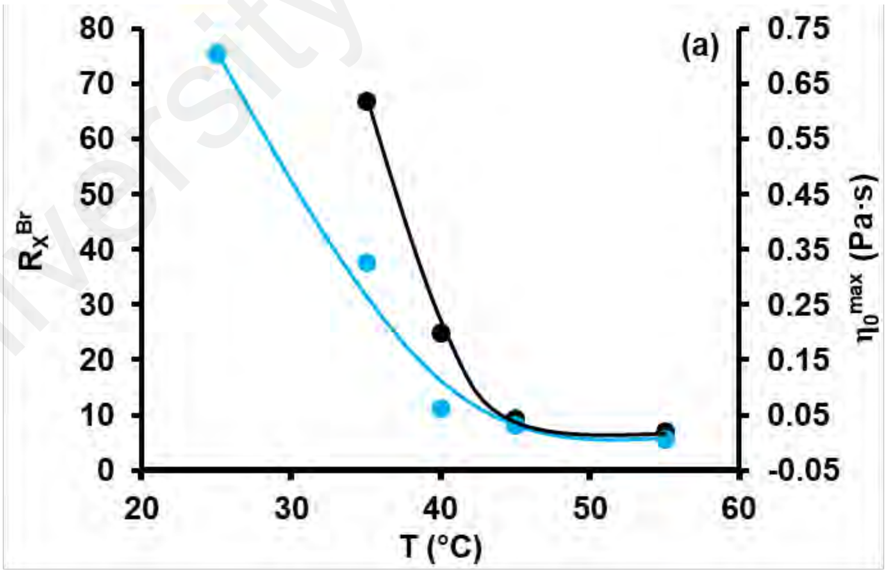

Figure 4.47: Plots showing the dependence of R_X^{Br} (black) and zero shear viscosity, η_0^{max} (blue) upon temperature at specific concentration of M_vX (v = 2) at which the viscosity maxima occur at 15 mM CTABr where (a): M_vX= 4-MeOSaNa$_v$; (b) and (c): M_vX= 3-MeSaNa$_v$ at which the respective first and second viscosity maximum occurs at 15 mM CTABr as well as (d) and (e): M_vX= 4-MeSaNa$_v$ at which the first and second viscosity maximum occurs at 15 mM CTABr, respectively.

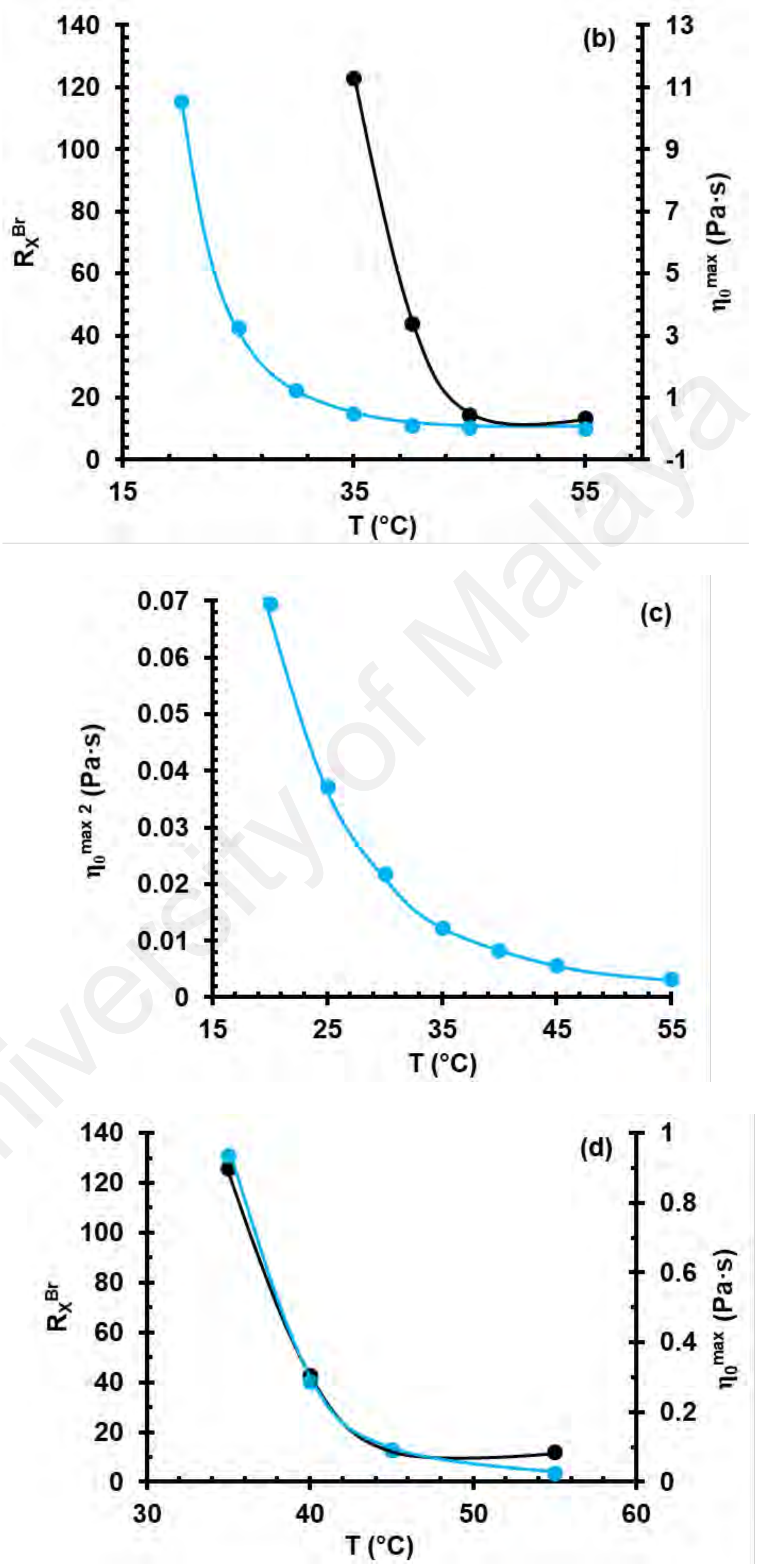

Figure 4.47, continued

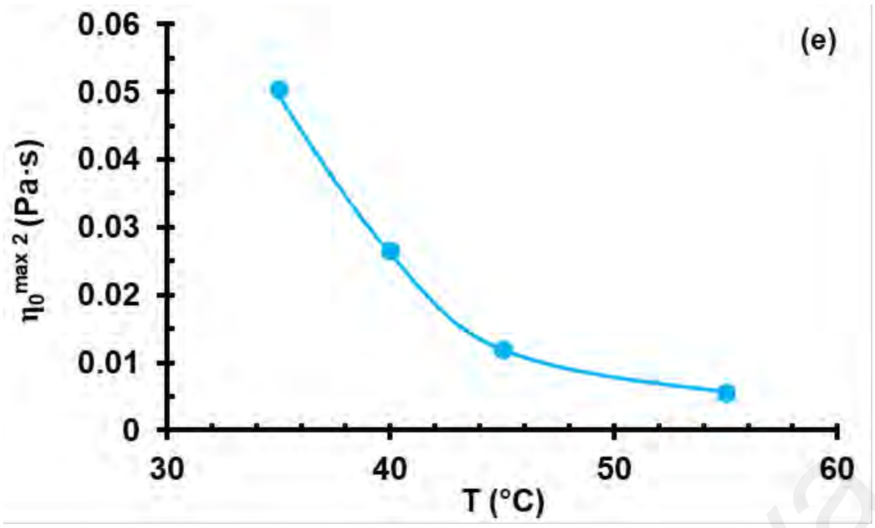

Figure 4.47, continued

It has been concluded elsewhere (Khan, 2010) that the micellar structural transition occurs due to the effects of hydrophobic interaction. The value of surfactant aggregate hydration number (R_W^{surf}) decrease upon surfactant aggregate structural transitions from SM-to-WM-to-Vs/bilayer aggregates. $R_W^{surf} = N_W/N_A$, where N_W and N_A represent respective total number of surfactant aggregate-bound water molecules and aggregation number of a monolayer of bilayer aggregate (Yusof & Khan, 2012). The nonlinear decrease in second zero shear viscosity maximum (η_0^{max2}) with the increasing temperatures (**Figure 4.47**) may be attributed to the decrease in the size of MLV (i.e. decrease in the magnitude of R_X^{Br} with increasing temperatures). However, the R_X^{Br} values, in the presence of flat bilayer sheets and MLV could not be determined by the present SEK method due to the absence of reliable break points in the plots of k_{obs} versus $[M_vX]$ (**Figures 4.5 –4.8** and **Figures S2 – S3**).

CHAPTER 5: CONCLUSIONS

It is evident from the study, that the counterion (X^{v-}) affinity to cationic micelles are correlated quantitatively to the X^{v-}- and temperature-induced micellar growth, where the quantitative correlation is made with the values of K_X^{Br} or R_X^{Br} = K_X/K_{Br}. The micellar binding constant of counterion (X^{v-}) varies in the order: K_X (SM) < K_X (WM) < K_X (Vs), which reveals the highest magnitude of R_X^{Br} in the presence of Vs, smaller in WM and the smallest in the presence of SM (i.e. R_X^{Br} (SM) < R_X^{Br} (WM) << R_X^{Br} (Vs).

The presence of break points in the plots of k_{obs} versus [M_vX] (M_vX = 3- and 4-MeSaNa$_v$) at 35, 40, 45 and 55 °C, reveals the structural transitions of CTABr/M_vX aggregates from SM-to-WM-to-PBLS-to-MLV, which are different from that SM-to-WM-to-BWM for 4-MeOSaNa$_v$. The magnitudes of K_X^{Br} or R_X^{Br} for 3- and 4-MeSaNa$_v$ are ~1.5 to 2.0-fold larger compared to that of 4-MeOSaNa$_v$. The η_0 versus [M_vX] plots of M_vX = 4-MeO-, 3- and 4-MeSaNa$_v$ showed strong and weak maximum for respective first and second peak, where the source of first peak is indicative of the presence of WM, while for the second peak, the source is concluded to be different. The K_X^{Br} or R_X^{Br} values of M_vX = aliphatic salts vary in the range ~0.3 - ~41, where the values increase with increasing hydrophobic chain length of aliphatic salts. The plots of η_0 versus [M_vX] show the absence of maximum where the η_0 values are similar and slightly higher than that of water , which reveals only SM or short RM present in that system. The occurrence of broad viscosity maxima for M_vX = 2,3-, 2,4-, 2,5- and 3,4-Cl_2BzNa reveals the presence of WM, while for 3,5-Cl_2BzNa, the source of such occurrence is almost similar to that obtained for M_vX = 3- and 4-MeSaNa$_v$. The magnitude of η_0 of similar aqueous CTABr/M_vX system varies in the order: η_0 (SM) ≈ η_0 (Vs) < η_0 (BWM) < η_0 (WM). The presence of turbidity in the present study indicates the presence of Vs.

The aqueous DDABr system exhibits the presence of cmc and cvc within the [DDABr] range ~0.0 – 0.8 mM. The values of $K_{Br/S}$ obtained in the presence of WM (= 76 M^{-1}) and Vs (= 437 M^{-1}) are nearly 3- and 17-fold larger, respectively than the value of $K_{Br/S}$ obtained in the presence of SM (= 25 M^{-1}) at 35 °C (Khan, 2010). Similarly, the values of K_S^0, for DDABr system with S = PSa^- were found to be ~2.5- and 5-fold larger in the presence of respective WM (= 18.7×10^3 M^{-1}) and Vs (=33.7×10^3 M^{-1}) compared to that in the presence of SM (= 7×10^3 M^{-1}) at 35 °C (Khan, 2010).

REFERENCES

Abdel-Rahem, R. (2008). The influence of hydrophobic counterions on micellar growth of ionic surfactants. *Advances in Colloid and Interface Science, 141*(1), 24-36.

Abdel-Rahem, R., & Hoffmann, H. (2007). Novel viscoelastic systems from cationic surfactants and hydrophobic counter-ions: Influence of surfactant chain length. *Journal of Colloid and Interface Science, 312*(1), 146-155.

Abezgauz, L., Kuperkar, K., Hassan, P. A., Ramon, O., Bahadur, P., & Danino, D. (2010). Effect of Hofmeister anions on micellization and micellar growth of the surfactant cetylpyridinium chloride. *Journal of Colloid and Interface Science, 342*(1), 83-92.

Aït-Ali, A., & Makhloufi, R. (1997). On the nonlinear rheology of a wormlike micellar system in the presence of sodium salicylate salt. *Journal of Rheology, 41*(2), 307-318.

Ali, A. A., & Makhloufi, R. (1999). Effect of organic salts on micellar growth and structure studied by rheology. *Colloid and Polymer Science, 277*(2-3), 270-275.

Bachofer, S. J., & Simonis, U. (1996). Determination of the ion exchange constants of four aromatic organic anions competing for a cationic micellar interface. *Langmuir, 12*(7), 1744-1754.

Brianáborak, J. (2010). Application of PET deprotection for orthogonal photocontrol of aqueous solution viscosity. *Chemical Communications, 46*(47), 8983-8985.

Brinchi, L., Di Profio, P., Germani, R., Goracci, L., Savelli, G., Gillitt, N. D., & Bunton, C. A. (2007). Premicellar accelerated decarboxylation of 6-nitrobenzisoxazole-3-carboxylate ion and its 5-tetradecyloxy derivative. *Langmuir, 23*(2), 436-442.

Brinchi, L., Germani, R., Braccalenti, E., Spreti, N., Tiecco, M., & Savelli, G. (2010). Accelerated decarboxylation of 6-nitrobenzisoxazole-3-carboxylate in imidazolium-based ionic liquids and surfactant ionic liquids. *Journal of Colloid and Interface Science, 348*(1), 137-145.

Broxton, T. J., Christie, J. R., & Chung, R. P. (1988). Micellar catalysis of organic reactions. 23. Effect of micellar orientation of the substrate on the magnitude of micellar catalysis. *The Journal of Organic Chemistry, 53*(13), 3081-3084.

Bunton, C. A. (1979). Reaction kinetics in aqueous surfactant solutions. *Catalysis Reviews Science and Engineering, 20*(1), 1-56.

Bunton, C. A., & Savelli, G. (1987). Organic reactivity in aqueous micelles and similar assemblies. *Advances in Physical Organic Chemistry, 22*, 213-309.

Candau, S., Hirsch, E., Zana, R., & Delsanti, M. (1989). Rheological properties of semidilute and concentrated aqueous solutions of cetyltrimethylammonium bromide in the presence of potassium bromide. *Langmuir, 5*(5), 1225-1229.

Carver, M., Smith, T. L., Gee, J. C., Delichere, A., Caponetti, E., & Magid, L. J. (1996). Tuning of micellar structure and dynamics in aqueous salt-free solutions of cetyltrimethylammonium mono-and dichlorobenzoates. *Langmuir, 12*(3), 691-698.

Chaimovich, H., Blanco, A., Chayet, L., Costa, L. M., Monteiro, P. M., Bunton, C. A., & Paik, C. (1975). Micellar catalysis of the reaction of 2, 4-dinitrofluorobenzene with phenoxide and thiophenoxide ions. *Tetrahedron, 31*(9), 1139-1143.

Davies, D. M., Gillitt, N. D., & Paradis, P. M. (1996). Catalysis and inhibition of the iodide reduction of peracids by surfactants: partitioning of reactants, product and transition state between aqueous and micellar pseudophases. *Journal of the Chemical Society, Perkin Transactions 2*(4), 659-666.

Davies, T. S., Ketner, A. M., & Raghavan, S. R. (2006). Self-assembly of surfactant vesicles that transform into viscoelastic wormlike micelles upon heating. *Journal of the American Chemical Society, 128*(20), 6669-6675.

Dreiss, C. A. (2007). Wormlike micelles: where do we stand? Recent developments, linear rheology and scattering techniques. *Soft Matter, 3*(8), 956-970.

Duynstee, E. F. J., & Grunwald, E. (1959a). Organic reactions occurring in or on micelles. I. Reaction rate studies of the alkaline fading of triphenylmethane dyes and sulfonphthalein indicators in the presence of detergent salts[1]. *Journal of the American Chemical Society, 81*(17), 4540-4542.

Duynstee, E. F. J., & Grunwald, E. (1959b). Organic reactions occurring in or on micelles. II. Kinetic and thermodynamic analysis of the alkaline fading of triphenylmethane dyes in the presence of detergent salts[1]. *Journal of the American Chemical Society, 81*(17), 4542-4548.

Engberts, J. B. F. N. (1992). Catalysis by surfactant aggregates in aqueous solutions. *Pure and Applied Chemistry, 64*(11), 1653-1660.

Fagge, I. I., Ahmad, W. H. W., Zain, S. M., & Khan, M. N. (2018a). Kinetics and mechanism of counterionic salt-catalysed piperidinolysis of anionic phenyl salicylate in the presence of cationic–nonionic mixed micelles. *Progress in Reaction Kinetics and Mechanism, 43*(1), 41-52.

Fagge, I. I., Khalid, K., Noh, M. A. M., Yusof, N. S. M., Zain, S. M., & Khan, M. N. (2016). Influence of mixed CTABr–$C_{16}E_{20}$ nanoparticles on relative counterion binding constants in aqueous solutions of inert salts (2-$NaOC_6H_4CO_2Na$ and NaBr): Kinetic and rheometric study. *RSC Advances, 6*(98), 95504-95511.

Fagge, I. I., Khalid, K., Noh, M. A. M., Yusof, N. S. M., Zain, S. M., & Khan, M. N. (2018b). Study of cationic and nonionic mixed micelles with NaBr and 3,5-$Cl_2C_6H_3CO_2Na$ by use of probe nucleophilic reaction of piperidine with ionized phenyl salicylate. *Journal of Oleo Science, 67*(1), 55-66.

Fagge, I. I., Yusof, N. S. M., Zain, S. M., & Khan, M. N. (2017). Effect of halo-substituted aromatic salts on counterion binding constants obtained from cationic nanoparticle catalyzed reactions of piperidine and phenyl salicylate. *Proceedings of the AIP Conference 1901.*

Gaidamauskas, E., Cleaver, D. P., Chatterjee, P. B., & Crans, D. C. (2010). Effect of micellar and reverse micellar interface on solute location: 2,6-Pyridinedicarboxylate in CTAB micelles and CTAB and AOT reverse micelles. *Langmuir, 26*(16), 13153-13161.

Gamboa, C., Rios, H., & Sepulveda, L. (1989). Effect of the nature of counterions on the sphere-to-rod transition in cetyltrimethylammonium micelles. *The Journal of Physical Chemistry, 93*(14), 5540-5543.

Gradzielski, M. (2011). The rheology of vesicle and disk systems—relations between macroscopic behaviour and microstructure. *Current Opinion in Colloid and Interface Science, 16*(1), 13-17.

Gravsholt, S. (1976). Viscoelasticity in highly dilute aqueous solutions of pure cationic detergents. *Journal of Colloid and Interface Science, 57*(3), 575-577.

Grillo, I., Penfold, J., Tucker, I., & Cousin, F. (2008). Spontaneous formation of nanovesicles in mixtures of nonionic and dialkyl chain cationic surfactants studied by surface tension and SANS. *Langmuir, 25*(7), 3932-3943.

Hassan, P. A., Narayanan, J., & Manohar, C. (2001). Vesicles and worm-like micelles: Structure, dynamics and transformations. *Current Science-Bangalore-, 80*(8), 980-989.

Herle, V., Manneville, S., & Fischer, P. (2008). Ultrasound velocimetry in a shear-thickening wormlike micellar solution: Evidence for the coexistence of radial and vorticity shear bands. *The European Physical Journal E, 26*(1-2), 3-12.

Ideta, R., Yanagi, Y., Tamaki, Y., Tasaka, F., Harada, A., & Kataoka, K. (2004). Effective accumulation of polyion complex micelle to experimental choroidal neovascularization in rats. *FEBS Letters, 557*(1), 21-25.

Israelachvili, J. N., Mitchell, D. J., & Ninham, B. W. (1976). Theory of self-assembly of hydrocarbon amphiphiles into micelles and bilayers. *Journal of the Chemical Society, Faraday Transactions 2: Molecular and Chemical Physics, 72*, 1525-1568.

Junquera, E., Arranz, R., & Aicart, E. (2004). Mixed vesicle formation on a ternary surfactant system: Didodecyldimethylammonium bromide/dodecylethyldimethyl ammonium bromide/water. *Langmuir, 20*(16), 6619-6625.

Kaur, R., Kumar, S., Aswal, V. K., & Mahajan, R. K. (2012). Interactional and aggregation behavior of twin tail cationic surfactants with pluronic L64 in aqueous solution. *Colloid and Polymer Science, 290*(2), 127-139.

Kawasaki, H., Imahayashi, R., & Maeda, H. (2002). Effects of hydrophobic counterions on the phase behavior of tetradecyldimethylhydroxylammonium chloride in aqueous solutions. *Langmuir, 18*(22), 8358-8363.

Kern, F., Lequeux, F., Zana, R., & Candau, S. (1994). Dynamic properties of salt-free viscoelastic micellar solutions. *Langmuir, 10*(6), 1714-1723.

Ketner, A. M., Kumar, R., Davies, T. S., Elder, P. W., & Raghavan, S. R. (2007). A simple class of photorheological fluids: Surfactant solutions with viscosity tunable by light. *Journal of the American Chemical Society, 129*(6), 1553-1559.

Khalid, K., Noh, M. A. M., Fagge, I. I., Zain, S. M., & Khan, M. N. (2016). Effects of cationic nanoparticles (CNP) on counterion binding constant (R_X^{Br}) and catalytic constant (k_{cat}) in micellar system. *Journal of Molecular Catalysis A: Chemical, 423*, 365-370.

Khalid, K., Noh, M. A. M., Khan, M. N., Ishak, R., Penney, E., Chowdhury, Z. Z., Hamzah, M. H., & Othman, M. (2017a). Giant vesicles (GV) in colloidal system under the optical polarization microscope (OPM). *Micron, 100*, 30-33.

Khalid, K., Zain, S. M., Suk, V. R. E., & Khan, M. N. (2017b). Microscopic evidence for the correlation of micellar structures and counterion binding constant for flexible nanoparticle catalyzed piperidinolysis of PS^- in colloidal system. *Tenside Surfactants Detergents, 54*(3), 224-229.

Khan, M. N. (1989). Intramolecular general base catalysis and the rate-determining step in the nucleophilic cleavage of ionized phenyl salicylate with primary and secondary amines. *Journal of the Chemical Society, Perkin Transactions 2*(3), 199-208.

Khan, M. N. (1995). Effects of anionic micelles on the intramolecular general base-catalyzed hydrolysis of phenyl and methyl salicylates. *Journal of Molecular Catalysis A: Chemical, 102*(2), 93-101.

Khan, M. N. (1996). Spectrophotometric determination of anionic micellar binding constants of ionized and non- ionized phenyl and methyl salicylates. *Journal of Physical Organic Chemistry, 9*(5), 295-300.

Khan, M. N. (1997). Effects of [NaOH] and [KBr] on intramolecular general base-catalyzed methanolysis of ionized phenyl salicylate in the presence of cationic micelles. *The Journal of Organic Chemistry, 62*(10), 3190-3193.

Khan, M. N. (2006). *Micellar catalysis*. Boca Raton: CRC Press.

Khan, M. N. (2010). A new semi-empirical kinetic method for the determination of ion exchange constants for the counterions of cationic micelles. *Advances in Colloid and Interface Science, 159*(2), 160-179.

Khan, M. N., & Ahmad, F. B. H. (2001a). Effects of organic salts on the rate of alkaline hydrolysis of phthalimide in the presence of cationic micelles. *Reaction Kinetics and Catalysis Letters, 72*(2), 321-329.

Khan, M. N., & Ahmad, F. B. H. (2001b). Kinetic probe to study the structure of micelles: Effects of inert inorganic and organic salts on the rate of alkaline hydrolysis of phthalimide in the presence of cationic micelles. *Colloids and Surfaces A: Physicochemical and Engineering Aspects, 181*(1), 11-18.

Khan, M. N., & Arifin, Z. (2000). Effects of inorganic ions on rate of alkaline hydrolysis of phthalimide in the presence of cationic micelles. *Journal of the Chemical Society, Perkin Transactions 2*(12), 2503-2510.

Khan, M. N., Arifin, Z., Ismail, E., & Ali, S. F. M. (2000). Effects of [NaBr] on the rates of intramolecular general base-catalyzed reactions of ionized phenyl salicylate (PS^-) with *n*-butylamine and piperidine in the presence of cationic micelles. *The Journal of Organic Chemistry, 65*(5), 1331-1334.

Khan, M. N., Arifin, Z., Lasidek, M. N., Hanifiah, M. A. M., & Alex, G. (1997). Effects of cationic micelles on rate of intramolecular general base-catalyzed aminolysis of ionized phenyl salicylate. *Langmuir, 13*(15), 3959-3964.

Khan, M. N., Arifin, Z., Yusoff, M. R., & Ismail, E. (1999). Effects of nonionic, cationic, and mixed nonionic–cationic surfactants on the acid–base behavior of phenyl salicylate. *Journal of Colloid and Interface Science, 220*(2), 474-476.

Khan, M. N., & Fagge, I. I. (2018). Kinetics and mechanism of cationic micelle/flexible nanoparticle catalysis: A review. *Progress in Reaction Kinetics and Mechanism, 43*(1), 1-20.

Khan, M. N., & Ismail, E. (2001). Spectrophotometric determination of cationic micellar binding constant of ionised phenyl salicylate in the presence of inert salts. *Journal of Chemical Research, 2001*(4), 143-145.

Khan, M. N., & Ismail, E. (2009). Kinetic assessment of relative counterion penetration into cationic micelles: Effects of inert salt on the rate of piperidinolysis of phenyl salicylate in alkaline cationic micelles. *Indian Journal of Chemistry. Section A, Inorganic, Bio-Inorganic, Physical, Theoretical & Analytical Chemistry, 48*(6), 781-787.

Khan, M. N., Ismail, E., & Misran, O. (2002). An empirical approach to study the occurrence of ion-exchange in the alkaline hydrolysis of phenyl benzoate under the presence of cationic micelles. *Journal of Molecular Liquids, 95*(1), 75-86.

Khan, M. N., Ismail, E., & Yusof, N. S. M. (2010). A new empirical kinetic method for the determination of ion-exchange constants for the counterions of cationic micelles: The rate of piperidinolysis and hydrolysis of anionic phenyl salicylate as the kinetic probes. *Colloids and Surfaces A: Physicochemical and Engineering Aspects, 361*(1), 150-161.

Khan, M. N., Naaliya, J., & Dahiru, M. (1988). Effects of anionic micelles on intramolecular general base-catalysed hydrolyses of salicylate esters: Evidence for a porous cluster micelle. *Journal of Chemical Research. Synopses* (4), 116-117.

Khan, M. N., Yusof, N. S. M., & Razak, N. A. (2013). A semi-empirical spectrophotometric (SESp) method for the indirect determination of the ratio of cationic micellar binding constants of counterions X–and Br–(K_X/K_{Br}). *Journal of Oleo Science, 62*(9), 695-708.

Koshy, P., Verma, G., Aswal, V., Venkatesh, M., & Hassan, P. (2010). Viscoelastic fluids originated from enhanced solubility of sodium laurate in cetyl trimethyl ammonium bromide micelles through cooperative self-assembly. *The Journal of Physical Chemistry B, 114*(32), 10462-10470.

Kreke, P. J., Magid, L. J., & Gee, J. C. (1996). ^{1}H and ^{13}C NMR studies of mixed counterion, cetyltrimethylammonium bromide/cetyltrimethylammonium dichlorobenzoate, surfactant solutions: The intercalation of aromatic counterions. *Langmuir, 12*(3), 699-705.

Kunitake, T., Okahata, Y., Ando, R., Shinkai, S., & Hirakawa, S. (1980). Decarboxylation of 6-nitrobenzisoxazole-3-carboxylate catalyzed by ammonium bilayer membranes. A comparison of the catalytic behavior of micelles, bilayer membranes, and other aqueous aggregates. *Journal of the American Chemical Society, 102*(27), 7877-7881.

Leng, S. Y., Khan, M. N., & Ariffin, A. (2004). Effects of tetraalkylammonium salts on alkaline hydrolysis of N-(2-Methoxyphenyl) Phthalimide. *Malaysian Journal of Science, 23*(2).

Lin, Y., Han, X., Huang, J., Fu, H., & Yu, C. (2009a). A facile route to design pH-responsive viscoelastic wormlike micelles: Smart use of hydrotropes. *Journal of Colloid and Interface Science, 330*(2), 449-455.

Lin, Y., Qiao, Y., Yan, Y., & Huang, J. (2009b). Thermo-responsive viscoelastic wormlike micelle to elastic hydrogel transition in dual-component systems. *Soft Matter, 5*(16), 3047-3053.

Lin, Z., Cai, J. J., Scriven, L. E., & Davis, H. T. (1994). Spherical-to-wormlike micelle transition in CTAB solutions. *The Journal of Physical Chemistry, 98*(23), 5984-5993.

Lin, Z., Zakin, J. L., Zheng, Y., Davis, H. T., Scriven, L. E., & Talmon, Y. (2001). Comparison of the effects of dimethyl and dichloro benzoate counterions on drag reduction, rheological behaviors, and microstructures of a cationic surfactant. *Journal of Rheology, 45*(4), 963-981.

Liu, J. F., Min, G., & Ducker, W. A. (2001). AFM study of adsorption of cationic surfactants and cationic polyelectrolytes at the silica-water interface. *Langmuir, 17*(16), 4895-4903.

LóPez-BarróN, C. R., Li, D., Derita, L., Basavaraj, M. G., & Wagner, N. J. (2012). Spontaneous thermoreversible formation of cationic vesicles in a protic ionic liquid. *Journal of the American Chemical Society, 134*(51), 20728-20732.

Macosko, C. W., & Larson, R. G. (1994). *Rheology: principles, measurements, and applications*. Weinheim, Germany: Wiley-VCH

Magid, L. J., Gee, J., & Talmon, Y. (1990). A cryogenic transmission electron microscopy study of counterion effects on hexadecyltrimethylammonium dichlorobenzoate micelles. *Langmuir, 6*(10), 1609-1613.

Magid, L. J., Han, Z., Warr, G. G., Cassidy, M. A., Butler, P. D., & Hamilton, W. A. (1997). Effect of counterion competition on micellar growth horizons for cetyltrimethylammonium micellar surfaces: electrostatics and specific binding. *The Journal of Physical Chemistry B, 101*(40), 7919-7927.

Manohar, C., Rao, U. R. K., Valaulikar, B. S., & Lyer, R. M. (1986). On the origin of viscoelasticity in micellar solutions of cetyltrimethylammonium bromide and sodium salicylate. *Journal of the Chemical Society, Chemical Communications* (5), 379-381.

Marques, E. F., Regev, O., Khan, A., Da Graça Miguel, M., & Lindman, B. (1999). Vesicle formation and general phase behavior in the catanionic mixture SDS-DDAB-water. The cationic-rich side. *The Journal of Physical Chemistry B, 103*(39), 8353-8363.

Menger, F. M. (1979). The structure of micelles. *Accounts of Chemical Research, 12*(4), 111-117.

Minero, C., & Pelizzetti, E. (1993). The generalized pseudophase model: Treatment of multiple equilibria in micellar solutions. *Pure and Applied Chemistry, 65*(12), 2573-2582.

Mitchell, D. J., & Ninham, B. W. (1981). Micelles, vesicles and microemulsions. *Journal of the Chemical Society, Faraday Transactions 2: Molecular and Chemical Physics, 77*(4), 601-629.

Modaressi, A., Sifaoui, H., Grzesiak, B., Solimando, R., Domanska, U., & Rogalski, M. (2007). CTAB aggregation in aqueous solutions of ammonium based ionic liquids; conductimetric studies. *Colloids and Surfaces A: Physicochemical and Engineering Aspects, 296*(1), 104-108.

Morariu, S., & Bercea, M. (2011). Effect of temperature and aging time on the rheological behavior of aqueous poly (ethylene glycol)/laponite RD dispersions. *The Journal of Physical Chemistry B, 116*(1), 48-54.

Murgia, S., Monduzzi, M., & Palazzo, G. (2011). Quantification of specific anion binding to non-ionic Triton X-100 micelles. *Langmuir, 28*(2), 1283-1289.

Nagarajan, R. (2002). Molecular packing parameter and surfactant self-assembly: The neglected role of the surfactant tail. *Langmuir, 18*(1), 31-38.

Nishiyama, N., Bae, Y., Miyata, K., Fukushima, S., & Kataoka, K. (2005). Smart polymeric micelles for gene and drug delivery. *Drug Discovery Today: Technologies, 2*(1), 21-26.

Oelschlaeger, C., Suwita, P., & Willenbacher, N. (2010). Effect of counterion binding efficiency on structure and dynamics of wormlike micelles. *Langmuir, 26*(10), 7045-7053.

Ono, Y., Kawasaki, H., Annaka, M., & Maeda, H. (2005). Effects of micelle-to-vesicle transitions on the degree of counterion binding. *Journal of Colloid and Interface Science, 287*(2), 685-693.

Otto, S., Engberts, J. B., & Kwak, J. C. (1998). Million-fold acceleration of a Diels-Alder reaction due to combined Lewis acid and micellar catalysis in water. *Journal of the American Chemical Society, 120*(37), 9517-9525.

Para, G., Jarek, E., & Warszynski, P. (2005). The surface tension of aqueous solutions of cetyltrimethylammonium cationic surfactants in presence of bromide and chloride counterions. *Colloids and Surfaces A: Physicochemical and Engineering Aspects, 261*(1), 65-73.

Penfold, J., Tucker, I., Staples, E., & Thomas, R. K. (2004). Adsorption of aromatic counterions at the surfactant/water interface: A neutron reflectivity study of hydroxybenzoate and chlorobenzoate counterions at the hexadecyl trimethylammonium surfactant/water interface. *Langmuir, 20*(19), 8054-8061.

Qi, Y., & Zakin, J. L. (2002). Chemical and rheological characterization of drag-reducing cationic surfactant systems. *Industrial and Engineering Chemistry Research, 41*(25), 6326-6336.

Raghavan, S. R., Edlund, H., & Kaler, E. W. (2002). Cloud-point phenomena in wormlike micellar systems containing cationic surfactant and salt. *Langmuir, 18*(4), 1056-1064.

Raghavan, S. R., & Kaler, E. W. (2001). Highly viscoelastic wormlike micellar solutions formed by cationic surfactants with long unsaturated tails. *Langmuir, 17*(2), 300-306.

Rao, U. R. K., Manohar, C., Valaulikar, B. S., & Iyer, R. M. (1987). Micellar chain model for the origin of the visoelasticity in dilute surfactant solutions. *Journal of Physical Chemistry, 91*(12), 3286-3291.

Razak, N. A., & Khan, M. N. (2013). Determination of flow activation energy at viscosity maximum for spherical and wormlike micelles of different lengths and flexibility. *Rheologica Acta, 52*(10-12), 927-937.

Razak, N. A., Yusof, N. S. M., & Khan, M. N. (2014). Kinetics and mechanism of nanoparticles (CTABr/MX/H_2O)-catalyzed piperidinolysis of ionized phenyl salicylate. 1. *Journal of the Taiwan Institute of Chemical Engineers, 45*(5), 2777-2785.

Razak, N. A., Yusof, N. S. M., & Khan, M. N. (2016). Rheological study on counter ion (X^{2-})-and temperature-induced cationic micellar growth: A quantitative correlation between X^{2-} binding affinity to cationic micelles and X^{2-}-and temperature-induced micellar growth. *Rheologica Acta*, 55(2), 125-136.

Rehage, H., & Hoffmann, H. (1991). Viscoelastic surfactant solutions: Model systems for rheological research. *Molecular Physics, 74*(5), 933-973.

Rojas, M. R., Müller, A. J., & Sáez, A. E. (2008). Shear rheology and porous media flow of wormlike micelle solutions formed by mixtures of surfactants of opposite charge. *Journal of Colloid and Interface Science, 326*(1), 221-226.

Romsted, L. S. (2007). Do amphiphile aggregate morphologies and interfacial compositions depend primarily on interfacial hydration and ion-specific interactions? The evidence from chemical trapping. *Langmuir, 23*(2), 414-424.

Ruan, K., Zhao, Z., & Ma, J. (2001). Effect of bromide salts on cationic micellar catalysis. *Colloid and Polymer Science, 279*(8), 813-818.

Santos, L. S., Knaack, L., & Metzger, J. O. (2005). Investigation of chemical reactions in solution using API-MS. *International Journal of Mass Spectrometry, 246*(1), 84-104.

Scarpa, M. V., Araujo, P. S., Schreier, S., Sesso, A., Oliveira, A. G., Chaimovich, H., & Cuccovia, I. M. (2000). Effect of vesicles of dimethyldioctadecylammonium chloride and phospholipids on the rate of decarboxylation of 6-nitrobenzisoxazole-3-carboxylate. *Langmuir, 16*(3), 993-999.

Schubert, B. A., Kaler, E. W., & Wagner, N. J. (2003). The microstructure and rheology of mixed cationic/anionic wormlike micelles. *Langmuir, 19*(10), 4079-4089.

Schubert, B. A., Wagner, N. J., Kaler, E. W., & Raghavan, S. R. (2004). Shear-induced phase separation in solutions of wormlike micelles. *Langmuir, 20*(9), 3564-3573.

Shikata, T., Hirata, H., & Kotaka, T. (1989). Micelle formation of detergent molecules in aqueous media. 3. Viscoelastic properties of aqueous cetyltrimethylammonium bromide-salicylic acid solutions. *Langmuir, 5*(2), 398-405.

Singh, K., Marangoni, D. G., Quinn, J. G., & Singer, R. D. (2009). Spontaneous vesicle formation with an ionic liquid amphiphile. *Journal of Colloid and Interface Science, 335*(1), 105-111.

Soltero, J. F. A., Bautista, F., Pecina, E., Puig, J. E., Manero, O., Proverbio, Z., & Schulz, P. C. (2000). Rheological behavior in the didodecyldimethylammonium bromide/water system. *Colloid and Polymer Science, 278*(1), 37-47.

Sotgiu, G., Schirone, L., & Rallo, F. (1996). Effect of surfactants in the electrochemical preparation of porous silicon. *Il Nuovo Cimento D, 18*(10), 1179-1186.

Sreejith, L., Parathakkat, S., Nair, S. M., Kumar, S., Varma, G., Hassan, P. A., & Talmon, Y. (2010). Octanol-triggered self-assemblies of the CTAB/KBr system: A microstructural study. *The Journal of Physical Chemistry B, 115*(3), 464-470.

Stuart, M. C., & Boekema, E. J. (2007). Two distinct mechanisms of vesicle-to-micelle and micelle-to-vesicle transition are mediated by the packing parameter of phospholipid–detergent systems. *Biochimica et Biophysica Acta (BBA)-Biomembranes, 1768*(11), 2681-2689.

Takeda, M., Kusano, T., Matsunaga, T., Endo, H., Shibayama, M., & Shikata, T. (2011). Rheo-SANS studies on shear-thickening/thinning in aqueous rodlike micellar solutions. *Langmuir, 27*(5), 1731-1738.

Vermathen, M., Stiles, P., Bachofer, S. J., & Simonis, U. (2002). Investigations of monofluoro-substituted benzoates at the tetradecyltrimethylammonium micellar interface. *Langmuir, 18*(4), 1030-1042.

Yang, J. (2002). Viscoelastic wormlike micelles and their applications. *Current Opinion in Colloid & Interface Science, 7*(5), 276-281.

Yunes, S. J., Gillitt, N. D., & Bunton, C. A. (2005). Examination of the pseudophase model of monomer-micelle interconversion in cetylpyridinium chloride. *Journal of Colloid and Interface Science, 281*(2), 482-487.

Yusof, N. S. M. (2011). *An empirical kinetic approach to study the occurrence of ion exchange in the piperidinolysis of phenyl salicylate in the presence of cationic micelles and inert salts.* (Unpublished master’s thesis). University of Malaya, Kuala Lumpur, Malaysia.

Yusof, N. S. M., & Khan, M. N. (2010). Determination of an ion exchange constant by the use of a kinetic probe: A new semiempirical kinetic approach involving the effects of 3-F-and 4-F-substituted benzoates on the rate of piperidinolysis of anionic phenyl salicylate in aqueous cationic micelles. *Langmuir, 26*(13), 10627-10635.

Yusof, N. S. M., & Khan, M. N. (2011). Kinetic and rheological measurements of the effects of inert 2-, 3-and 4-bromobenzoate ions on the cationic micellar-mediated rate of piperidinolysis of ionized phenyl salicylate. *Journal of Colloid and Interface Science, 357*(1), 121-128.

Yusof, N. S. M., & Khan, M. N. (2012). Quantitative correlation of counterion (X) affinity to ionic micelles and X-and temperature-induced micellar growth (spherical–wormlike micelles–vesicles) for X= 5-methyl-and 5-methoxysalicylate ions. *The Journal of Physical Chemistry B, 116*(7), 2065-2074.

Yusof, N. S. M., Razak, N. A., & Khan, M. N. (2013). Quantitative correlation between counterion (X) affinity to cationic micelles and X-induced micellar growth for X= 2, 4-; 2, 5-; 2, 6-and 3, 4-dichlorobenzoate ions. *Journal of Oleo Science, 62*(5), 257-269.

Zhang, J., & Liu, S. (2011). Kinetics of thermo-induced micelle-to-vesicle transitions in a catanionic surfactant system investigated by stopped-flow temperature jump. *Physical Chemistry Chemical Physics, 13*(27), 12545-12553.

Zheng, Y., Lin, Z., Zakin, J. L., Talmon, Y., Davis, H. T., & Scriven, L. E. (2000). Cryo-TEM imaging the flow-induced transition from vesicles to threadlike micelles. *The Journal of Physical Chemistry B, 104*(22), 5263-5271.

Ziserman, L., Abezgauz, L., Ramon, O., Raghavan, S. R., & Danino, D. (2009). Origins of the viscosity peak in wormlike micellar solutions. 1. Mixed catanionic surfactants. A cryo-transmission electron microscopy study. *Langmuir, 25*(18), 10483-10489.

LIST OF PUBLICATIONS AND PAPERS PRESENTED

Khan, M. N., Yusof, N. S. M. and Razak, N. A. (2013). A semi-empirical spectrophotometric (SESp) method for the indirect detremination of the ratio of cationic micellar binding constants of counterions X^- and Br^- (K_X/K_{Br}). *Journal of Oleo Science, 62(9)*, 695-708.

Razak, N. A., Fagge, I. I. & Khan, M. N. (2017). Effect of [NaBr] on the rate of intramolecular base-assisted piperidinolysis of ionized phenyl salicylate in the presence of double-tail cationic surfactant aggregates: DDABr/NaBr/H_2O nanoparticles catalysis. *Indian Journal of Chemistry*, *56A*, 1132-1142.

Razak, N.A and Khan, M. N. (2013). Determination of flow activation energy at viscosity maximum for spherical and wormlike micelles of different lengths and flexibility. *Rheologica Acta, 52*, 927-937.

Razak, N.A and Khan, M. N. (2014). Kinetics and machanism of nanoparticles-catalyzed piperidinolysis of anionic phenyl salicylate. *The Scientific World Journal, 2014*.

Razak, N. A., Yusof, N. S. M. and Khan, M. N. (2014). Kinetics and mechanism of nanoparticles (CTABr/MX/H_2O)-catalyzed piperidinolysis of ionized phenyl salicylate. 1. *Journal of the Taiwan Institute of Chemical Engineers, 45*, 2777-2785.

Razak, N. A., Yusof, N. S. M. and Khan, M. N. (2016). Rheological study on counter ion (X^{2-})- and temperature-induced cationic micellar growth: a quantitative correlation between X^{2-} binding affinity to cationic micelles and X^{2-}- and temperature-induced micellar growth. *Rheologica Acta, 55*, 125-136.

Yusof, N. S. M., Razak, N. A. and Khan, M. N. (2013). Quantitative correlation between counterion (X) affinity to cationic micelles and X-induced micelar growth for X = 2,4-; 2,5-; 2,6- and 3,4-dichlorobenzoate ions. *Journal of Oleo Science, 62(5)*, 257-269.